Hexagonal packing of Drosophila wing epithelial cells by the Planar Cell Polarity pathway

DISSERTATION

zur Erlangung des akademischen Grades

Doctor rerum naturalium

(Dr.rer.nat.)

vorgelegt

der Fakultät Mathematik und Naturwissenschaften

der Technischen Universität Dresden

von

Anne-Kathrin Claßen

Diplom-Biologin

geboren am 10. Juli 1976 in Berlin, Deutschland

Gutachter:

Prof. Dr. Michael Brand	Technische Universität, Dresden
Dr. Suzanne Eaton	Max Planck Institut für Molekulare Zellbiologie und Genetik, Dresden
Prof. Dr. Elizabeth Knust	Heinrich Heine Universität, Düsseldorf

I herewith declare that I have produced this paper without the prohibited assistance of third parties and without making use of aids other than those specified; notions taken over directly or indirectly from other sources have been identified as such. This paper has not previously been presented in identical or similar form to any other German or foreign examination board.

The thesis work was conducted from October 15th, 2002 to April 12th, 2006 under the supervision of Dr. Suzanne Eaton at the Max Planck Institute of Molecular Cell Biology and Genetics, Dresden.

Dresden, April 12th, 2006

Anne-K. Claßen

Acknowledgement

Writing this thesis would not have been possible without the contributions, encouragement and support from many great people, some of which I would like to acknowledge here:

Suzanne, thank you so much for everything!!! Working with you is literally ‘mind-blowing’. I stopped counting the number of times I had to get my brain rewired in the past three years due to your sudden sparks of enlightenment. Thank you so much for that and for all the enthusiasm, never-ending discussions, patience, trust and amazing support!

Kurt, thank you so much for working with me on this project! It’s been a lot of fun! I would also like to thank the members of my TAC committee, Tony Hyman and Michael Brand, for great discussions and comments in our meetings. Especially, I would like to thank Michael Brand and Elizabeth Knust for reviewing this thesis. Furthermore, I want to acknowledge Francois Graner and his lab; they have made major contributions to the conceptual development of this thesis.

Dear lab, I am lacking the right words to say what would need to be said! You are truly the best bunch of people I could have only dreamed of working with. Thank you for the great science and the beers, and great science over beers! A huge hug in deep appreciation for the Eaton-girls Christina, Daniela, Radiosa, Maria and Sarah - you are the best! Ali, Jens, Falco, Chandra, Eric and Marko (the Eaton boys) - thank you for always putting a smile to my face. Sniff, I already miss you like crazy!!!

I would like to thank my family, and especially my mom and dad. I would not be where I am now without you. Thank you for all your support and patience, no matter what ;) !
I am furthermore indebted to Martin, Andrea, Jörg, Amy, Steph, Nina, Jules, Anna, Maike, Alex, Phillipp, Tony, Alicia, Bas, Bryony, Imke, Thomas, Anette, Thilo, Britta, Julia, Antje and Sören for: beer coffee chocolate food sofas hugs listening occasionally kicking my a… inspiration support and big chunks of love :) !

Zusammenfassung

Die Etablierung einer regelmäßigen Gewebegeometrie ist essentiell für die Funktionalität vieler Organe, wobei Signaltransduktionswege, die die Ausbildung einer solchen Gewebegeometrie kontrollieren nicht bekannt sind. In dieser Arbeit haben wir zellulären Mechanismen untersucht, welche verantwortlich dafür sind, dass sich Haare, die von einzelnen *Drosophila* Flügelepithelzellen gebildet werden, in einem regelmäßigen hexagonalen Muster anordnen.

Hier zeigen wir auf, dass Epithelzellen in der frühen Entwicklung des *Drosophila* Flügelgewebes unregelmäßig arrangiert sind. Kurz vor der Haarausbildung allerdings gliedern sich die Epithelzellen in ein gleichmäßiges hexagonales Packmuster ein. Dabei werden individuelle Zellkontakte zurückgebildet und neue Kontakte werden aufgebaut. Diese Prozesse führen zu lokalen Zellrearrangements, die eine hexagonale Musterbildung ermöglichen. Dieses hochdynamische Verhalten von Zellkontakten ist im Wesentlichen abhängig vom effizienten intrazellullären Transport des Zelladhäsionsprotein E-cadherin und wird gesteuert durch die GTPasen Dynamin und Rab11.

Wir zeigen außerdem, dass die hexagonale Musterbildung die Aktivität des Planaren Zellpolarität Signaltransduktionsweges bedarfs. Planarpolaritäts-Proteine sind evolutionär stark konservierte Komponenten eines nicht-klassischen Wnt-Signaltransduktionsweges, welcher bei der Koordination von Zellpolarität und Zellverhalten in unterschiedlichsten Systemen eine Rolle spielt. Genetische Interaktionen zwischen *dynamin*- und Planarpolaritätsmutanten weisen darauf hin, dass Planare Zellpolaritätsproteine den Dynamin-regulierten intrazellulären Transport von E-cadherin modulieren um so den Auf- und Abbau von Adhäsionskontakten zu ermöglichen. Außerdem beschreiben wir die Rekrutierung von Sec5, einer Exocyst-Komponente, durch das Planare Polaritätsprotein Flamingo. Wir zeigen die Kolokalisierung von Sec5 mit Vesikeln die E-cadherin und Flamingo enthalten. Basierend auf diesen Daten postulieren wir, dass Flamingo über Sec-5 E-

cadherin-haltige Vesikel rekrutiert, und damit einen zielgerichteten Transport von E-cadherin zu individuellen Zellkontakten ermöglicht. Das so lokalisierte Freisetzen von E-cadherin stabilisiert dynamische Zellkontakte - eine wichtige Grundlage für die Ausbildung einer regelmäßigen Gewebegeometrie.

Diese vorgelegte Dissertation legt dar, dass eine wesentliche Funktion des Planaren Zellpolarität Signaltransduktionsweges die dynamische Modulierung von Zelladhäsionskontakten in der Embryonalentwicklung ist. Darüber reguliert im *Drosophila* Flügel dieser Signaltransduktionsweg die hexagonales Musterbildung von Epithelzellen. Wir haben intrazelluläre Exocyst-regulierte Transportwege als potentiell grundlegende molekulare Effektoren identifiziert, die die Funktion des Signaltransduktionsweges in verschiedenen Prozessen der Embryonalentwicklung näher bestimmen können.

Summary

The mechanisms that order cellular packing geometry are critical for the functioning of many tissues, but are poorly understood. Here we investigate this problem in the developing wing of Drosophila. The surface of the wing is decorated by hexagonally packed hairs that are uniformly oriented towards the distal wing tip. They are constructed by a hexagonal array of wing epithelial cells.

We find that wing epithelial cells are irregularly arranged throughout most of development but become hexagonally packed shortly before hair formation. During the process, individual cell junctions grow and shrink, resulting in local neighbor exchanges. These dynamic changes mediate hexagonal packing and require the efficient delivery of E-cadherin to remodeling junctions; a process that depends on both the large GTPase Dynamin and the function of Rab11 recycling endosomes. We suggest that E-cadherin is actively internalized and recycled as wing epithelial cells pack into a regular hexagonal array.

Hexagonal packing furthermore depends on the activity of the Planar Cell Polarity proteins. The Planar Cell Polarity group of proteins coordinates complex and polarized cell behavior in many contexts. No common cell biological mechanism has yet been identified to explain their functions in different tissues.

A genetic interaction between Dynamin and the Planar Cell Polarity mutants suggests that the planar cell polarity proteins may modulate Dynamin-dependent trafficking of E-cadherin to enable the dynamic remodeling of junctions. We furthermore show that the Planar Cell Polarity protein Flamingo can recruit the exocyst component Sec5. Sec5 vesicles also co-localizes with E-cadherin and Flamingo. Based on these observations we propose that during the hexagonal repacking of the wing epithelium these proteins polarize the trafficking of E-cadherin-containing exocyst vesicles to remodeling junctions.

The work presented in this thesis shows that one of the basic cellular functions of planar cell polarity signaling may be the regulation of dynamic cell adhesion. In doing so, the planar cell polarity pathway mediates the acquisition of a regular packing geometry of *Drosophila* wing epithelial cells. We identify polarized exocyst-dependent membrane traffic as the first basic cellular mechanism that can explain the role of PCP proteins in different developmental systems.

Table of Contents

Table of Figures

Abbreviations

AP	Anterior posterior
APF	After Puparium Formation
Dpp	Decapentaplegic
DV	Dorsal ventral
GFP/YFP/CFP	Green/yellow/cyan fluorescent protein0
Hh	Hedgehog
Hrs	Hours
MDCK	Madin Darby Canine Kidney (cell line)
Min	Minutes
MTOC	Microtubule Organizing Centre
OR	Oregon R (fly strain)
P (P2A-P2D)	Pupal (Waddington stage Pupal 2A-2D)
PCP	Planar Cell Polarity
PP	Prepupal
SD	Standard deviation
TP	Time point
Wnt/Wg	Wnt/Wingless
WT	Wild type

1. Introduction

1.1. Tissue geometry and tissue function

The function of many epithelial tissues critically depends on the exact geometry of their constituent cells (Figure 1). Sensory epithelia of the inner ear comprise an ordered array of hair cells and support cells (McKenzie et al 2004, Tilney & Saunders 1983, Tilney et al 1986, Wang et al 2005). To respond to mechanical perturbations caused by sound or motion, stereocilia bundles on sensory hair cells must be precisely aligned (Roberts et al 1988). The optical properties of vertebrate and invertebrate eyes depend on cellular packing geometry. In Dipteran eyes, which utilize neural superposition to increase their sensitivity, axons of photoreceptors in different ommatidia responding to the same spatial information converge to the same place in the lamina, superimposing their signals (Nilsson 1989). Small deviations in packing within or between ommatidia would make this system unworkable. In the vertebrate eye, hexagonal packing of lens fiber cells minimizes light scattering by cell membranes and is essential for transparency (Tardieu 1988). The *Drosophila* wing is covered by a hexagonally packed array of hairs, each constructed by a single wing epithelial cell. Hairs are oriented distally and parallel to the longitudinal wing veins, and have been proposed to guide air flow over the surface of the wing during flight (Wootton 1992); regular hair spacing and orientation would clearly be important for this function.

Intriguingly, many tissues with regular packing geometries also display planar cell polarity, a polarity along an axis orthogonal to the apical-basal axis of epithelial cells. Planar cell polarity is achieved by high coordination of behavior of cells with that of their neighbors, leading to local and global alignment with the axis of polarity. On *Drosophila* wings, all hairs are oriented towards the distal wing margin. Photoreceptor positioning within ommatidia is stereotypical and coordinated with the positioning in neighboring ommatidia. Stereocilia bundle orientation in the mouse inner ear is coordinated throughout several rows of cells; hexagonal cells in dipteran eyes align their pointed vertices along one axis (white arrows in Figure 1).

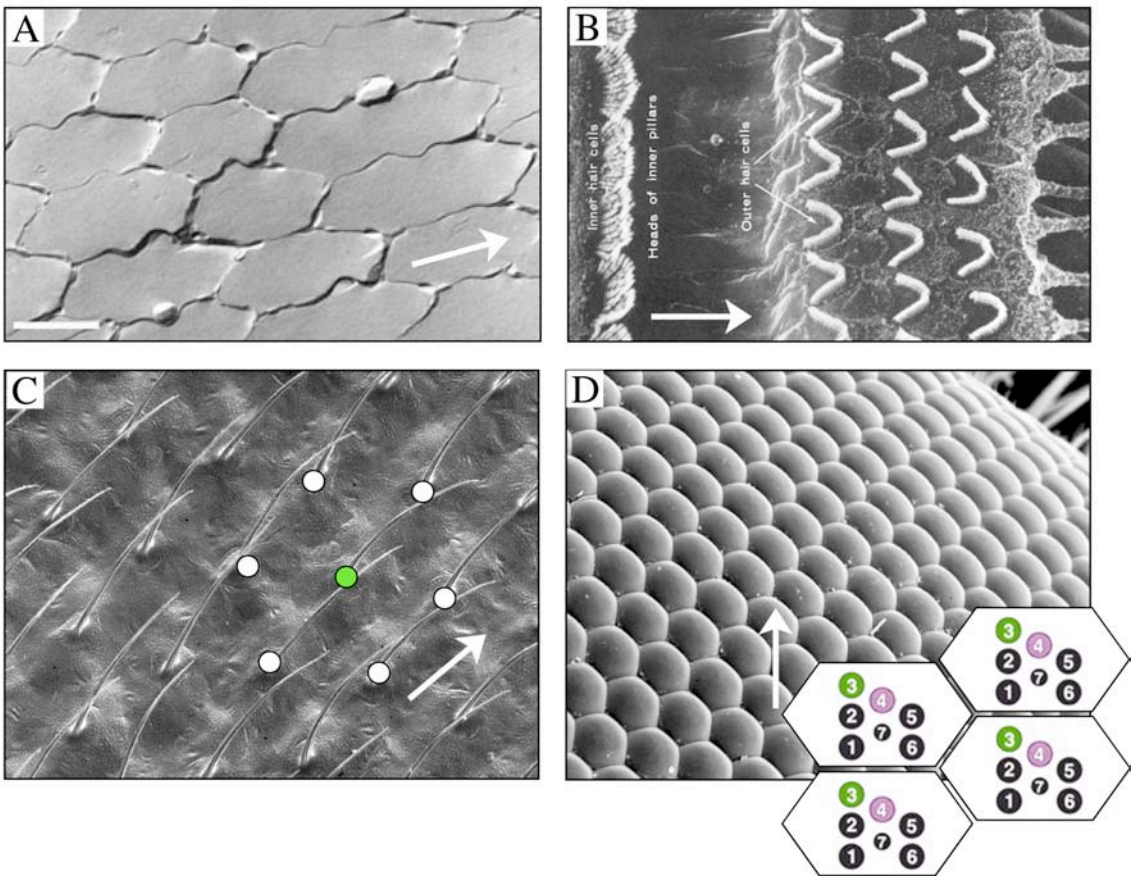

Figure 1 **Regular tissue geometry in vertebrates and *Drosophila***

(A) Fish eye lens fiber cells are hexagonally packed (from www.biol.lu.se/funkmorf/vision/ronald/ultra1.jpg). **(B)** The mammalian Organ of Corti in the inner ear consists of regularly aligned rows of sensory hair cells giving rise to stereocilia bundles. **(C)** *Drosophila* wing hairs are regularly spaced and hexagonally packed. **(D)** Hexagonal lattice of ommatidia in the *Drosophila* eye (from www.bath.ac.uk/ceos/images/blowFly/bfeye.jpg). Each ommatidia hexagon consists of a cluster of 8 photoreceptor cells (7 shown) that are arranged in a precise triangular pattern. All tissues not only possess a highly regular geometry but also exhibit planar cell polarity or tissue polarity along the axis indicated by a white arrow.

In *Drosophila*, genetic analysis has identified a group of 'tissue polarity' or 'planar cell polarity' genes essential for global orientation of hairs on the wing surface (Gubb & Garcia-Bellido 1982). In planar cell polarity (PCP) mutant wings, hairs are organized in whorls exhibiting good coordination between neighboring cells, but lacking the normal long-range proximal-distal polarity (Figure 3A). In wild type, each cell in the wing epithelium gives rise to a single apical hair at the distal cell side. In some PCP mutants, hair outgrowth is not focused to a single point causing multiple hairs to form (Adler 2002, Adler et al 1994, Lee & Adler 2002). At this developmental stage the wing epithelium consists of two at their basolateral side apposed epithelial sheets that

already outline adult wing shape. This wing shape arises during pupal metamorphosis from the larval wing imaginal disc primordium. The primordium is a single-layered epithelia sac that has undergone massive cell proliferation during larval stages to construct the tissue mass required to model adult structures (Figure 2) (Fristrom 1988, Waddington 1941).

The research presented in this thesis addresses the intriguing question of how epithelial cells form precise geometrical arrays in the developing pupal wing of *Drosophila*. We found that the planar cell polarity group of genes has an essential role in generating a regular and hexagonal packing topology of wing epithelial cells just prior to hair formation.

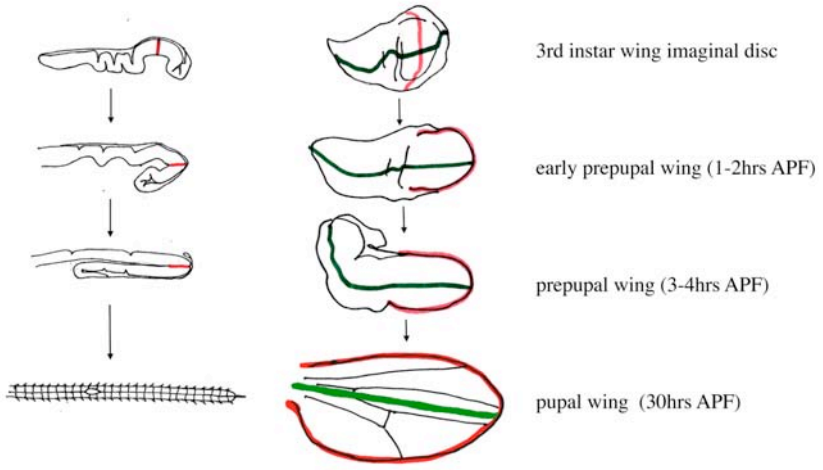

Figure 2 ***Drosophila* wing development**

Transverse sections (left) and dorsal views (right) of the developing wing epithelium. During larval stages the wing primordium, the imaginal disc, proliferates and is patterned by the action of the Dpp, Hedgehog and Wingless morphogens into different compartments. These are separated by the dorsal-ventral compartment boundary (red) and anterior-posterior compartment boundary (green), which maintain the different wing territories throughout morphogenesis. During prepupal development (0-17hrs APF (after puparium formation), see timeline in Table1) the single-layer epithelium of the disc evaginates and gives rise to the two flat cell sheets apposed at their basal sides that are characteristic of the adult wing. During early pupal development the wing tissue acquires its final adult shape and pattern. Hairs form at the two apical surfaces of the epithelium.

1.2. Planar cell polarity and morphogenesis

The core-components of the PCP-signaling pathway appear to be highly conserved and required to coordinate cell behavior in seemingly very different developmental context (Figure 3). In addition to wing hair polarity, the same group of PCP genes also coordinates photoreceptor

positioning in *Drosophila* (Figure 3B) (Gubb 1993, Wehrli & Tomlinson 1995), alignment of stereocilia bundles in the mouse inner ear (Figure 3C) (Wang et al 2005), alignment of mouse skin hairs (Figure 3E) (Guo et al 2004) and guides cell movements during convergent extension in vertebrate gastrulation (Figure 3D) (Mlodzik 2002). Strikingly, many mammalian syndromes such as spina bifida (Ueno & Greene 2003), hearing and balance disorders (Hawkins & Lovett 2004), congenital heart defects (Garriock et al 2005, Henderson et al 2006, Phillips et al 2005) and polycystic kidney disease (Fischer et al 2006) have been associated with PCP signaling deficiencies. Taken together, these findings identify PCP signaling as a new major contributor to tissue morphogenesis in human development of strong medical interest and potential.

Recent advances in the studies of PCP establishment have begun to reveal the molecular machinery underlying coordinate cell behavior in a planar sheet of cells. PCP signaling appears to function through a non-canonical Wg/Wnt signaling pathway that is different from the classical β-catenin-dependent Wg/Wnt pathway resulting in transcriptional regulation of TCF/Lef-1 target genes. Rather, PCP signaling impinges on cell-cell communication (Saburi & McNeill 2005), cytoskeletal organization (Turner & Adler 1998) and gene transcription (Fanto et al 2003).

At the heart of the pathway lies a highly conserved core machinery of gene products that include transmembrane proteins like Frizzled (Gubb & Garcia-Bellido 1982, Vinson & Adler 1987, Vinson et al 1989), Strabismus (Taylor et al 1998, Wolff & Rubin 1998), Flamingo (Usui et al 1999) and the cytoplasmic proteins Prickle, Prickle-Spiney leg, Dishevelled (Gubb & Garcia-Bellido 1982), Diego (Feiguin et al 2001) and Widerborst (Hannus et al 2002). Recently, also components of heterotrimeric G-protein signaling, such as the $G\alpha_o$-subunit (Go), have been placed at this level of the pathway (Katanaev et al 2005).

Frizzled and dishevelled are also central to the canonical Wg/Wnt-pathway mediating stabilization of cytoplasmic β-catenin. Dishevelled is positioned at the site of divergence between the functionally distinct canonical and non-canonical Wnt-pathway (Boutros & Mlodzik 1999). The cytoplasmic protein Dishevelled directly binds the single-pass transmembrane receptor protein Frizzled (Chen et al 2003, Cong et al 2004, Wong et al 2003) and transduces receptor activation to downstream effectors via its DIX, DEP or PDZ domain. Dishevelled canonical signaling specifically requires the N-terminal DIX (Dsh/Axin) domain (Itoh et al 2000, Kishida et al 1999). The DEP (Dsh/egl-10/Pleckstrin) domain appears to function both in the canonical and PCP-pathway (Axelrod et al 1998, Penton et al 2002) and may confer membrane-association in response to Frizzled signaling (Axelrod et al 1998, Pan et al 2004). Repressive binding of the canonical Wnt-inhibitors Naked Cuticle (Rousset et al 2001, Yan et al 2001) or Frodo and Dapper (Wong et

al 2003) to the PDZ-domain of Dishevelled may bias Dishevelled function towards PCP signaling. Dishevelled is also targeted by core PCP proteins for binding; Strabismus (Bastock et al 2003) or Prickle and Diego (Jenny et al 2005) where shown to bind Dishevelled and modulate Dishevelled signaling.

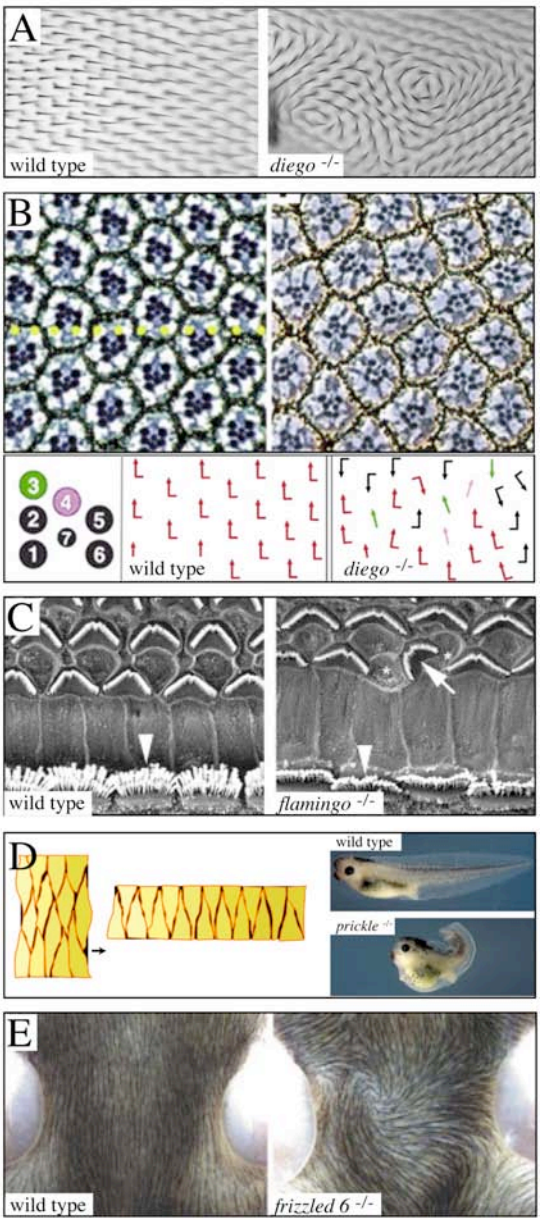

Figure 3 **Planar cell polarity in vertebrates and *Drosophila***

(A) *Drosophila* wing hair patterns in wild type (left) and in the PCP mutant *diego* (right). **(B)** *Drosophila* eye neuroepithelium in wild type (left) and in PCP mutants (right). Note the nice hexagonal packing of ommatidia units in wild type. There, the arrangement of photoreceptors in one ommatidial unit is coordinated with the arrangement of photoreceptors in the neighboring ommatidial unit (red arrows, lower left panel). In PCP mutants this coordination is lost (lower right panel). **(C)** Mouse inner ear neuroepithelium in wild type (left) and in the PCP mutant *flamingo* (right). **(D)**

During convergent-extension cells intercalate towards the tissue midline to elongate the tissue along the midline axis. This process is used to extend the vertebrate body axis during gastrulation. In *prickle* mutants proper cell intercalation fails leaving the body axis short and fat. **(E)** Mouse skin hair patterns in wild type (left) and in the PCP mutant *frizzled* (right).

The current common view in the field emphasizes that PCP proteins are recruited to the cell cortex at the level of adherens junctions only late during *Drosophila* pupal wing development prior to hair formation (Figure 4A). This recruitment is thought to result from the activation of Frizzled-receptor signaling via Dishevelled and specifically requires the 7-pass transmembrane protein Flamingo and the 4-pass transmembrane protein Strabismus (Bastock et al 2003, Strutt 2001). In the absence of Flamingo other core PCP-components like Dishevelled may not localize to the cellular cortex (Shimada et al 2001).

It is speculated that after uniform cortical recruitment a small bias of fz-signaling activity of unknown origin towards one side of the cell (Adler et al 1997) initiates a cellular cascade to amplify this bias and establish a stable polarity cue. The cellular cascade involves recruitment and competitive recruitment inhibition of core PCP components into two spatially distinct complexes (Bastock et al 2003, Das et al 2004, Jenny et al 2005, Strutt 2002, Tree et al 2002b). As a consequence, PCP proteins become asymmetrically localized within individual cells to proximal and distal cortical domains. Cortical domains appear to be tightly coupled between neighboring cells by the atypical Cadherin Flamingo, which may facilitate cell-cell communication. Cell-cell communication is a central feature of the feedback loop model proposed by Tree et al (Figure 4B); positive and negative feedback loops reinforce and stabilize asymmetric protein localization between neighboring cells enabling them to coordinate cellular behavior (Adler 2002, Eaton 2003, Strutt 2002, Tree et al 2002a, Tree et al 2002b).

Recently, the problem of PCP establishment was addressed using mathematical modeling approaches (Adler 2002, Amonlirdviman et al 2005, Le Garrec et al 2006, Webb & Owen 2004). Amonlirdviman et al established a rule set of partial differential equations to describe protein-protein interactions in proximal and distal complexes. The model predicted PCP protein-protein interactions to be sufficient for domineering non-autonomy of cortical domains. Domineering non-autonomy is a puzzling phenomenon observed where *frizzled* or *strabismus* mutant cells can reorient cortical domain polarity in neighboring wild type cells; secreted factors affecting neighboring cells in this way have not been identified in *Drosophila*. These studies demonstrated

that mathematical modeling of the PCP signaling network may be a powerful tool to elucidate the complex behavior of proteins during establishment of tissue polarity.

So far, polarized PCP protein distribution has not been observed during convergent-extension movements in vertebrate embryos. Rather, PCP proteins appear to localize to small patches of cell-cell contacts in the mesenchymal cells of the involuting mesoderm (pers. comm. Sabine Witzel in the Heisenberg lab). However, during ascidian gastrulation Prickle becomes subcellularly polarized (Jiang et al 2005). Even more strikingly though, inner ear development employs PCP-dependent convergent-extension-like epithelial cell intercalation for anterior-posterior axis elongation in the organ of Corti (McKenzie et al 2004, Wang et al 2005). Towards the final stages, at the time of stereocilia cell alignment, Dishevelled2 is asymmetrically localized (Wang et al 2005). Thus, polarized distribution of core PCP components may depend on tissue specific (mesenchymal vs. epithelial) context.

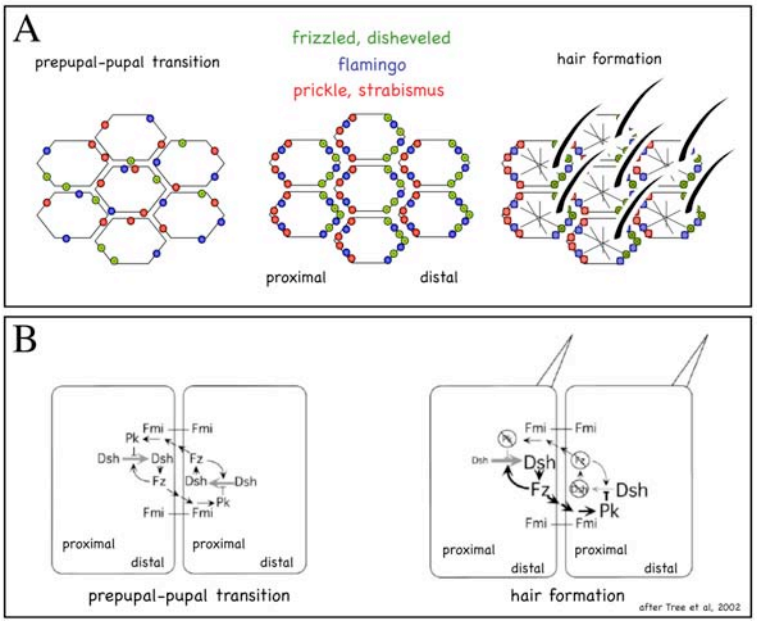

Figure 4 Establishment of planar cell polarity in the *Drosophila* wing

(A) According to the current view core planar polarity proteins become recruited to the apical cell cortex at the prepupal-pupal transition (see timeline in Table 1). Over the course of several hours these proteins become asymmetrically localized within each wing epithelial cell to either the proximal or distal boundaries (red or green proteins, respectively). Flamingo (blue) localizes to both the proximal and the distal cell boundary. These asymmetric cortical domains then organize and focus hair outgrowth at the distal side of the cell. **(B)** A small bias of Fz-activity towards the distal cell boundary is amplified by mutual recruitment and stabilization of Dsh and Fz to the distal side of the cell, as well as active

inhibition of their localization to the proximal side; this is mediated by Prickle-dependent inhibition of Dsh localization. A positive feedback loop acting through homophilic Flamingo-interactions across cell boundaries may promote the evolution of asymmetry by modulating the ability of Fz, Dsh and Pk to associate with cortical domains.
Large bold letters indicate proteins accumulating to high levels; smaller letters indicate lower levels. Bold arrows represent predominant reactions. Circles with slashes indicate proteins whose levels are decreased or absent from the designated locations. Multiple arrows between Fz and Pk indicate that Fz induces accumulation of Pk on the opposite boundary through an undefined mechanism, possible using Flamingo intercellular signaling (Tree et al 2002b).

1.3. Upstream regulation of planar cell polarity

Members of the Frizzled family of receptors are important for PCP-signaling in many developmental contexts, but also function as Wnt-receptors in the canonical Wnt-pathway. Therefore Wnt-family members are good molecular candidates that may also regulate PCP. At least vertebrates appear to rely on Wnt/Wg-ligands to mediate long-range PCP signaling across a field of cells. Certain Wnt-ligand/frizzled-receptor combinations initiate PCP but not canonical Wnt/Wg signaling. In zebrafish, the Wnt-ligands Silberblick (Wnt-11) (Heisenberg et al 2000, Ulrich et al 2003) and Pipetail (Wnt-5) (Kilian et al 2003, Zhu et al 2006), as well as the frizzled-receptor 7 (Carreira-Barbosa et al 2003), confer specificity of Frizzled-activation to the non-canonical pathway. In addition, the inability of some Wnts to bind canonical Frizzled co-receptors, such as LRP-5/6 (Liu et al 2005), or the absence of canonical frizzled co-receptors such as *Drosophila* Arrow (Povelones et al 2005), may promote non-canonical PCP-pathway signaling.

In *Drosophila*, the mechanisms that initiate PCP signaling and may determine the axis of polarity have been more obscure. Only some evidence for a distant role of wingless/DWnt in establishing PCP has been found (Cho & Irvine 2004, Lawrence et al 2002, Lim et al 2005, Rulifson et al 2000). The lack of upstream Wnt-related factor initiating core PCP signaling in *Drosophila* have led many to propose the existence of a hypothetical unknown factor X (Fanto et al 2003, Lawrence et al 2002, Struhl et al 1997, Wehrli & Tomlinson 1998). Only recently however, the large atypical Cadherins Fat and Dachsous, as well as the Type II transmembrane protein Four-Jointed, have emerged to play an important but little understood role in the regulation of frizzled/PCP-polarity. These proteins are not directly required for frizzled activation and polarization per se, but lie genetically upstream of Fz and mediate long-range coordination of polarity in *Drosophila* eye and wing (Ma et al 2003, Saburi & McNeill 2005, Strutt & Strutt 2005). Four-jointed may affect Dachsous and Fat function by directing post-translational modification of

these two proteins in the Golgi (Brodsky & Steller 1996, Saburi & McNeill 2005, Strutt et al 2004). Four-jointed and Dachsous both act via effects on Fat; Dachsous and Fat may interact at adjoining cell surfaces of neighboring cells. This interaction appears to modulate an activity of Fat towards Frizzled (Adler et al 1994, Clark et al 1995, Ma et al 2003, Matakatsu & Blair 2004, Strutt & Strutt 2002a, Yang et al 2002).

Intriguingly, it has become clear that both Dachsous and Frizzled signaling must be active during late larval or prepupal stages to correctly specify the axis of cortical domain polarity (Adler et al 1994, Matakatsu & Blair 2004, Strutt & Strutt 2002a). However, cortical domains are not thought to actually polarize until much later during pupal development.

1.4. Cellular responses to planar cell polarity signaling

In the course of identifying the cellular response pathways of polarized cortical domains several different downstream effectors of PCP signaling have been described. In *Drosophila*, polarized cortical domains appear to provide a spatial cue for the subcellular site of hair outgrowth (Shimada et al 2001, Strutt 2002). On the wing, each single cell forms one distally pointing hair, which is derived from an actin and microtubule-filled apical membrane outgrowth (Eaton et al 1996, Turner & Adler 1998). Cortical domains position the initial actin accumulation towards the distal side of the cell. In the absence of some of the core PCP proteins wing hair outgrowth initiates in the center of the cell (Wong & Adler 1993). The molecular mechanisms whereby polarized cortical domains mediate changes in cytoskeletal organization also in other developmental systems remain unclear. Downstream PCP targets do include known actin-regulators such as RhoA and Rho-kinase (Kim & Han 2005, Strutt et al 1997, Winter et al 2001, Zhu et al 2006), the actin motor Myosin II (Winter et al 2001), the small Rho GTPases Cdc42 and Rac (Djiane et al 2000, Eaton et al 1996, Fanto et al 2000), and less well-characterized *Drosophila* proteins like Tricorned, Inturned, Furry, or Multiple wing hairs (Adler 2002, Adler et al 2004, Collier et al 2005, Lee & Adler 2002, Yun et al 1999). In vertebrates, the formin-homology domain protein Daam1 (Dishevelled associated activator of morphogenesis 1) directly links PCP signaling of Dishevelled to Rho (Habas et al 2001). This is one of the few molecular clues to how PCP proteins activate downstream effectors. However, *Drosophila* Daam does not appear to be required for *Drosophila* PCP (Matusek et al 2006).

Depending on context other PCP effector modules are engaged, such as the STE20-like kinase Misshapen (Paricio et al 1999) and the JNK-type MAPK cascade (Kim & Han 2005, Noselli & Agnes 1999, Strutt 2002). Both effectors are implicated either in *Drosophila* eye development or in vertebrate gastrulation. Several studies have moreover uncovered the ability of PCP-signaling to modulate gene transcription in *Drosophila* development (Fanto et al 2003, Fanto et al 1998, Fanto & Mlodzik 1999, Fanto et al 2000, Lee & Adler 2004). PCP-signaling in the eye biases Notch-Delta activity to specify R3/R4 photoreceptor cell fate (Das et al 2002, Fanto et al 1998, Fanto & Mlodzik 1999). The transcriptional co-repressor Atrophin directly interacts with the cytoplasmic tail of fat; this may be required to control four-jointed expression in eye morphogenesis (Fanto et al 2003).

It has always been puzzling that, in other developmental contexts, the genes of the well-conserved PCP cassette organize processes that involve dynamic cell adhesion, as during vertebrate gastrulation (Mlodzik, 2002) or ommatidial rotation (Strutt & Strutt 2003), rather than the formation of polarized structures.

We found that PCP proteins act to remodel junctional adhesive contacts and that this is a prerequisite for the establishment of an orderly hexagonal packing of wing epithelial cells. Therefore, our data strongly suggests that dynamic modulation of intercellular contacts may be a common feature of processes requiring the conserved planar polarity cassette.

1.5. Cell adhesion and tissue remodeling during morphogenesis

Dynamic modulation of intercellular contacts during epithelial morphogenesis is not a trivial task to accomplish. An epithelium is a contiguous sheet of tightly adjoining cells that posses a clear apico-basal polarity. Organelle distribution, microtubule and actin cytoskeleton networks, membrane lipid composition and integral and peripheral membrane protein allocation have distinctive properties in apical and basolateral cellular domains. Another hallmark of epithelia is the distribution of intercellular junctions along the apico-basal axis. They provide firm adhesion between cells and maintain the characteristic barrier function between apical/luminal and basal/substratum territories. In *Drosophila*, mature epithelia generally posses a subapical zone, adherens junctions, septate junctions and more basally gap junctions (Figure 5A). These junctions are assembled from a vast repertoire of different proteins that establish and maintain junctions as distinct subdomains (Lecuit & Wieschaus 2002, Tepass et al 2001). In *Drosophila* pupal wings, characteristic features of all these junctions are evident (Figure 5B).

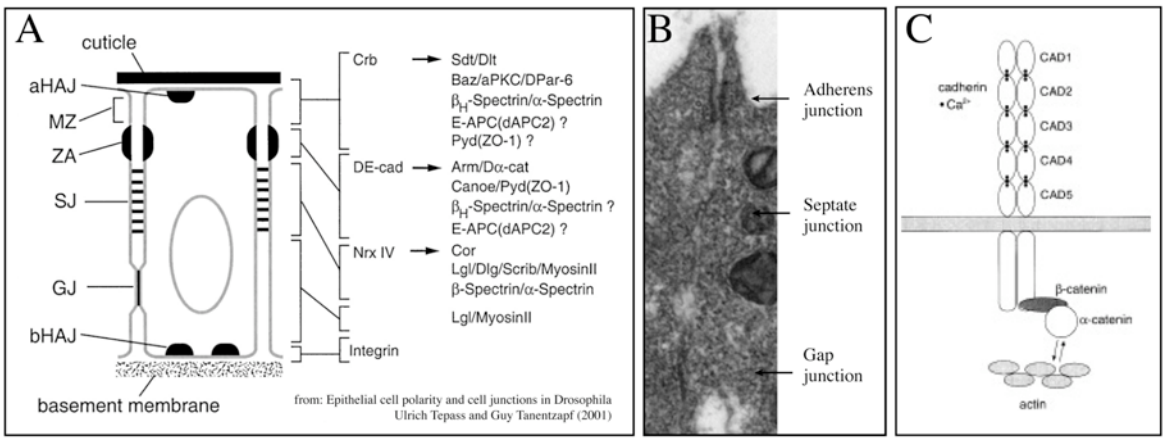

Figure 5 **Epithelial junctions in *Drosophila***

(A) Schematic of epithelial cell junctions in mature *Drosophila* epithelia during larval development. The type of a cellular junction is indicated to the left and proteins found in the respective subdomains are listed on the right. The question marks indicate that the localization of these proteins at the given position requires confirmation. (aHAJ, apical hemi adherens junction; bHAJ, basal HAJ; DE-cad, DE-cadherin; ECM, extracellular matrix; GJ, gap junction; MZ, marginal zone; SJ, septate junction; ZA, zonula adherens) (Tepass et al 2001). **(B)** Electron micrograph of a pupal wing epithelium before hair formation. **(C)** Schematic representation of the E-cadherin complex proposed to assemble at adherens junctions: E-cadherin has 3-5 cadherin-repeat ectodomains; the most distal binds E-cadherin molecules from the opposite cell surface. The more membrane-proximal domains coordinate Ca^{2+} ions using motifs resembling EF-hand domains. Two E-cadherin molecules form transdimers and cluster laterally, which is required for good adhesion. The current dogma views the cytoplasmic tail of E-cadherin to interact with β-catenin, linking the adhesive complex via α-catenin to the actin cytoskeleton. (image: http://www.cs.stedwards.edu/chem/Chemistry/CHEM43/CHEM43/Cadherins/FUNCTION.html)

Examples of the concerted morphogenesis of epithelial sheets in *Drosophila*, which do require the dynamic modulation of intercellular contacts include leg imaginal disc morphogenesis (Fristrom 1988), tracheal development (Lee & Kolodziej 2002, Metzger & Krasnow 1999, Tanaka-Matakatsu et al 1996), embryonic dorsal closure (Jacinto et al 2001) and germband extension (Bertet et al 2004). Molecular mechanisms and principles described in *Drosophila* are recapitulated in vertebrate epithelia, for example, during wound healing, vertebrate epiboly, inner ear development, skin formation and gut or kidney morphogenesis. During epithelial sheet transformation it is crucial to maintain close cell adhesion, apico-basal polarity and epithelial barrier function; nevertheless, junctions need to be mobilized. Possible mechanisms may be concertina stretching of junctional belts (Fristrom 1982, Hull & Staehelin 1976) or de novo assembly and disassembly of the junctional molecular machinery (Gumbiner 2005). To multiply the level of complexity to be considered, junctions are formed between two neighboring cells,

hence at least two cells are engaged in a decision to activate junctional mobilization. This suggests that the process of epithelial sheet morphogenesis is a highly complex process that needs to be tightly controlled and involves extensive cell-cell communication.

One of the first molecules to be recognized as being important for cellular rearrangements in epithelia was E-cadherin (Figure 5C). It is encoded by the *Drosophila* Shotgun locus and appears to be specifically required to maintain epithelial integrity during tissue morphogenesis. *Shotgun* mutant cells in *Drosophila* retain good apico-basal polarity in static embryonic tissues but catastrophically disintegrate in dynamic epithelia (Le Bivic 2005, Tanaka-Matakatsu et al 1996, Tepass et al 1996, Tepass et al 2001, Uemura et al 1996). E-cadherin localizes to the electron-dense transmembrane core at adherens junctions (Figure 5B). E-cadherin has multiple extracellular Ca^{2+}-binding cadherin repeats that are coordinated by Ca^{2+}-ions into stiff rods (Figure 5C). Adhesion is activated by E-cadherin transdimers that mediate homophilic binding to E-cadherin at the surface of neighboring cells via the most membrane-distal ectodomain (Gumbiner 2000). The cytoplasmic tail of E-cadherin binds β-catenin, which, in turn, links the E-cadherin complex to the cortical actin cytoskeleton via the adaptor α-catenin (Yap et al 1997). Many studies suggest that these interactions may be highly dynamic and subject to regulation at many different levels, thereby tailoring adhesion strength to suit different epithelial contexts (Gates & Peifer 2005, Gumbiner 2000, Gumbiner 2005, Lilien & Balsamo 2005, Perez-Moreno et al 2003, Wheelock & Johnson 2003).

Intriguingly, the PCP downstream effector RhoA can directly bind to two *Drosophila* adherens junction proteins: α-catenin and p120ctn (Magie et al 2002). RhoA and α-catenin mutually depend on each other for proper localization and affect epithelial integrity during dorsal closure (Bloor & Kiehart 2002). Further studies outline both positive and negative consequences of Rho activity on adhesion (Braga 2002); these may reflect the function of Rho in modulating actin dynamics at adherens junctions. Regulation at the level of microtubules and lipid-dependent signaling cannot be excluded (Fukata et al 2003). In general though, altering E-cadherin based adhesion is proposed to function in epithelial-mesenchymal and mesenchymal-epithelial transitions that occur during embryonic development. Furthermore, for a long time now it has been recognized that downregulation of E-cadherin adhesion also often correlates with the acquisition of a malignant metastatic phenotype by tumor cells (Katoh 2005).

Our data presented in this thesis suggests that *Drosophila* E-cadherin is dynamically internalized and recycled back to the cell surface. Endocytic trafficking of DE-cadherin turns out to

be crucially important to mediate dynamic adhesion and epithelial integrity at the time when packing geometry in the pupal wing epithelium changes.

1.6. Intracellular membrane trafficking

An essential element of cell homeostasis is intracellular membrane flow whereby organelles and the plasma membrane communicate by means of vesicular carriers called endosomes sorting protein cargo to their destination. Two main routes of membrane flow are distinguished: endocytic trafficking of cell surface proteins to degradation in lysosomes or back to the plasma membrane via recycling endosomes, and the delivery of biosynthetic cargo via ER and Golgi to the plasma membrane. Multiple points of intersection exist between both routes.

Linearity and specificity of cargo trafficking is controlled by a vast array of proteins mediating cargo-recruitment into vesicular carriers, fission of the vesicle from the donor membrane, cytoplasmic transport along microtubules and actin filaments, docking to specific target membranes and the fusion of vesicles with the target membranes. Adaptor-proteins such as the mammalian AP-family of proteins, COP-proteins and GGA's can recruit specific protein cargo into coated membrane patches (Robinson 2004, Robinson & Bonifacino 2001). The large GTPase Dynamin acts as a pinchase the pinch off budding vesicles from donor membranes (Hinshaw 2000). Dynein and kinesin are minus-end and plus-end directed microtubule motor proteins respectively, whereas myosin is an actin-dependent motor protein; these motor proteins are recognized to move endocytic vesicles along cytoskeletal tracks (Apodaca 2001, Murray & Wolkoff 2003, Seabra & Coudrier 2004). The Syntaxin and SNARE-family of proteins tether incoming vesicles to target membranes and play an active role in membrane bilayer fusion (Ungermann & Langosch 2005).

However, the principal chief regulators of membrane trafficking in all cells are Rab-proteins belonging to the Ras-family of small GTPases. They function as molecular switches that exchange between GTP- and GDP-bound conformations (Deneka et al 2003, Gruenberg 2001, Pfeffer 2001, Zerial & McBride 2001). They can spatially and temporally control the recruitment of some the regulatory proteins described above to membrane subdomains. Thereby, the small GTPases confer identity to distinct membranes that act as donor or acceptor environments for cargo vesicles (Figure 6A). This assignment of domain identity ensures specificity and linearity in

endocytic trafficking. Some of the best-characterized Rab-proteins are Rab5, Rab7 and Rab11. Rab5 interacts with downstream effectors such as EEA-1 (Early Endosome Autoantigen-1) and Rabaptin-5, thereby regulating the formation and maturation of early endosomes after budding from the plasma membrane (Christoforidis et al 1999, Gaullier et al 1999, Simonsen et al 1998). Rab7 can mediate the sorting of endocytic cargo towards degradation in lysosomes by interacting with RILP (Rab-interacting lysosomal protein) (Cantalupo et al 2001). Rab11 is a marker for recycling endosomes, which act as transient way-stations for endocytic cargo to be recycled to the plasma membrane (Hoekstra et al 2004, Maxfield & McGraw 2004). Some biosynthetic cargo can also be delivered to the plasma membrane via first trafficking through Rab11 endosomes (Langevin et al 2005).

In recent years another main determinant of endocytic sorting specificity has been characterized; a protein-interaction network of eight proteins Sec3p, Sec5p, Sec6p, Sec8p, Sec10p, Sec15p, Exo70p and Exo84p was originally described in the budding yeast Saccharomyces cerevisiae to be essential for exocytosis (Lipschutz & Mostov 2002). These different proteins are now collectively called the exocyst. Some exocyst subunits localize to vesicles, others localize to the plasma membrane; interactions between the vesicle-bound and plasma membrane-bound exocyst-components are thought to mediate the polarized recruitment, docking and fusion of exocyst-marked vesicles (Figure 6B). In yeast, the exocyst provides a membrane patch at the growing daughter bud tip (TerBush et al 1996) and at the cytokinetic furrow (Fielding et al 2005) for the polarized delivery of cargo, driving active cell surface expansion during different stages of the cell cycle. It is now clear that exocyst function is highly conserved throughout evolution. In mammalian epithelial cells the exocyst is thought to mediate the polarized delivery of basolateral cargo to junctions from the Golgi and from recycling endosomes (Figure 6C) (Ang et al 2004, Grindstaff et al 1998, Yeaman et al 2004, Zhang et al 2004). The exocyst subunits may interact as different subcomplexes depending on tasks and context. Variable complex composition could increase the number of specific sorting events that the exocyst can faithfully negotiate (Lipschutz & Mostov 2002, Prigent et al 2003, Sommer et al 2005, Zajac et al 2005, Zhang et al 2004).

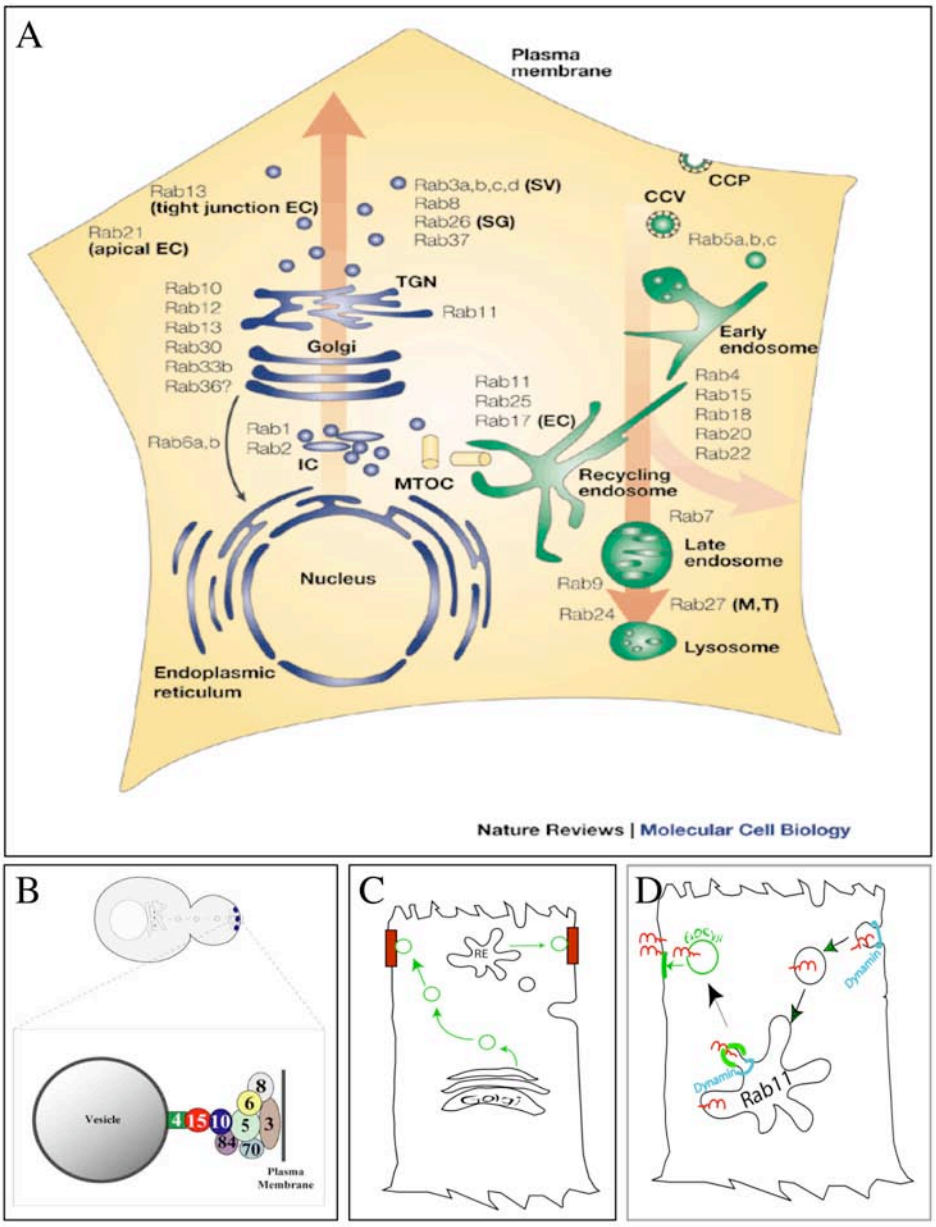

Figure 6 **Membrane traffic in eukaryotic cells**

(A) Map of intracellular localization of Rab proteins, (reproduced from (Zerial & McBride 2001) The map summarizes the intracellular localization of the different members of the Rab-family of proteins in mammalian cells. Different Rabs identify different membrane subdomains. (CCV, clathrin-coated vesicle; CCP, clathrin-coated pit; EC, epithelial cells; IC, ER–Golgi intermediate compartment; M, melanosomes; MTOC, microtubule-organizing centre; SG, secretory granules; SV, synaptic vesicles; T, T-cell granules; TGN, trans-Golgi network.) **(B)** The exocyst complex regulates polarized delivery of cargo. The exocyst consists of multiple subunits, some localizes to vesicles, others localizes to the plasma membrane. Interactions between the vesicle and plasma membrane bound exocyst-components are thought to mediate the recruitment, docking and fusion steps of the vesicles. In yeast budding, the exocyst provides a membrane patch at the growing bud tip for the polarized delivery of biosynthetic cargo (from http://www.umassmed.edu/celldynamics/faculty/munson.cfm). **(C)** In epithelial cells the exocyst is thought to mediate the polarized delivery of cargo to junctions from the Golgi and from recycling endosomes. **(D)** In MDCK cells, E-cadherin (red) enters the

endocytic route through various Rab5-dependent and independent routes. In MDCK cells, endocytic and biosynthetic E-cadherin traffics through the Rab11-positive recycling endosome on its way out to the plasma membrane. In the *Drosophila* thoracic epithelium and in MDCK cells, the exocyst complex is required to deliver E-cadherin derived from the recycling endosome to epithelial cell junctions. In many vertebrate and invertebrate cells, the GTPase Dynamin acts as a pinchase to pinch off a specific population of budding vesicles from the plasma membrane, the recycling endosome and the Golgi.

1.7. E-cadherin trafficking

Intriguingly, in the thoracic epithelium of *Drosophila*, E-cadherin delivery from Rab11 recycling endosomes to adherens junctions depends on exocyst components Sec5, Sec6 and Sec15 (Langevin et al 2005). Our work suggests that specifically this process of exocyst-targeted delivery of E-cadherin to junctions is essential for efficient modulation of adhesive contacts during the establishment of regular tissue geometry in the wing. A range of studies before us have established that the state of E-cadherin based adhesion between epithelial cells is based on a dynamic equilibrium between adhesive E-cadherin complexes at the cell surface and intracellular E-cadherin in endosomes and membrane compartments (Bryant & Stow 2004). E-cadherin endocytosis, degradation or recycling to junctions appears to be frequently utilized to modulate cell adhesion.

E-cadherin endocytosis in cultured epithelial cells correlates with downregulation of adhesion. The molecular machinery identified to facilitate E-cadherin endocytosis incorporate some more general membrane trafficking regulators such as Rab5 (Kamei et al 1999, Le et al 1999, Palacios et al 2005), the large GTPase pinchase Dynamin (Palacios et al 2002, Paterson et al 2003), the membrane coat-protein Clathrin (Ivanov et al 2004b, Palacios et al 2002), and a member of the ARF-family of GTPases Arf6 (Palacios et al 2001, Palacios et al 2002, Paterson et al 2003). Protein kinase C (Le et al 2002) and the small GTPases Rac1, Cdc42 and Rho1 (Kaibuchi et al 1999, Palacios et al 2002) are also implicated in the control of E-cadherin endocytosis. They are part of a complex signaling network at adherens junctions, which coordinates E-cadherin complex dissociation and actin dynamics during endocytosis. In general it emerged though that depending on epithelial context different players may be involved (compare Ivanov et al 2004b, Paterson et al 2003).

In many cell types, E-cadherin endocytosis takes place constitutively (Le et al 1999, Paterson et al 2003); but the rate of endocytosis appears to be upregulated in response to various

signals such as Calcium-depletion (Ivanov et al 2004a, Ivanov et al 2004b, Le et al 1999), Hepatocyte-growth factor/Met activation (Kamei et al 1999, Palacios et al 2001) and signaling by other receptor-tyrosine kinases (Daniel & Reynolds 1997). Endocytosis may also be triggered in response to signals such as ubiquitination by the Hakai E3-ubiquitin ligase; ubiquitination occurs as a consequence of Src-induced tyrosine phosphorylation in E-cadherin (Fujita et al 2002, Pece & Gutkind 2002). Importantly, ubiquitination of cell surface receptors is often associated with an enhanced rate of their endocytosis and subsequent degradation via the lysosome (Hicke & Riezman 1996, Riezman et al 1996) or the proteasome (Jeffers et al 1997). In addition to transcriptional suppression, Rab7-dependent lysosomal degradation of E-cadherin after endocytosis may indeed contribute to a permanent downregulation of E-cadherin based adhesion (Palacios et al 2005). However, it is not clear whether the often observed multiple mono-ubiquitination of cell surface proteins, per default, leads to degradation - as it is the case for poly-ubiquitinated proteins (multiple ubiquitins added to the same residue). Instead, after their endocytosis, cell surface receptors often become dissociated from their ligands in endosomes and are then recycled back to the cell surface via Rab11-recycling endosomes. A putative ubiquitination and de-ubiquitination cycle could bias the fate of mono-ubiquitinated cell surface protein towards recycling (for exampleNikko et al 2003). Consistent with this, the deubiquitination enzyme FAM interacts specifically with β-catenin and E-cadherin at multiple points of sorting to the plasma membrane (Murray et al 2004).

Unfortunately, also very little is known about E-cadherin trafficking to the cell surface. The cytoplasmic tail of E-cadherin contains a conserved dileucine motif, which ensures faithful targeting to the basolateral membrane in polarized cells (Miranda et al 2001). Delivery of E-cadherin may be enhanced by association with β-catenin at exit from the ER (Chen et al 1999). β-catenin is however not required for basolateral targeting (Miranda et al 2001). Endocytosed and newly synthezised E-cadherin traffics through the Rab11-positive recycling endosome on its way out to the cell surface (Lock & Stow 2005). As in the *Drosophila* thorax, delivery of E-cadherin to the junctions in mammalian cells depends on the exocyst complex (Yeaman et al 2004) and is positively regulated by the exocyst-stimulating GTPase Ral1 (Shipitsin & Feig 2004). Once E-cadherin is inserted into the membrane lateral clustering of transdimers, homophilic binding of E-cadherin at the neighboring cell and actin recruitment to the complex are components of a positive feedback loop that reinforces junctional assembly (reviewed in Braga 2002). Again, universal actin-regulators, such as Rac1 and Cdc42, and signaling molecules such as PKC are implicated to function in the formation of adherens junctions as well (Braga 2002, Le et al 2002).

2. Scope of the thesis

Despite the fact that regular epithelial geometry is a widespread universal phenomenon and closely linked to epithelial function only a few studies have attempted to describe, quantify and understand tissue topology (Honda et al 1982, Zallen & Zallen 2004). So far no molecular and cell biological mechanism has been implicated in the control of epithelial geometry. To start to address how cells form precise geometrical arrays within epithelia we choose to work in the developing wing of *Drosophila*. It provides an attractive genetic and cell biological system easy to access and manipulate; and it undergoes dramatic changes in cell packing towards a regular hexagonal array during pupal stages. Our first objective was to establish a method to describe and quantify cell packing during development. We opted for computer-aided automated analysis of microscopy images taken of wing epithelia at different development stages. Several parameters such as neighbor number and cell shape were to be documented and statistically evaluated (Section Results 3.1.-3.2.; Appendix II + III). To identify the cellular mechanism responsible for hexagonal packing of epithelial cells we wanted to interfere with hexagonally repacking by perturbing the machinery impinging on dynamic cell adhesion. Because endocytic trafficking of junctional components may contribute to disassembly and reassembly of adhesive contacts during morphogenesis we analyzed a series of different endocytic mutants for effects on cell adhesion and epithelial geometry (Section Results 3.3.-3.5.). Surprisingly, we found that PCP proteins have an essential role in generating orderly hexagonal packing of wing epithelial cells just prior to hair formation. (Section Results 3.6.-3.10.). We furthermore provide evidence for a molecular mechanism whereby the PCP pathway functions in hexagonal packing: the PCP protein Flamingo may be able bias E-cadherin delivery to specific junctions in the remodeling wing epithelium (Section Results 3.11.). To conclude, we explored how biasing endocytic trafficking may account for the function of PCP proteins in hair formation (Section Results 3.12.-3.16.) .

To date, no common cell biological mechanism has been proposed to explain the function of the planar cell polarity group of proteins in different tissues. Based on the work presented in this thesis we suggest that PCP proteins act to remodel adhesive contacts in the *Drosophila* wing

indicating that dynamic modulation of intercellular contacts may be a common feature of processes requiring the conserved planar polarity machinery. We furthermore propose that a universal molecular mechanism whereby the PCP pathway functions is to mediate polarization of membrane trafficking by regulating the exocyst complex - a currently unknown downstream effector of PCP signaling.

The work presented in this thesis was partially done in collaboration with Kurt Anderson. Eric Marois, Benjamin Dollet, Francois Graner and Suzanne Eaton have also contributed to this thesis as indicated in the text or figure legends.

3. Results

3.1. The wing epithelium becomes hexagonally packed shortly before hair formation

During pupal stages the wing epithelium undergoes dramatic changes in epithelial packing geometry (Figure 7A,B). At the prepupal-pupal moult, several hours before hair formation, cell shape and neighbor number are highly variable. Yet, at the time of hair formation epithelial cell packing is almost hexagonal, and cell shapes are much more isometric. This striking evolution of epithelial geometry is likely to involve highly complex cellular mechanisms responsible for sensing, regulating, mediating and coordinating changes in epithelial packing geometry, which we wanted to understand.

To study changes in epithelial packing, we developed an automated image analysis program in collaboration with Kurt Anderson using Definion's Cellenger software (see Materials and Methods). After staining developing wings for E-cadherin, we used the program to identify each cell, measure the length of each cell-cell contact, the total perimeter and area of each cell, and the number of its neighbors (Figure 7C-E). We also identified 3 and 4-cell vertices in the epithelium (Figure 7G). These parameters allowed us to quantify several aspects of packing geometry: perimeter and area reveal differences in the distribution of cell sizes; cell-cell contact length variation mirrors isometry of cell shape; the percentage of cells in an image with a specific number of neighbors describes the deviation of packing topology from hexagonal packing. Number of neighbors and vertex identity are related by Euler's formula (F+V-E=2), which describes the mathematical relationship between the total number of faces (F), vertices (V) and edges (E). The analysis was performed at larval and pre-pupal stages, and at 5 pupal time points beginning at the P2B stage of Waddington (Waddington 1941), and ending at the time of hair outgrowth (Figure 7F; see timeline in Table 1 on page 42).

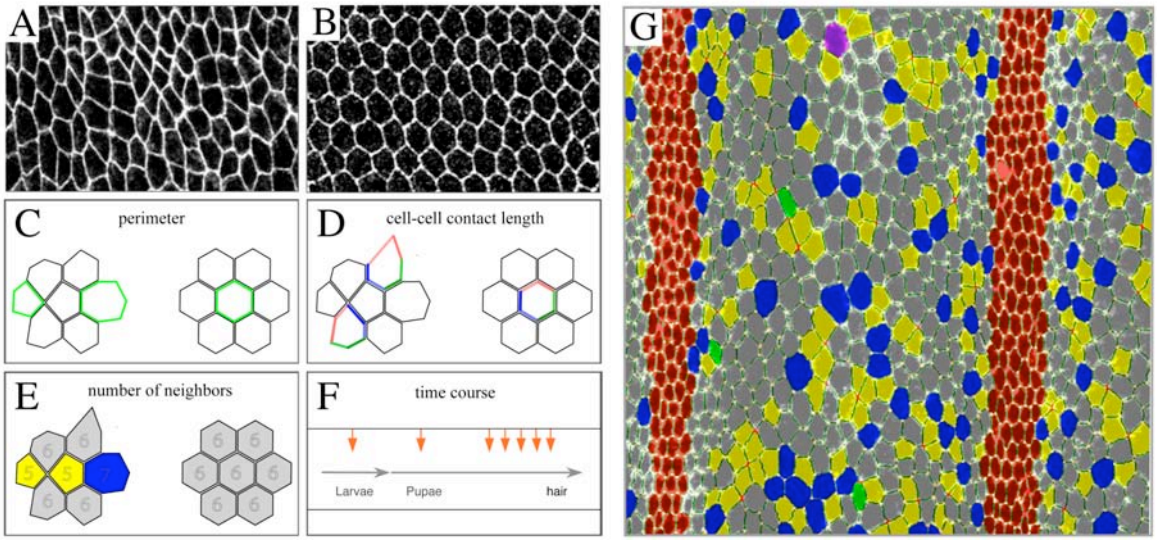

Figure 7 **Analysis of tissue geometry parameters using Cellenger Software**

(A) Irregular cell packing in the *Drosophila* wing epithelium at prepupal to pupal transition. **(B)** Hexagonal packing of the *Drosophila* wing epithelium at hair outgrowth. **(C)** Cell perimeter describes cell size. **(D)** Cell-cell contact length variation describes cell shape. The six sides of a regular hexagon are all of the same length (right); irregular polygons have higher contact length variation (left). **(E)** The neighbor number of a cell defines its polygon class (pentagons, hexagons, heptagons). Cells were color-coded according to their respective polygon class for better visualization of polygon identity. **(F)** Cellenger analysis was performed at larval, prepupal and five evenly spaced time points from early pupal development to hair outgrowth. **(G)** Image output from Cellenger program: spring green, tetragons; yellow, pentagons; grey, hexagons; blue, heptagons; purple, octagons; red cells, vein; dark green, individual cell edges; orange vertex, three-way vertex; red vertex, four-way vertex.

Figures 8 and 9 show processed images of distal (Figure 8), anterior and posterior (Figure 9) wing regions at different developmental stages in which tetragonal, pentagonal, hexagonal, heptagonal and octagonal cells are indicated by different colors. For each developmental stage intervein regions of 3 dorsal wing surface were quantified and averaged to generate the plots shown in Figure 8 and 9 (see also Appendix II + III).

Wing epithelial cells are irregularly packed throughout larval and pre-pupal development (Figure 8A,B). Less than half the cells are hexagonal, and of non-hexagonal cells the majority are pentagons; on average, each cell has less than 6 (5.55) neighbors. The wing epithelium is repacked into a quasi-hexagonal array beginning shortly after the prepupal-pupal moult, and ending just before hair formation. Figure 8C-G show regions surrounding longitudinal vein 3 (L3, see cartoon). Results for intervein cells are quantified in Figure 8I. Similar repacking occurs in anterior and posterior regions of the wing (Figure 9). The increase in hexagons occurs mainly at the expense of pentagons, although smaller decreases in the number of 4,7 and 8-sided cells occur as well (Figure 8I; Figure 9G,H).

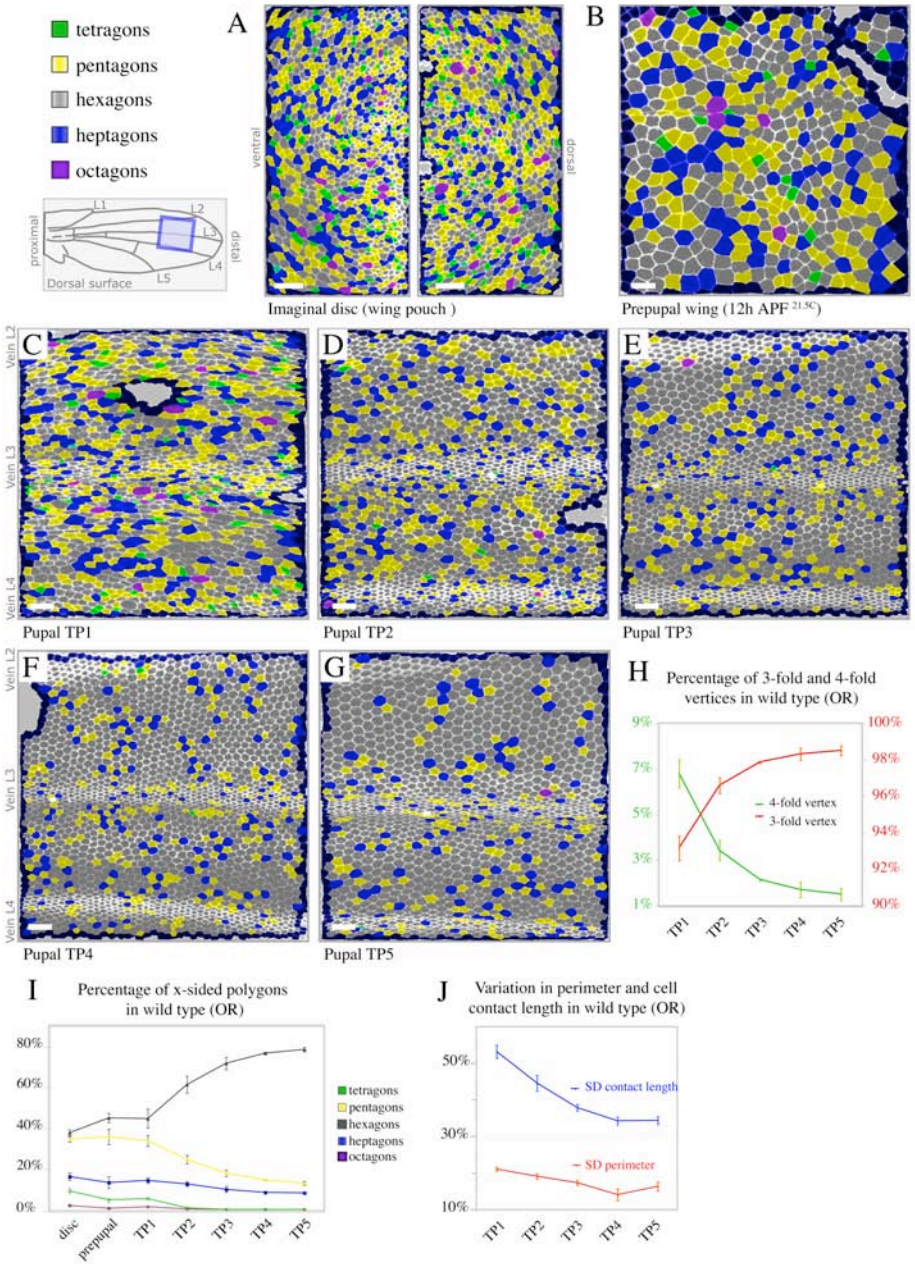

Figure 8 Packing geometry of wild type wing epithelial cells during development I

The wing cartoon highlights the distal region of the wing between vein L2 and L4 shown in B-G. **(A-G)** Images of E-cadherin-stained wing tissues were analyzed using Cellenger automated image analysis software. Cells in images of larval (A) and prepupal (B) stages and at 5 different pupal times (TP1-TP5) from Waddington stage P2B to P2C (C-G) were color-coded for neighbor number. **(H)** Percentage of 3-fold and 4-fold vertices during pupal stages TP1-TP5. Consistent with Euler's formula F+V-E=2 (faces (F), vertices (V), edges (E)) the percent of 3-fold vertices increases as the epithelium becomes more hexagonal. **(I)** Percentage of cells with 4,5,6,7 or 8 neighbors (color-coded as indicated) at different developmental times. **(J)** Variability in total cell perimeter and individual cell edge length decreases between TP1 and TP4. Standard deviations are expressed as a percentage of the average perimeter (or average cell edge length) to control for cell size differences. Intervein regions, amounting to a total of approximately 2500 cells per data point, were averaged to obtain the data in H-J. Only intervein cells on the dorsal side of the wing surface were analyzed.

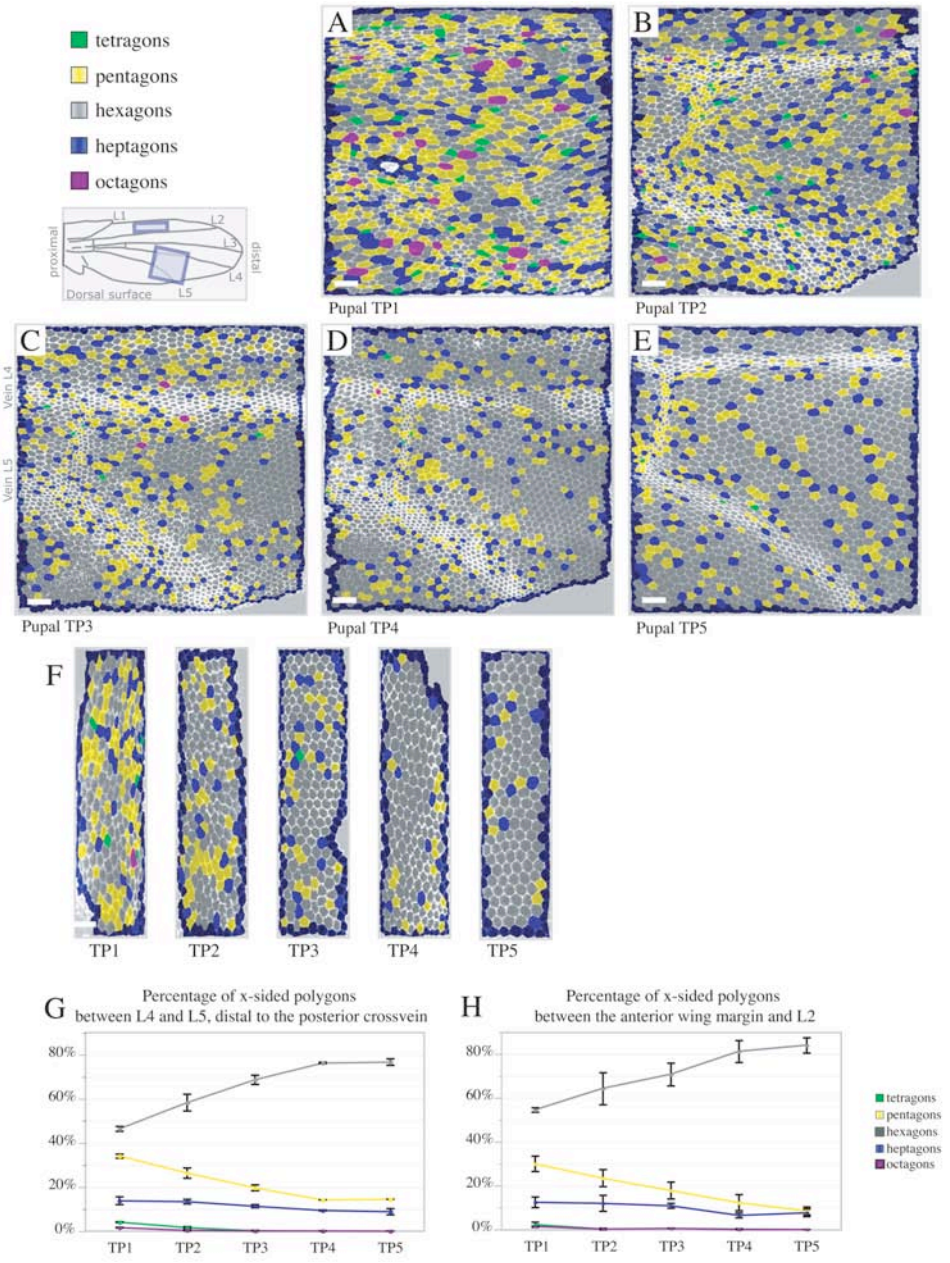

Figure 9 **Packing geometry of wild type wing epithelial cells during development II**

The wing cartoon highlights the anterior and posterior region of the wing shown in (A-F). **(A-E)** Images of the region distal to the posterior crossvein analyzed by Cellenger and color-coded for polygon identity as indicated. Representative examples of Time Point 1 (A) to Time Point 5 (E) are shown. **(F)** Images of the region between the anterior wing margin and L2 analyzed by Cellenger software and color-coded for polygon identity as indicated. Representative examples of Time Point 1 to Time Point 5 are shown. **(G)** Percentage of x-sided polygons between L4 and L5 distal to the posterior crossvein during pupal development (TP1-TP5). **(H)** Percentage of x-sided polygons between the anterior wing margin and L2. Graphs are color-coded for polygon identity as before. Only intervein cells on the dorsal side of the wing surface were analyzed.

Consistent with Euler's formula (Figure 8H) the number of four cell vertices decreases and the number of three cell vertices increases as the average neighbor number grows from 5.55 to 5.96. This means that there is a net increase in the number of cell contacts.

Regularization of epithelial packing is also reflected in decreased variability of area (not shown) and perimeter (Figure 8J) of wing cells. Variation in individual cell-cell contact lengths (Figure 8J) decreases even more than that of cell perimeter, consistent with junctional material becoming more symmetrically distributed between neighbors. Although the absolute number of cell contacts increases during hexagonal packing, total perimeter is minimized by hexagonal packing, suggesting that total junctional material need not increase. By the time hairs form, intervein regions of the wing consist of 78% hexagons. These are arrayed in neat rows of coordinate orientation, occasionally interrupted by pentagons and heptagons.

According to the honeycomb conjecture hexagonal packing of polygons is the 'minimal energy configuration' were perimeter and surface energy are optimally minimized (Hales, 2000), which should be advantageous to epithelial cells. The data presented above, however, shows that the generation of a hexagonally packed array of epithelial cells is a discrete developmental event and not a "ground state" of epithelia. Intriguingly, similar regularization of cell packing occurs in the moth wing before scale formation (Nardi & Magee-Adams 1986).

3.2. Intercellular junctions shrink and grow during hexagonal repacking

The transition from irregular to quasi-hexagonal packing in the pupal wing epithelium must involve extensive remodeling of intercellular contacts to accommodate the net increase in the number of cell contacts as the average neighbor number grows from 5.55 to 5.96.

To study how cell contacts were remodeled, we performed live confocal imaging on pupal wings expressing E-cadherin:GFP (Oda & Tsukita 2001) (Figure 10A). We often observed intercellular junctions shrinking to form a 4-way vertex. 4-way vertices then resolved into a pair of 3-way vertices (colored cell boundaries in Figure 10A, schematized in Figure 11), sometimes by re-expanding the original cell boundary (green boundary between cells D and D' in Figure 10A), or alternatively by assembling a junction between different cells in the perpendicular direction (red boundary between A and A', turquoise boundary between C and C', and pink boundary between B and B').

These events resemble the junctional remodeling observed during *Drosophila* embryonic convergent extension (Bertet et al 2004, Oda & Tsukita 1999, Zallen & Zallen 2004). However, they are not as strongly directional. This is consistent with the absence of dramatic concurrent changes in the proportions of the wing epithelium.

It is clear that this type of junctional remodeling is able to mediate the changes in packing topology that are required to achieve hexagonal packing (Figure 11).

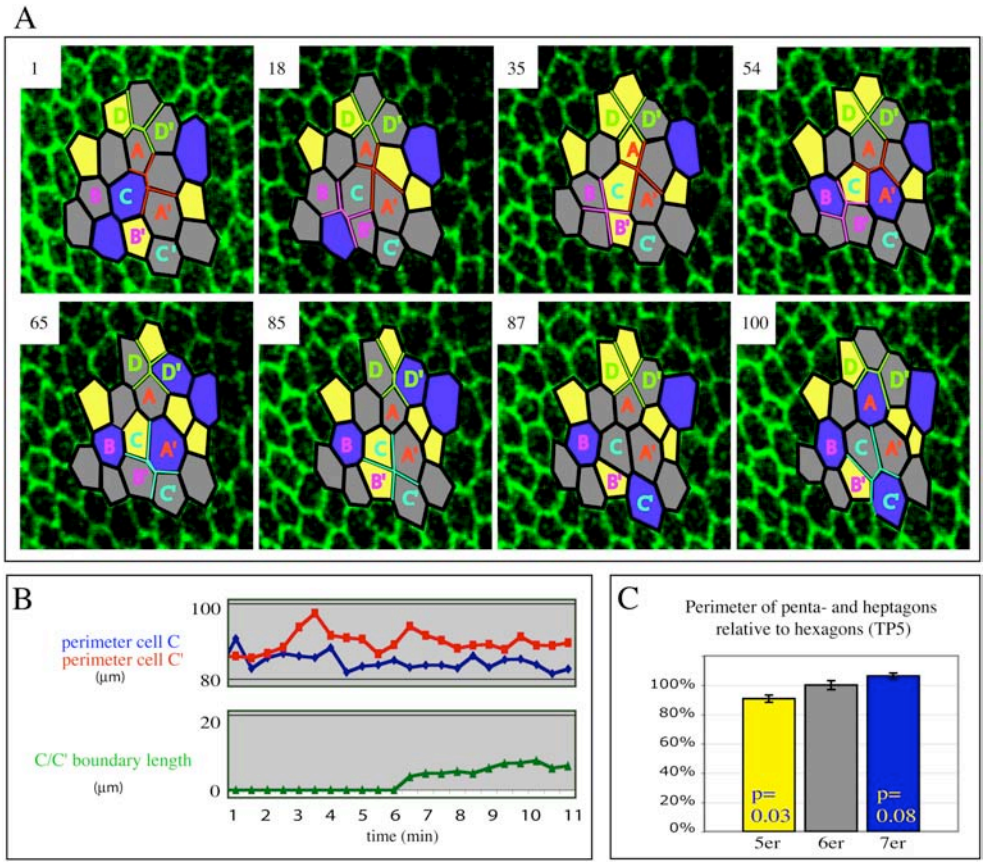

Figure 10 Junctions are dynamically remodeled during hexagonal repacking

(A) Single images from time-lapse series of stage P2B pupal wings expressing E-cadherin:GFP under the control of a tubulin promoter. Frame numbers (separated by 30 seconds) are indicated in the upper left corner of each image. Overlaid on each frame is a color-coded cartoon of the region undergoing junction remodeling. Blue indicates heptagons, grey hexagons and yellow pentagons. Cells and junctions that undergo remodeling are highlighted in different colors. **(B)** Changes in the length of the perimeter of cells C and C', and the growing boundary between them. **(C)** Average perimeters of pentagonal, hexagonal and heptagonal cells. In theory, a pentagon may have 5/6 or 83.3% the perimeter of a hexagon. On average, however, pentagon perimeters are 91% of that of hexagons. Equally, heptagons have a perimeter of 106% of hexagons, compared to a theoretical value of 116.6% (7/6 of hexagon perimeter). Therefore, new cell contacts may utilize material derived from contacts with other cells. P-values indicate the significance in perimeter difference of pentagons and heptagons to hexagons.

Assembly of new cell contacts takes place within 6-15 minutes – much more rapidly than junctions assemble de novo in embryonic epithelia (Tepass & Hartenstein 1994). Thus, we wondered whether the junctional material that accumulates at these boundaries might derive from pre-existing cell contacts rather than the biosynthetic pathway. To approach this question, we asked whether growth of a new cell boundary added to the total cellular perimeter. Measuring the perimeter of cells C and C' during the elongation of the boundary between them (Figure 10B) revealed that the length of the cell perimeter fluctuates over a period of several minutes. These fluctuations do not correlate with development of the new cell boundary, however. Consistent with this, average perimeter of 5, 6 and 7-sided cells did not differ by the length of one cell boundary, although we found small but significant differences between them (Figure 10C). These data suggest that formation of new cell contacts may utilize material derived from contacts with other cells.

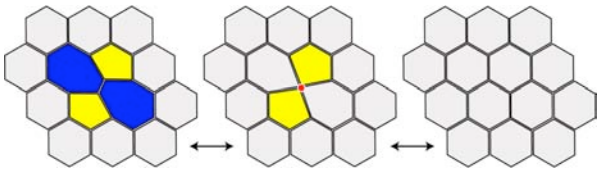

Figure 11 Local cell rearrangements mediate hexagonal packing

Two cells shrink the junction between them to a four-way vertex, thereby losing a side each. The four-way vertex is then used to assemble a new junction, which will lie perpendicular to the original junction; thereby two cells gain a side each. Local cell rearrangements by junctional remodeling are reversible at four-way vertices: the point of decision between which two opposite cells to expand the new junction.

3.3. Dynamin is needed for normal E-cadherin distribution during junction remodeling

How might E-cadherin or other junctional material be added to a growing boundary (Figure 12)? In other epithelia, E-cadherin is dynamically endocytosed and recycled to modulate cell adhesion (Bryant & Stow 2004). To test whether this might happen in the pupal wing, we used the temperature sensitive *shibire* (*shi*) mutation of Dynamin (Figure 6D). Dynamin is required for scission of endocytic vesicles (Sever 2002), and vesicles formed from Rab11 recycling endosomes (Pelissier et al 2003, van Dam & Stoorvogel 2002). 30-45 minutes after shifting mutant animals to the restrictive temperature of 34ºC, gaps form in junctional E-cadherin in *shibire* mutant wings that are not found in wild type control wings (Figure 13A,B), even after 3 hours of temperature shift (see Figure 20A). The gaps form exclusively in intervein regions, and occur primarily at or adjacent to vertices.

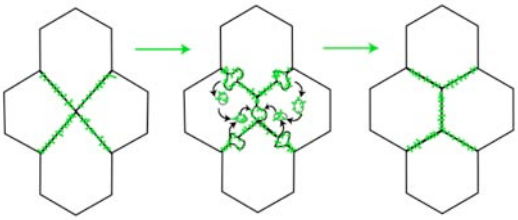

Figure 12 Endocytosis and recycling of E-cadherin may driving junctional remodeling

Cells may disassemble shrinking boundaries by endocytosis of junctional components and reassemble growing boundaries by recycling of endocytic junctional components towards growing boundaries. E-cadherin (green) is one of the main cell-cell adhesion molecules in epithelia and its endocytosis and recycling is known to be important for modulating intra-epithelial adhesion.

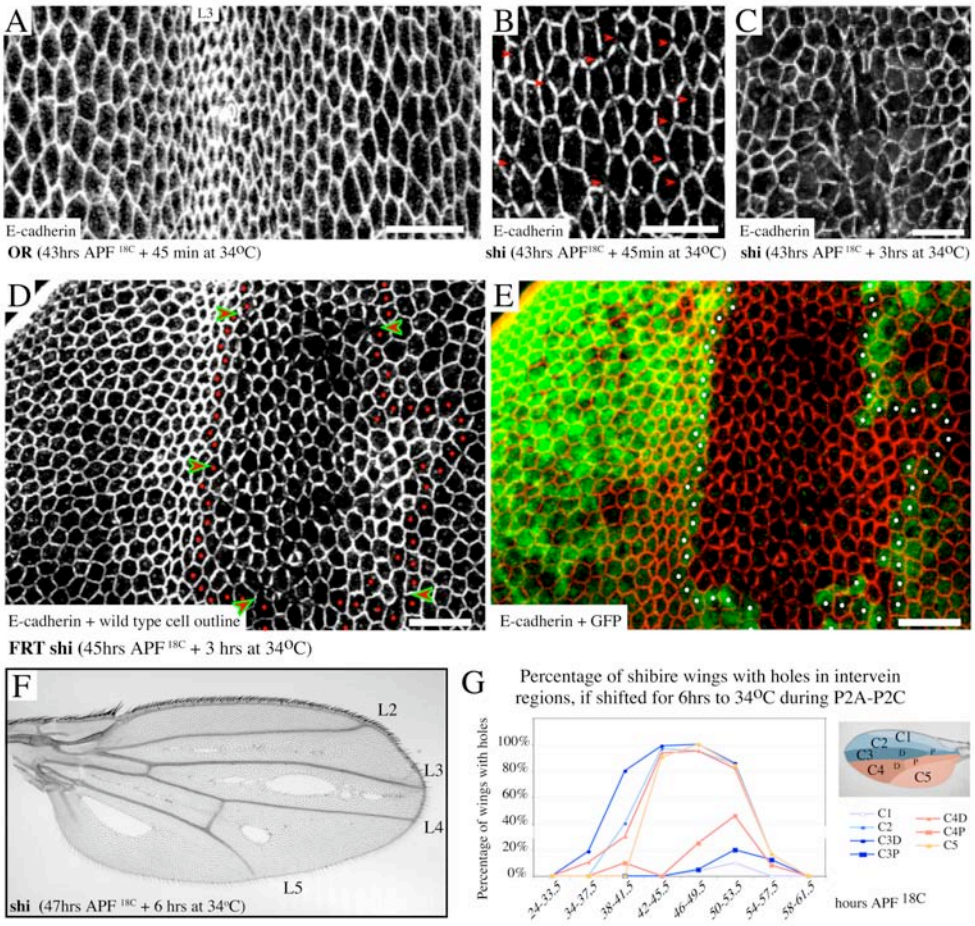

Figure 13 Dynamin is required for E-cadherin trafficking during junctional remodeling

(A-C) are projections of E-cadherin stained wings between veins L3 and L4 that include all sections with junctional E-cadherin. **(A)** Intervein regions surrounding L3 of a wild type wing stained for E-cadherin after a 45 minute-shift to 34°C starting at stage P2B. The row of smaller cells stained more intensely for E-cadherin in the center of the image

corresponds to vein L3. **(B)** *Shibire* pupal wing stained for E-cadherin after a 45 min shift to 34°C starting in stage P2B. Red arrows indicate gaps in E-cadherin. **(C)** *Shibire* wing stained for E-cadherin after a shift for 3 hours to 34ºC starting in P2B. **(D, E)** A wing containing a *shibire* mutant clone stained for E-cadherin (D, red in E). The clone is marked by the absence of GFP (green in E) and is outlined by dots in the last shell of wild type cells. Arrows in (D) point to junctions between wild type and *shibire* mutant cells that have gaps in E-cadherin localization. **(F)** A *shibire* adult wing shifted for 6 hours to 34°C starting at P2B. **(G)** Quantification of hole formation in different regions of *shibire* mutant wings in response to a 6-hour shift to 34°C at different times during early pupal development (210 wings analyzed). The x-axis indicates the time APF at 18°C at which shifts were started. The y-axis shows the percentage of wings with holes in the intervein compartments as indicated in the cartoon. P indicates the compartment proximal to the crossvein, and D the compartment distal to the crossvein.

Similar results are obtained in clones of *shibire* mutant cells (Figure 13D,E). This suggests that loss of E-cadherin in *shibire* cells is autonomous to the dorsal and the ventral wing surface. Interestingly, gaps were also observed between wild type and *shibire* mutant cells (arrows in Figure 13D) indicating the requirement for two neighboring cells to possess functional Dynamin for normal E-cadherin localization between them.

After 3 hours at 34ºC, *shibire* mutant cells show even larger gaps in E-cadherin (Figure 13C). By 6 hours, cell-free areas are seen in the inter-vein region by E-cadherin staining (not shown). After these animals are restored to the permissive temperature of 18ºC, emerging adults have holes in wing intervein regions (Figure 13F). Development of holes in intervein regions where E-cadherin gaps form suggests that loss of junctional proteins disturbs epithelial integrity.

To ask whether only E-cadherin depends on Dynamin for proper localization during remodeling, we examined the behavior of different junctional proteins in *shibire* mutant tissue. Armadillo, another adherens junction protein, is lost from the cortex where E-cadherin gaps form (Figure 14A,B). In contrast, the septate junction protein Coracle (Figure 14C-F) and basolaterally localized CD2:GFP and gpi:GFP (not shown) were undisturbed by loss of Dynamin. These data suggest that Dynamin is required to maintain uniform localization of adherens junction, but not septate junction or basolateral proteins, during repacking.

Dynamin function is required specifically during pupal stages to maintain E-cadherin at the cortex; no change in E-cadherin localization is observed when temperature shifts are performed on third instar larvae (Figure 15D,E), even for longer times. Loss of E-cadherin is not a consequence of cell death; E-cadherin is lost before Caspase is found in the nucleus (Figure 15C-E).

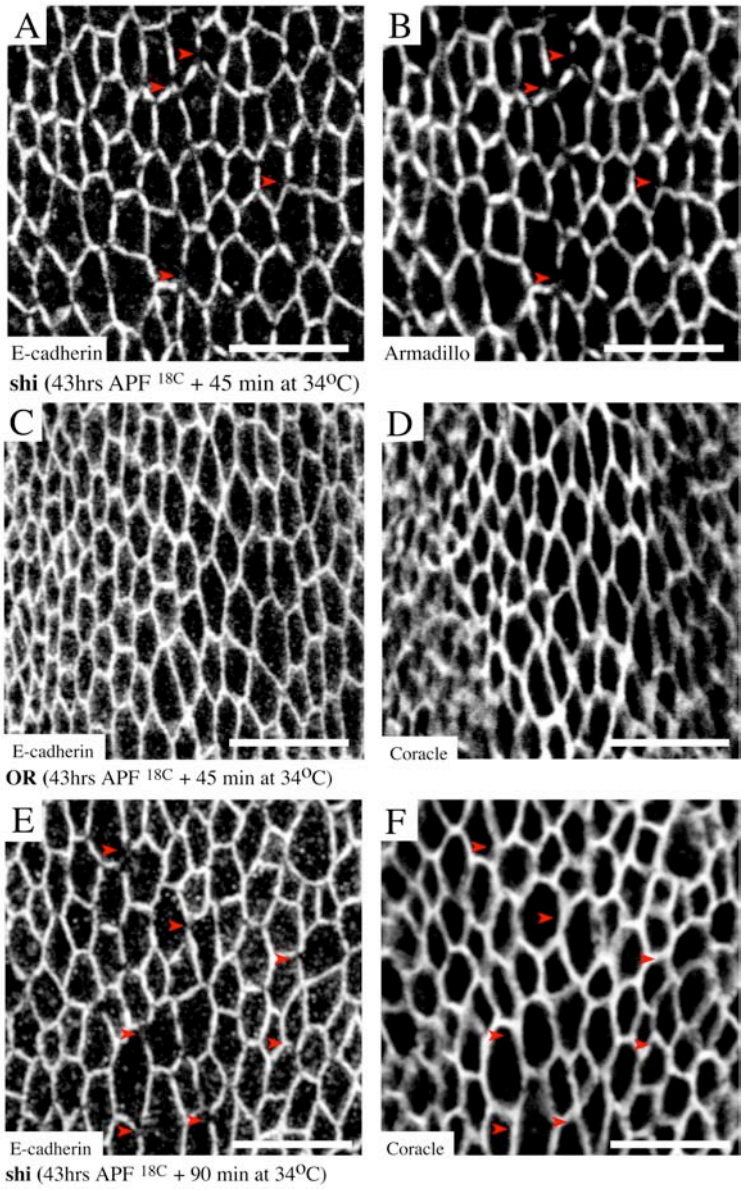

Figure 14 **Dynamin function is not required for septate junction integrity**

(A-C,E) are projections of sections containing staining for adherens junction markers. (D, E) are projections of the first 5 section containing staining for the septate junction marker Coracle. **(A, B)** *Shibire* pupal wing stained for E-cadherin (A) and Armadillo (B) after a 45 minute shift to 34°C starting in stage P2B. Red arrows indicate gaps in both E-cadherin and Armadillo. **(C, D)** A wild type wing stained for E-cadherin after a 45 minute shift to 34°C starting at stage P2B stained for E-cadherin (C) and Coracle (D). **(E, F)** A *shibire* mutant wing shifted to 34ºC for 90 minutes and stained for E-cadherin (E) and Coracle (F). Red arrows indicate gaps in E-cadherin. In contrast, no gaps in Coracle staining were observed.

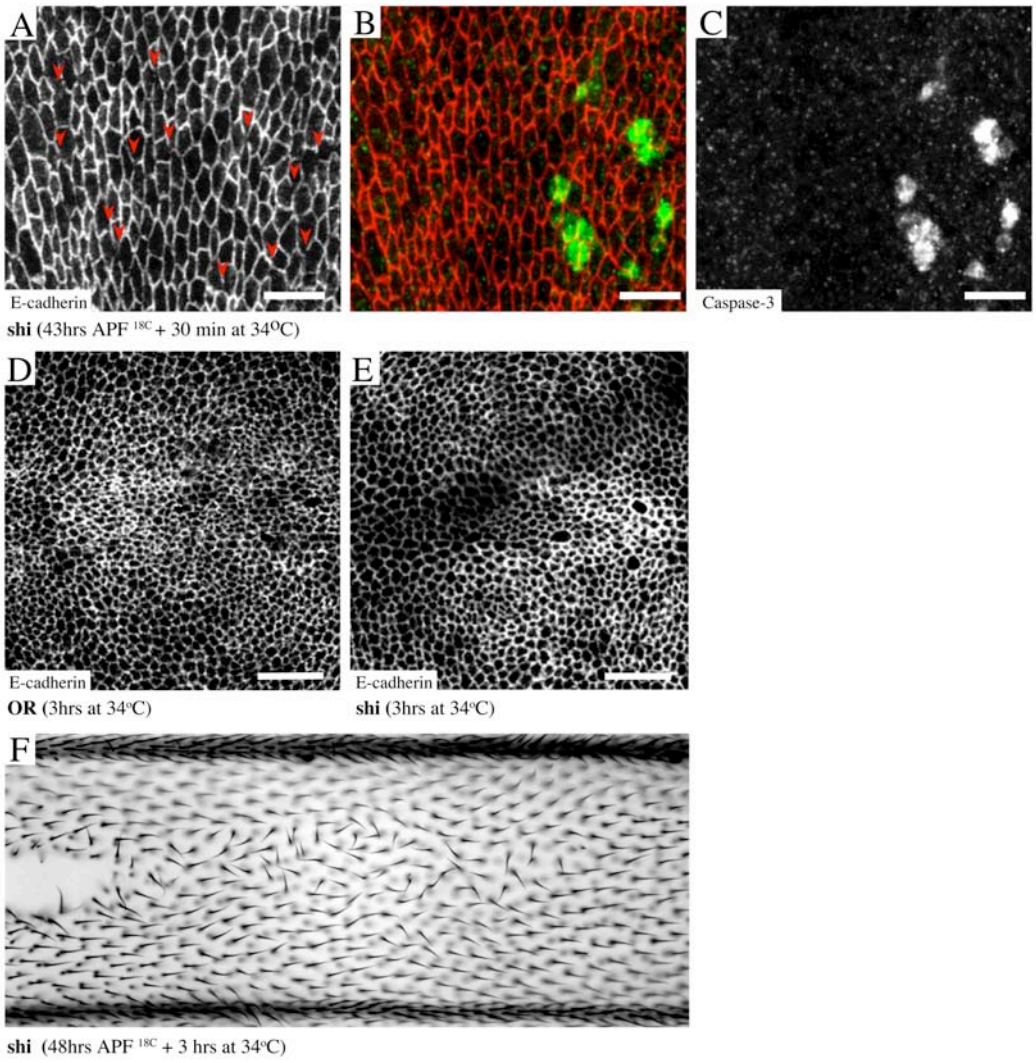

Figure 15 E-cadherin gaps are not due to cell death

(A-C) A *shibire* pupal wing shifted at P2B for 30 minutes to 34ºC stained for E-cadherin (A, red in B) and activated Caspase-3 (C, green in B). Red arrows indicate gaps in junctional E-cadherin. Overlay of E-cadherin and activated Caspase shows that cells form E-cadherin gaps before activated Caspase accumulates in the nucleus. **(D)** A wild type wing imaginal disc stained for E-cadherin after a 3hrs shift to 34°C. **(E)** A *shibire* mutant wing imaginal disc stained for E-cadherin after a 3hrs shift to 34°C. **(F)** A *shibire* adult wing shifted for 3 hours to 34°C starting at P2B. Hairs next to vein cells point into wild type direction.

To precisely define the developmental stages at which Dynamin was required to maintain E-cadherin mediated epithelial integrity, we systematically shifted *shibire* mutants to 34ºC during a sliding 6-hour window starting just after pupariation, and ending after hair formation. We quantified frequency and placement of holes in the adult wing as a read-out for loss of E-cadherin mediated adhesion because antibody penetration is prevented by cuticle throughout much of pupal

development. Although we observed a variety of phenotypes (summarized in Table 1), only temperature shifts initiated between P2A and mid-P2C (before hair formation) cause holes in the wing (Figure 13G). These data show epithelial repacking is temporally coincident with the requirement for Dynamin.

We noticed that, when Dynamin function was removed for 3 rather than 6 hours, holes formed less frequently and were replaced in identical positions by mispolarized wing hairs (Figure 15F). The window in which hexagonal packing by junctional remodeling occurs corresponds precisely to the period in which Frizzled function is required for normal hair polarization (Adler et al 1994). This observation suggests that the mechanisms controlling epithelial cell packing and hair polarization might be related.

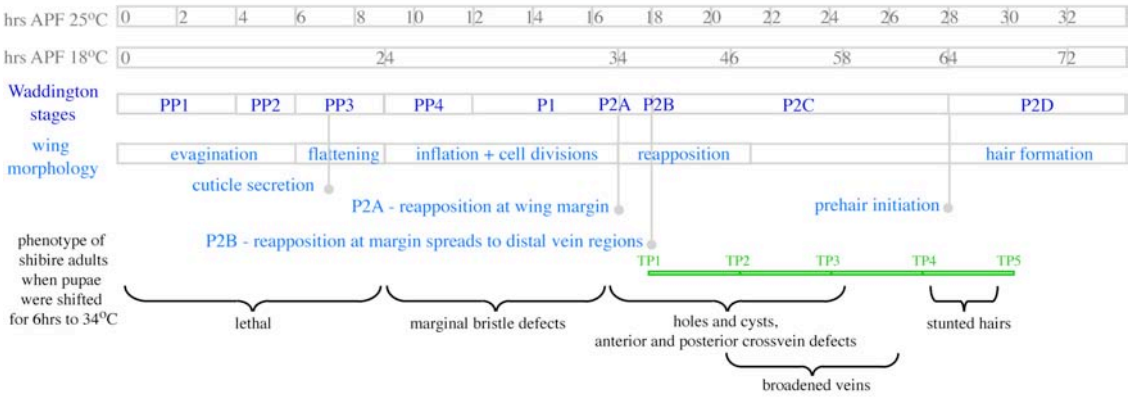

Table 1 Waddington stages of pupal wing development

Waddington's stages (dark blue) are outlined below the times that they occur at 18°C or 25°C temperatures (grey). Post-larval development is divided into pre-pupal (PP) and pupal (P) stages, separated by a molt. Landmark events in wing morphogenesis are indicated in light blue. Phenotypes caused by starting a 6 hours shift of *shibire* mutants to 34°C at different developmental stages are indicated in black. TP1-TP5 (green) indicate the times chosen for pupal packing analysis. APF = After Puparium Formation. OR = Oregon R, Wild type.

3.4. Rab11 and the exocyst are needed for normal E-cadherin distribution during junctional remodeling

To provide evidence that gaps of E-cadherin in *shibire* wing tissue are indeed due to a failure of endocytic function, we wanted to confirm that E-cadherin enters intracellular traffic at the time of hexagonal repacking. To this end, we stained E-cadherin:GFP-expressing pupal wings (stage P2B) with FM4-64. FM4-64 labels the plasma membrane and endosomes that form after its

addition. The majority of pupal wing cells contain multiple internal spots of E-cadherin:GFP that colocalize with FM4-64 after 15-30 minutes (Figure 16A-C). Thus, E-cadherin is actively endocytosed during repacking.

To ask which type of endosomes contained E-cadherin, we used flies that ubiquitously expressed Rab11:YFP or Rab5:CFP at low levels under the control of the tubulin promoter (Marois et al 2006). Rab11 labels recycling endosomes, and Rab5 marks early endosomes (Zerial & McBride 2001). E-cadherin was observed in both types of endosomes (Figure 16D-I), supporting the idea that it is endocytosed and recycled.

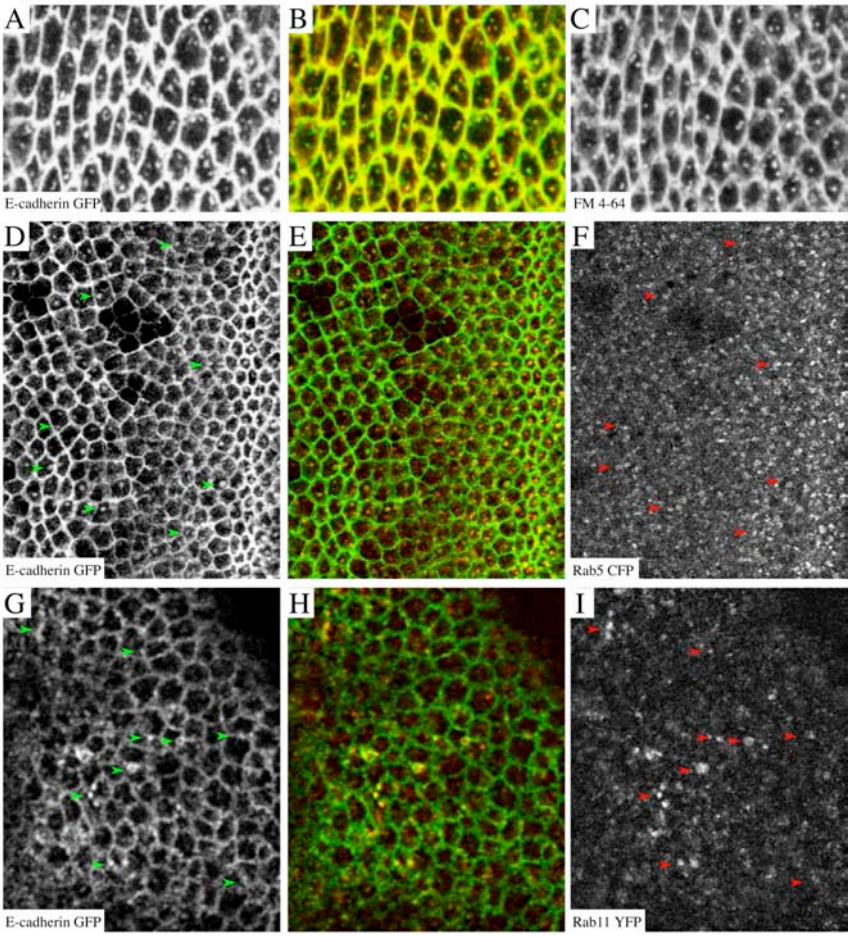

Figure 16 E-cadherin undergoes endocytic trafficking in *Drosophila* wing cells

(A-C) Image from a time-lapse movie of stage P2B pupal wings expressing E-cadherin:GFP (A, green in B) that were incubated with the membrane dye FM4-64 (C, red in B) for 30 min. E-cadherin:GFP strongly colocalizes with FM4-64 in a recently endocytosed intracellular compartment (B). **(D-E)** Image from a time-lapse movie of stage P2B pupal wings expressing E-cadherin:GFP (A, green in B) and Rab5:CFP (C, red in B). E-cadherin:GFP strongly colocalizes with the early endosome marker Rab5 in intracellular punctae (arrows). **(G-I)** Image from a time-lapse movie of a wing imaginal disc expressing E-cadherin:GFP (A, green in B) and Rab11:YFP (C, red in B). E-cadherin:GFP localizes to a compartment labeled by the recycling endosome marker Rab11 (arrows).

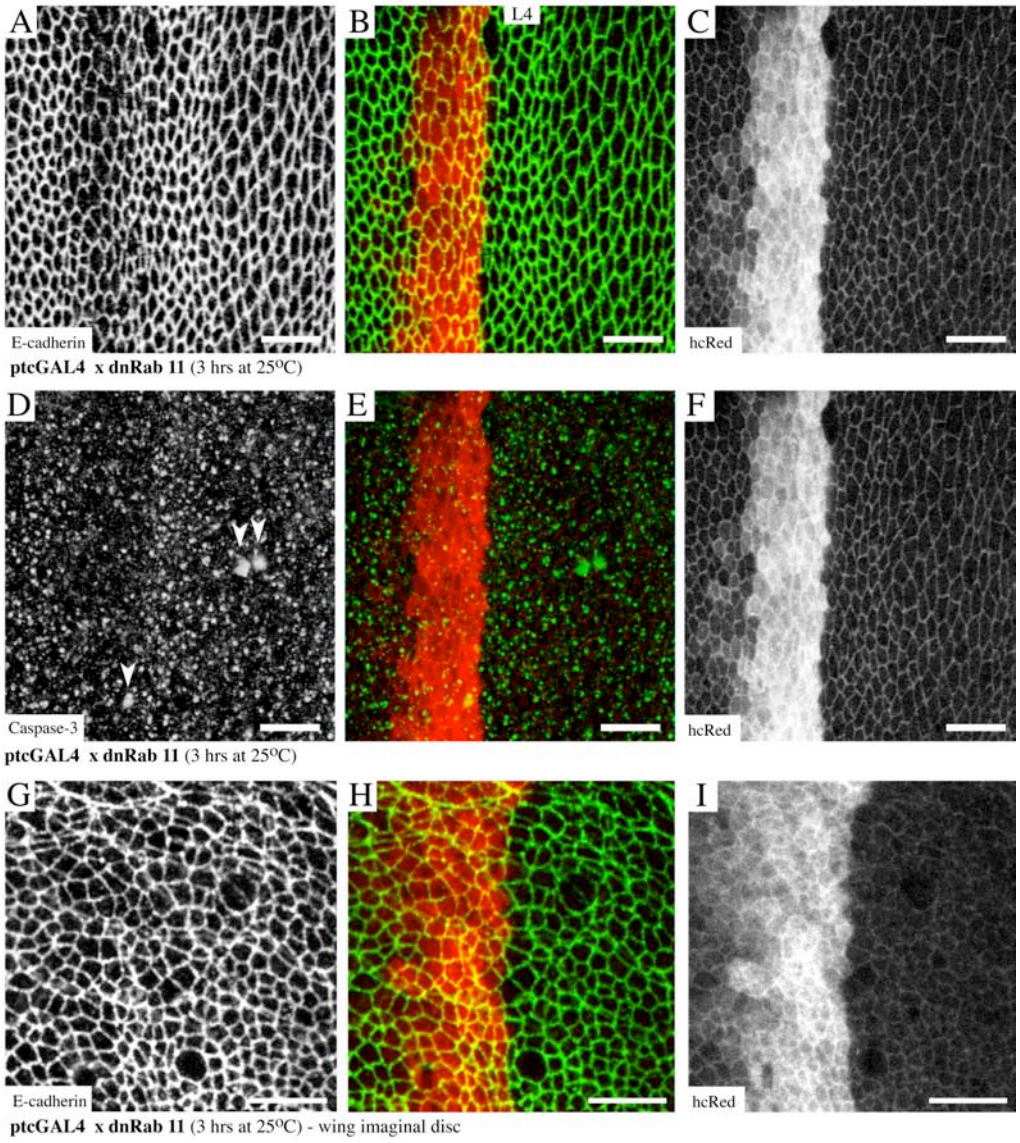

Figure 17 Rab11 is required for E-Cadherin trafficking during junctional remodeling

(A-C) depicts a stage P2B pupal wing that has expressed dominant-negative Rab11SN for 3 hours. Rab11SN is expressed using the pUHR vector (Marois et al 2006) in which expression can be initiated after excision of an HcRed containing FLP cassette between the UAS promoter and the cDNA. E-cadherin (A, green in B) begins to disappear from cell boundaries of Rab11SN-expressing cells (residual HcRed fluorescence in C, red in B). **(D-F)** show the same wing depicted in (A-C) imaged for HcRed fluorescence, (F, red in E) and activated Caspase staining (D, green in E). Activated Caspase is found in the nuclei of three cells (indicated by arrowheads), only one of which is inside the dnRab11 expression domain. **(G-I)** show a third instar larval wing disc that has expressed dominant-negative Rab11SN in the stripe of HcRed-expressing cells shown in (I, red in H) for 3 hours. E-Cadherin staining (G, green in H) is not different in dnRab11SN-expressing and in wild type cells.

In MDCK cells, E-cadherin is delivered through Rab11 endosomes (Lock & Stow 2005). To ask whether this occurs in the wing, we disturbed Rab11 function by short-term expression of a dominant negative Rab11SN construct (Marois et al 2006). 3 hours after initiating Rab11SN expression, E-cadherin begins to be lost from the junctional region – a phenotype similar to that of the *shibire* mutant (Figure 17A-C). These cells are not apoptotic (Figure 17D-F). No gaps form when Rab11SN is expressed for similar times in larval wing discs (Figure 17G-I). Thus, Rab11 is required to deliver E-cadherin to junctions, and this requirement is acute during epithelial repacking. Loss of junctional E-cadherin in *dynamin* mutant cells may reflect Dynamin's function at Rab11 endosomes. Consequently, loss of junctional E-cadherin in *dynamin* and Rab11 mutant cells may be due to the failure to deliver E-cadherin from recycling endosomes to growing boundaries during junctional remodeling and hexagonal packing (Figure 19).

The exocyst is a multiprotein complex that mediates polarized membrane delivery from recycling endosomes and from the Golgi in many different cell types (Lipschutz & Mostov 2002, Prigent et al 2003, Sommer et al 2005, Zhang et al 2004). In the Drosophila thorax, E-Cadherin delivery from recycling endosomes to the zonula adherens depends on exocyst components (Langevin et al 2005). To test whether E-cadherin was recycled via the exocyst during repacking in the wing, we utilized a mutation in Sec5 (*sec5*^{E13}) that has been suggested to preferentially perturb recycling (Sommer et al 2005). E-cadherin accumulates in internal vesicles and along the plasma membrane in *sec5*^{E13} mutant cells (Figure 18). Accumulation of internal vesicles suggests that delivery of E-cadherin is slowed. We do not know whether higher levels of peripheral E-cadherin staining reflect accumulated unfused vesicles, or whether Sec5 may also function at some other step in E-cadherin trafficking (Figure19).

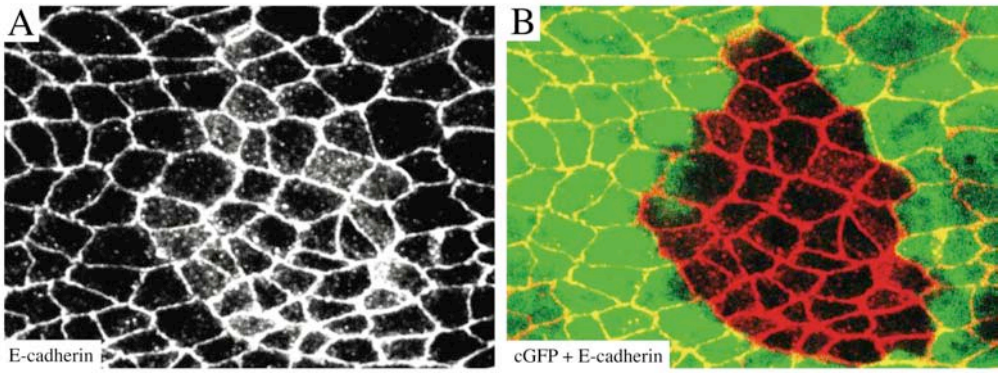

Figure 18 The exocyst complex is required for E-cadherin trafficking

(A,B) *Sec5*^{E13} clone stained for E-cadherin (A, red in B) and marked by absence of GFP (green in B). E-cadherin accumulates in internal vesicles and at cell junctions in mutant tissue.

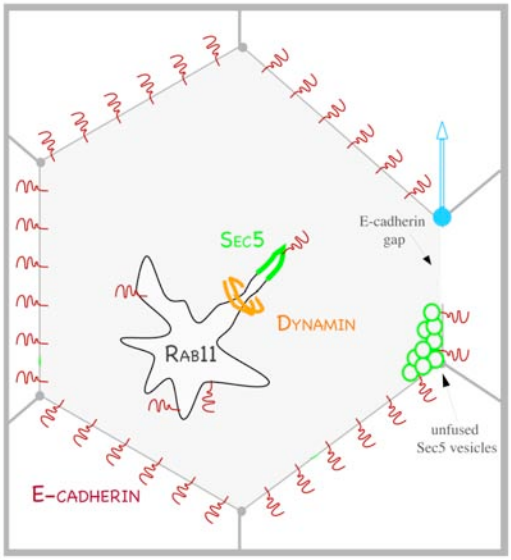

Figure 19 A failure to recycle E-cadherin may cause gaps in E-cadherin

Rab11 is required for E-cadherin recycling to the plasma membrane and Dynamin is required to pinch off vesicles from recycling endosomes. If, in *shibire* or Rab11 mutant tissue, delivery of E-cadherin to expanding boundaries (blue arrow) fails then gaps in E-cadherin may expected. The exocyst is required for delivery of E-cadherin from the recycling endosome to junctions and, later, potentially for the fusion of vesicles at the plasma membrane. In Sec5 mutant cells E-cadherin may be either retained in internal vesicles or in unfused vesicles at the plasma membrane.

3.5. Hexagonal packing is disturbed by inhibiting Dynamin function or stabilizing E-Cadherin contacts

To ask whether perturbing endocytosis and recycling caused defective cell packing by interfering with junctional remodeling during hexagonal repacking, we analyzed *shibire* mutant wings shortly after shift to the restrictive temperature. Compared with wild type shifted to the same temperature, *shibire* tissue was less hexagonal with higher variability in the length of individual cell contacts (Figure 20A-C). This is consistent with the possibility that Dynamin-dependent recycling of junctional components is needed to remodel and expand growing junctions and to achieve hexagonal packing. However, packing may have been perturbed by some other Dynamin-dependent process.

To test whether turnover of E-cadherin itself was required for hexagonal packing, we induced expression of an E-cadherin:α-Catenin fusion protein (Dumstrei et al., 2002) at the time of repacking using the GAL4/GAL80 system (McGuire et al 2004). A similar vertebrate construct is

not regulated by α-catenin (Figure 20D-F), causes abnormally stable adhesiveness and inhibits motility in L cells (Nagafuchi et al 1994). Expression of this construct disrupts hexagonal packing and increases variability of cell contact lengths (Figure 20 G,H; Figure 21C-E; Table 2; Appendix II+III). This is consistent with the idea that junction remodeling depends on disassembly of E-cadherin-mediated contacts at shrinking junctions, although we cannot rule out additional effects potentially mediated by an irreversible linkage of the fusion protein to the actin cytoskeleton.

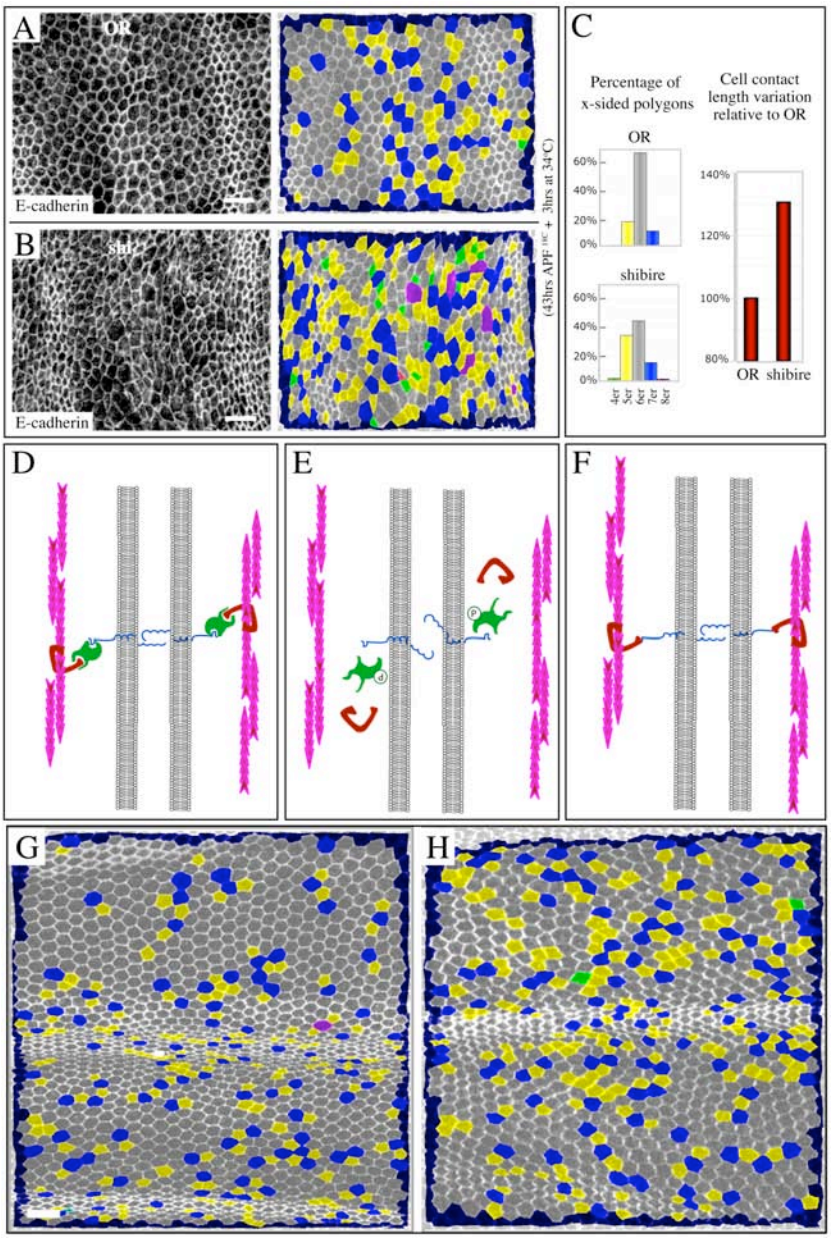

Figure 20 Cell packing defects caused by *shibire* and the E-cadherin:α-catenin fusion protein

(A) A wild type wing shifted at P2B to 34ºC for 3hrs, stained for E-cadherin (left). Right panel is color-coded as before (Figure 8) to show cell neighbor number. **(B)** A *shibire* mutant wing shifted at P2B to 34ºC for 3hrs stained for E-cadherin (left). Cell packing (right) is disturbed. **(C)** Quantification of neighbor number and variability of individual cell-

cell contact lengths in wild type and *shibire* wings shown in (A,B). Cell-cell contact length variability is normalized for perimeter variation to a 100% in wild type. **(D)** The current view on E-cadherin adherens junction architecture depicts the cytoplasmic tail of E-cadherin (blue) to be bound by β-catenin (green) which in turn binds α-catenin (red) associated with cortical actin (pink). This conformation is thought to stabilize E-cadherin complexes at the junctions. **(E)** The stable linkage of E-cadherin to the cortical actin cytoskeleton can be dissociated by phosphorylation of β-catenin. **(F)** Fusion of α-catenin to the cytoplasmic tail of E-cadherin should result in a stable E-cadherin-actin linkage that cannot be regulated by phosphorylation of β-catenin. **(G)** Image of distal wing tissue between L2 and L4 at the time of hair outgrowth analyzed using Cellenger for polygon identity. **(H)** Image of distal wing tissue at the time of hair outgrowth that has expressed an E-cadherin:α-catenin fusion protein during pupal stages under the control of the GAL4/GAL80 system. The image was analyzed for polygon identity (Figure 21C,D; Table2) and cell shape (Figure 20E) using Cellenger.

3.6. Planar Cell Polarity proteins are needed for hexagonal repacking

We suspected a link between the Planar Cell Polarity (PCP) pathway and epithelial repacking, because inhibition of Dynamin function during junctional remodeling can cause hair polarity defects (Figure 15F). Furthermore, hexagonal repacking occurs at the same time that PCP proteins are thought to polarize. We therefore quantified neighbor number and junction length variability at the time of hair outgrowth in different PCP mutants (Figure21A,C-E; Table 2; Appendix II + III). For *pk-sple13/26* mutant wing, we also quantified neighbor number over time (Figure 21B).

pk-sple13/26 wings begin repacking at the same time as wild type (Figure 9G,H; compare with Figure 8I), however the process is less successful. Whereas wild type wings reduce the percentage of pentagonal cells from 34% to 13% by the time that hairs begin to emerge, *pk-sple13/26* wings retain 21% (Figure 21C,D; Table 2). Thus, about 40% of the pentagonal cells that normally assemble boundaries with new neighbors (and become hexagonal) fail to do so in *pk-sple13/26* mutants. Consistent with this, *pk-sple13/26* wing epithelia contain abnormally high numbers of four-way vertices between cells (Figure 21F). *pk1* mutant wings are even more irregularly packed than *pk-sple13/26* (Figure 21A,C-F; Table 2). 62% of the pentagonal cells that would normally become hexagonal fail to assemble boundaries with new neighbors in *pk1* wings. Even four-sided cells accumulate significantly in *pk1* mutant wings (Table 2). Individual cell contact lengths are also much more variable; while *pk-sple13/26* boundary lengths were 9% more variable than wild type, those of *pk1* were 42% more variable (Figure 21E and Table 2). These data are consistent with the earlier observation that adult *pk* wings contain frequent pentagonal cells (Gubb et al 1999). They suggest that assembly of new cell boundaries and regularization of junction length do not occur efficiently in the absence of products of the Pk-Sple locus.

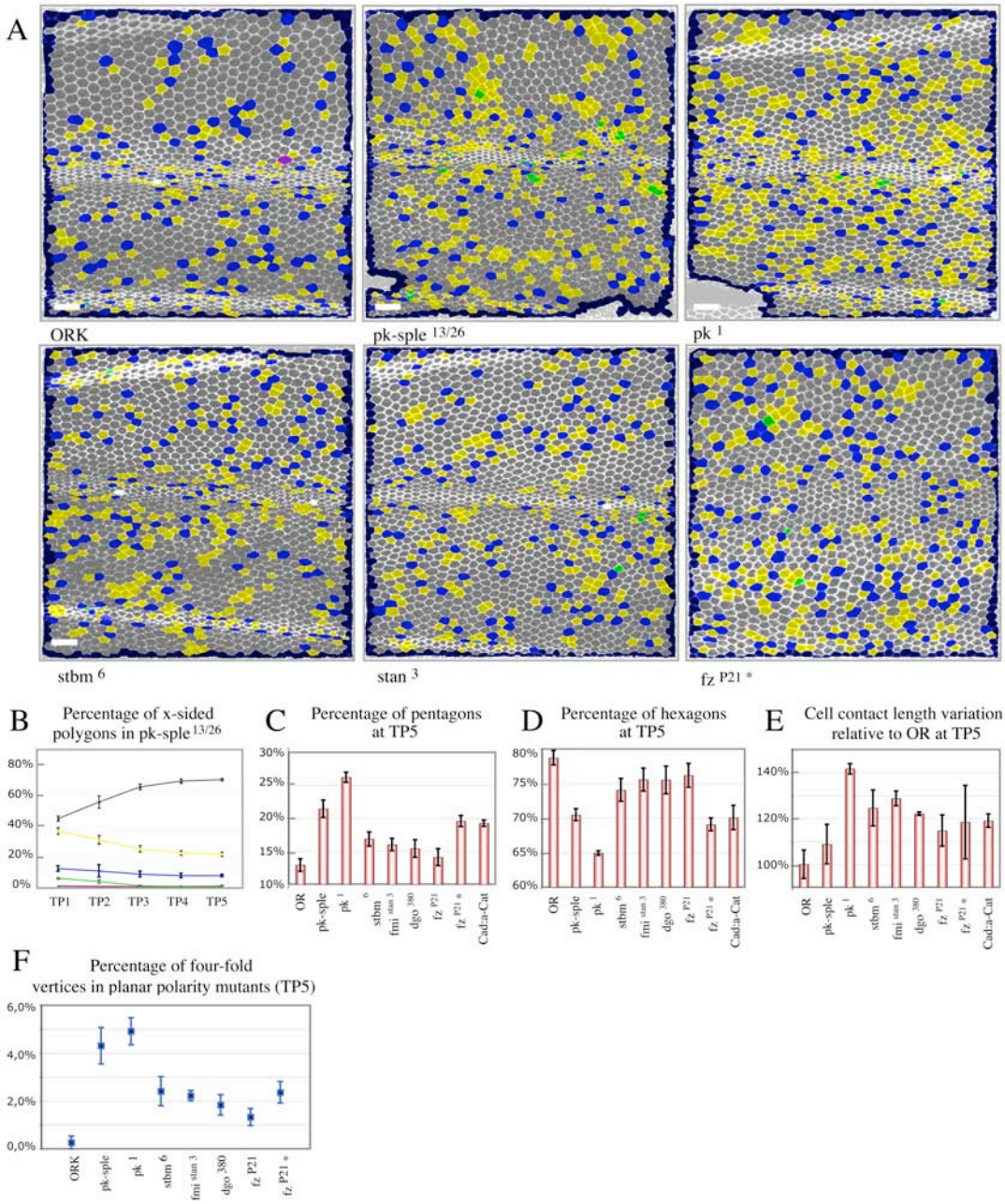

Figure 21 Cell packing defects in planar cell polarity mutants

fzP21* denotes *fzP21* mutant wings that have not formed hairs (see text). Cad:a-Cat denotes wings expressing the non-regulatable E-cadherin:α-catenin fusion protein. **(A)** Polygon identity at TP5 (hair outgrowth) for wings of the indicated genotypes. Polygon identity is color-coded as in Figure 8. **(B)** Time course of cell packing of *pk-sple* from TP1-TP5. **(C)** Percentage of cells with 5 neighbors at TP5 in wild type and PCP mutant wings. **(D)** Percentage of cells with 6 neighbors at TP5 in wild type and PCP mutant wings. **(E)** The standard deviation of length of individual cell boundaries is normalized to the standard deviation of the cell perimeters for 3 wings per genotype to correct for perimeter variability. For each mutant, this ratio is depicted as a percentage of the wild type ratio. The average and standard deviation of the perimeters (in μm) of the different genotypes range from 16.8 +/- 2.6 (for OregonR) to 15.1 +/- 1.9 (for *pk1*). **(F)** Percentage of four-fold vertices in wild type and PCP mutants at hair outgrowth.

Packing defects of the hypomorphic Flamingo (fmi) allele, *fmi(stan)3*, are mild but significant (Figure 21A,C-F; Table 2). The null allele *fmiE59* produces much stronger defects (Figure 22; Table 2). The variability of individual junctional lengths in these cells is more than twice that of wild type and only 69% of *fmiE59* mutant cells become hexagonal, compared with 78% in wild type (Table 2). Pentagonal cells persisted in *fmiE59* mutants (27% compared with 13% in wild type). This suggests that the majority of pentagonal cells fail to assemble boundaries with new neighbors when Flamingo is missing.

We examined the packing geometry of two different *frizzled (fz)* alleles; *fzR52* and *fzP21*. *fzP21* mutant wings fall into two classes. While the majority of wild type and PCP mutant wings initiate hair formation by 42hr APF (at 22ºC), a subset of *fzP21* mutant wings does not. Since these wings were not apoptotic (as indicated by Caspase staining, data not shown), we included them in our analysis, quantifying them separately. Even at 50hr APF, their packing is much more irregular than that of wild type (Figure 21A,C-F; Table 2). Defects in *fzP21* mutant wings that do initiate hair formation by 42 hrs APF are milder but still significant (Figure 21A,C-F; Table 2). *fzR52* homozygotes do not produce viable pupae in our hands, and homozygous mutant clones are small. These clones have even stronger packing defects than those of *fzP21*; cells in the clone shown in Figure 22 are 37% pentagonal, suggesting little repacking occurs in *fzR52* homozygous tissue. Thus, Frizzled is needed to develop regular hexagonal packing.

strabismus6 and *diego380* mutant wings have milder, but significant alterations in the ratio of pentagons, hexagons and heptagons and of four way vertices (Figure 21A,C-F; Table 2). Both mutants, however, affect junction length variability more strongly than *pk-sple13/26* (Figure 21E; Table 2). Taken together, these data indicate that PCP mutant cells fail to efficiently assemble boundaries with new neighbors and cannot regularize their packing geometry.

	tetragons			pentagons			hexagons			heptagons			cell contact variation		
	% average	SD	p-value	% average	SD	p-value	% average	SD	p-value	% average	SD	p-value	% average	SD	p-value
ORK	0.1	0.0		12.9	0.9		78.7	1.0		8.2	0.3		100.0	6.2	
pk-sple	0.6	0.4	0.0574	21.4	1.3	0.0006	70.5	0.9	0.0003	7.5	0.8	0.1178	108.8	8.6	0.1281
pk1	0.3	0.1	0.0034	26.2	0.8	0.0000	64.9	0.3	0.0004	8.5	0.4	0.2030	141.6	2.3	0.0009
stbm^{6}	0.2	0.1	0.2029	16.9	1.1	0.0046	74.1	1.7	0.0103	8.8	0.6	0.1094	124.6	7.9	0.0143
fmi ^{stan3}	0.2	0.2	0.1270	16.0	0.9	0.0079	75.6	1.7	0.0301	8.2	0.9	0.4918	128.7	3.2	0.0021
dgo^{380}	0.1	0.1	0.2049	15.4	1.3	0.0303	75.5	2.0	0.0450	8.9	0.5	0.0744	122.1	0.7	0.0116
fz ^{P21}	0.1	0.1	0.2234	14.1	1.3	0.1367	76.2	1.7	0.0541	9.6	0.4	0.0050	114.7	6.8	0.0330
fz $^{P21\ s}$	0.5	0.3	0.0596	19.6	0.8	0.0004	69.1	0.9	0.0002	10.8	0.2	0.0006	118.4	16.0	0.1148
CadaCat	0.1	0.1	0.3080	19.2	0.5	0.0001	70.1	1.8	0.0002	10.5	1.2	0.0350	118.9	2.9	0.0085
fmi^{E59}	0.2	0.4	0.1189	26.6	6.5	0.0006	68.6	5.3	0.0009	4.6	2.3	0.0050	221.3	23.6	0.0000

Table 2 Cell packing in PCP-mutants at hair outgrowth

Average percentage of polygon classes and contact length variability in wings or clones (*fmiE59*) of different genotypes are indicated, along with standard deviations (SD) and the P-value of the Student t-test. Contact length variability is

calculated by dividing the SD of the contact length (as percentage of the average) by the SD of the perimeter (as percentage of the average) to correct for cell-size variation and expressing it as a percentage of the wild type value. The average perimeter of *fmiE59* mutant cells is 12.2 +/- 0.7 µm, compared to 16.8 +/- 2.6 µm for OregonR. P-values <0.05 are highlighted in orange. P-values <0.005 are highlighted in red.

3.7. Frizzled mutant cells alter the packing of adjacent tissue

To ask whether interfering with PCP polarity could alter the geometry of packing in wild type cells, we examined cells surrounding PCP mutant clones with either autonomous (*fmiE59*) or non-autonomous (*fzR52*) effects on polarity. We examined the frequency of pentagons, hexagons and heptagons in *fzR52* and *fmiE59* mutant clones, and in areas of disturbed and normal Flamingo polarity surrounding both. The mutant cells within both *fzR52* and *fmiE59* clones are abnormally packed (Figure 22C,D,G,H). However, whereas the packing defects caused by *fmi* clones are predominantly restricted to the clone and directly adjacent cells (Figure 22E-H), *fz* clones alter packing over long distances in wild type tissue (Figure 22A-D) in the same regions where Flamingo polarity is disturbed. The abnormal packing of wild type cells surrounding *fzR52* clones is unlikely to be a consequence of altered cell packing within the mutant clone, because *fmiE59* mutant clones pack just as abnormally but do not perturb packing in surrounding tissue. This suggests that dominant reorientation of Flamingo polarity by *frizzled* mutant clones disturbs repacking of wild type cells.

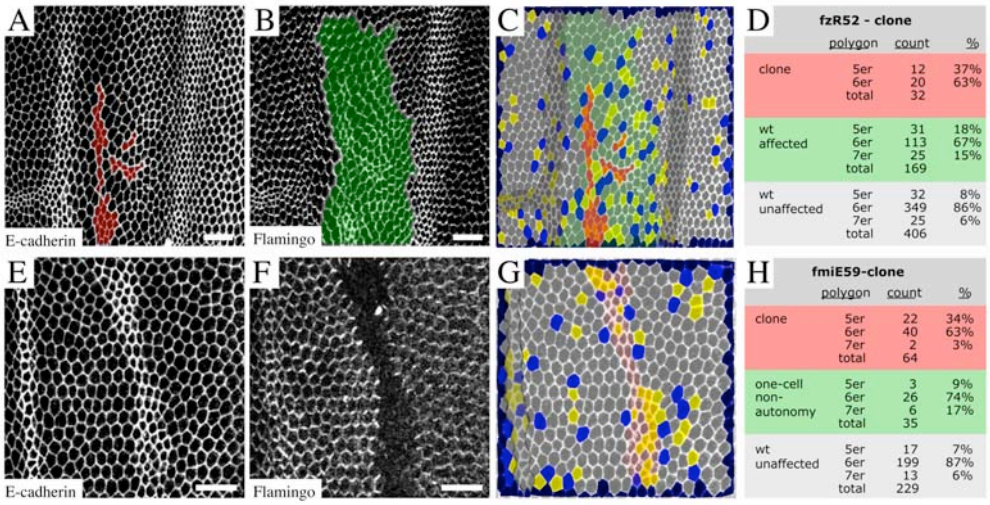

Figure 22 **Cell packing is non-autonomously perturbed by *fzR52* mutant clones**

Color code for different sided polygons as in Figure 8. **(A-B)** A *fzR52* clone (red in A and C) stained for E-cadherin (A), and Flamingo (B). Cells with altered Flamingo polarity are colored green. E-cadherin levels are normally elevated in the

anterior compartment in pupal wings, accounting for brighter staining in the right half of the image. **(C)** Image shown in (A) color-coded for polygon identity and overlaid with colors indicating clone (red), non-autonomously mispolarized cells (green) and vein cells (dark grey). **(D)** Different polygon classes in *fzR52* mutant cells (red), wild type cells with altered Flamingo polarity (green) and unaffected wild type cells (grey) from images shown in (A-C). **(E-G)** A *fmiE59* clone stained for E-cadherin (E), Flamingo (F) and analyzed for neighbor number (G). The clone is shaded pink. *fmiE59* mutant cells are smaller than wild type and have elevated E-cadherin at apical junctions. The row of small cells to the left is a vein. **(H)** Different polygon classes in *fmiE59* mutant cells (red), wild type cells directly adjacent to clone (green) and more distant wild type cells (grey) derived from images shown in (E-G).

3.8. Flamingo polarity is transiently disturbed during junction remodeling

To investigate how the PCP proteins were localized during repacking, we imaged pupal wings for Flamingo before, during and after hexagonal packing. Since it is thought that PCP proteins do not polarize until shortly before hair formation, we were surprised to find that the subcellular distribution of Flamingo is polarized in many areas of the wing before junction remodeling initiates, even in late third instar wing discs and pre-pupal wings (Figure 23A-D; Appendix I A-D). Frizzled:GFP (Strutt 2001), Strabismus, Diego and Dishevelled are distributed similarly (Appendix I J,K and not shown). This polarity may have been missed because it exhibits less long-range coherence in imaginal discs and pre-pupal wings than it does later.

In pre-pupal wings, Flamingo polarity is roughly proximal-distal in the region surrounding L3 (Figure 23A-C, Appendix I C,D). Coherent Flamingo polarity is lost at the beginning of the pupal period (Figure 23D-F, Appendix I E,F): exactly the time at which junction remodeling initiates. Although polarity is not coherent, Flamingo is not uniformly distributed along cell boundaries. This can be clearly seen when Flamingo localization (Figure 23E) is compared to that of E-Cadherin (Figure 23D).

At analysis time point TP1, Flamingo polarization begins in vein cells as they contract their apical cross section (Figure 23G-I, Appendix I G,H). Intervein regions contain only small groups of cells with coherent polarity, and its axis is not always proximal-distal (Figure 23G-I). By TP2, Flamingo polarity is coherent between larger groups of cells, although the axis of polarity is still mixed (Figure 23J-L, Appendix I I). Flamingo polarity is aligned in large coherent domains along the proximal distal axis by TP4, when hexagonal packing is completed, and remains unchanged at TP5 when hairs emerge (Figure 23M-O). No difference in timing of coherent polarity emergence was observed between distal and proximal wing regions (Appendix I I).

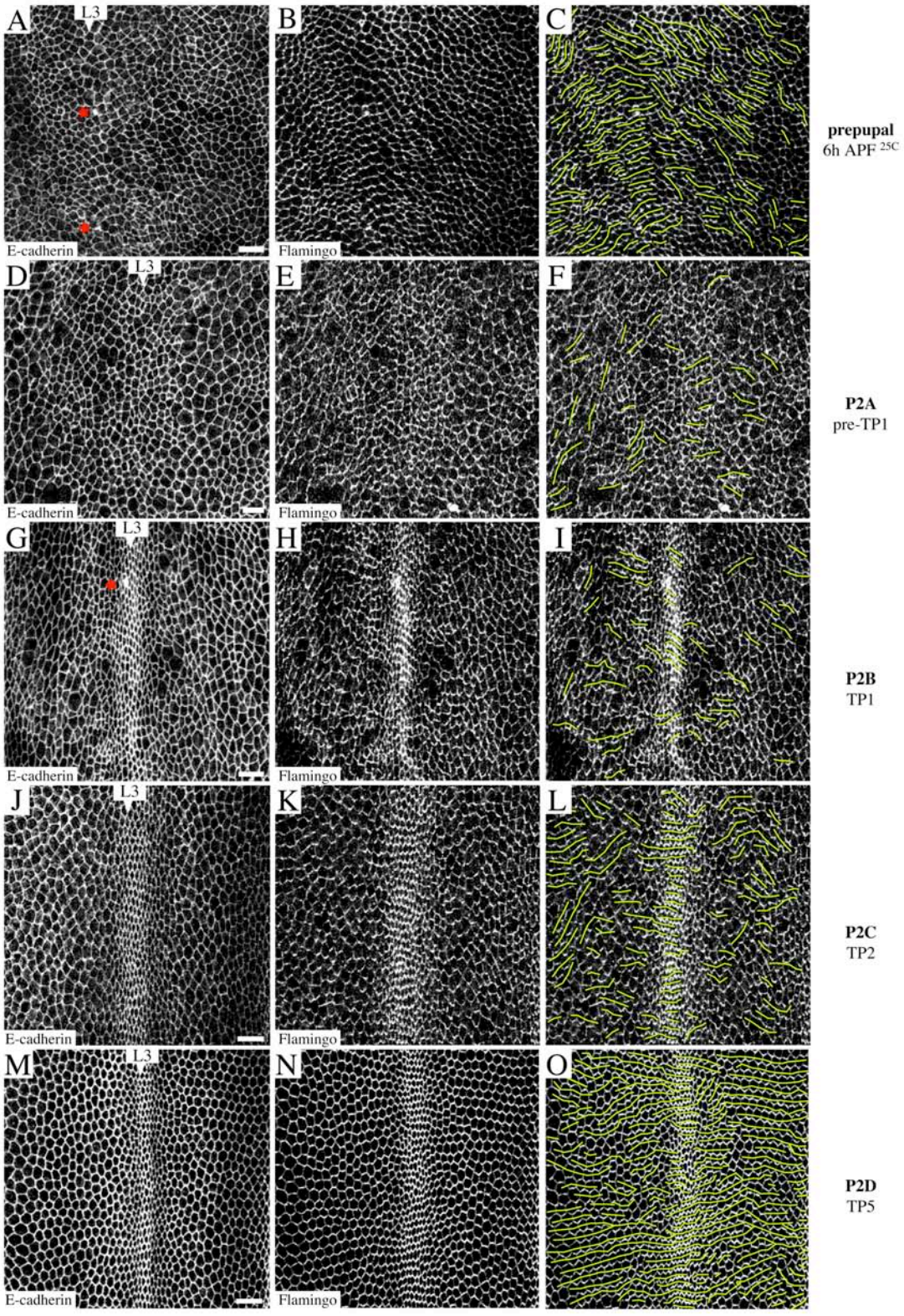

Figure 23 Flamingo polarity is perturbed during junction remodeling

(A-O) depict Flamingo and E-cadherin staining in the region surrounding L3 (arrowhead) at different developmental stages. Distal is up. Asterisks indicate the developing campaniform sensillum on L3. Green lines in C,F,I,L,O are drawn between neighboring cells with coherent Flamingo polarity, through boundaries with lower Flamingo levels. **(A-C)** a

pre-pupal wing imaged for E-cadherin:GFP (A) and Flamingo (B,C). **(D-F)** Early pupal wing (Waddington P2A) stained for E-cadherin (D) and Flamingo (E,F). **(G-I)** a pupal wing (Waddington P2B, TP1) stained for E-cadherin (G) and Flamingo (H,I). **(J-L)** a pupal wing at early P2C (TP2) stained for E-cadherin (J) and Flamingo (K,L). **(M-O)** a pupal wing at Waddington stage P2D (TP5) stained for E-cadherin (M) and Flamingo (N,O).

In summary: PCP proteins polarize during larval and pre-pupal stages, alignment of polarity between cells is disturbed when junction remodeling begins, and long-range polarity is re-established as hexagonal packing is completed. Early polarization of PCP proteins is consistent with the genetic requirement for Frizzled and Dachsous activity at this time to determine the axis of polarity (Adler et al 1994, Matakatsu & Blair 2004, Strutt & Strutt 2002a), and suggests that the feedback loop that organizes coupled proximal and distal domains (Amonlirdviman et al 2005, Tree et al 2002b) probably acts during these early stages.

3.9. Blocking Dynamin function prevents alignment of Flamingo polarity

Because mild temperature shifts of *shibire* mutant animals at the stage P2B cause hair polarity defects in adult wings (Figure 15F) we wondered whether the re-establishment of coherent Flamingo polarization might depend on successful remodeling of intercellular junctions. To test this, we shifted *shibire* mutant pupae (stage P2B) to 34ºC for 3 hours and compared Flamingo localization to that of wild type controls shifted under the same conditions. While the overall levels of Flamingo at the cortex do not change, and Flamingo remains polarized within individual cells, the alignment of Flamingo polarity between neighboring cells is disturbed (Figure 24A,B). This occurs only during stages where junctional remodeling and hexagonal repacking occurs; no effects are observed in third instar *shibire* discs shifted for even longer times (Figure 24C,D). The fact that *dynamin* mutant cells cannot efficiently align domains of Flamingo enrichment with that of their neighbors suggests that the remodeling of intercellular contacts is needed to develop long-range coherence of Flamingo polarity.

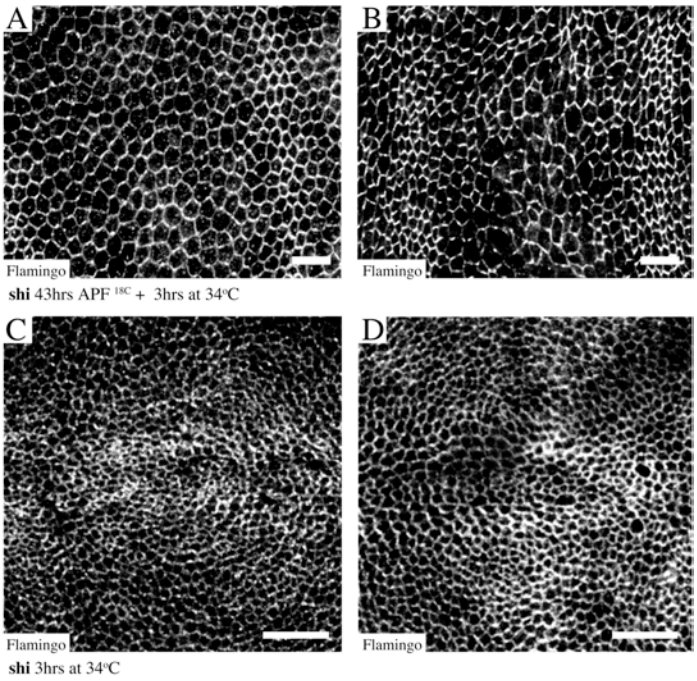

Figure 24 Blocking Dynamin activity prevents long-range alignment of Flamingo polarity

(A) A wild type wing shifted to for 3 hours to 34ºC at stage P2B and stained for Flamingo. Corresponding E-cadherin image in Figure 20A. **(B)** A *shibire* mutant wing shifted to for 3 hours to 34ºC at stage P2B and stained for Flamingo. Corresponding E-cadherin image in Figure 20B. Alignment of Flamingo polarity between neighboring cells is disturbed. **(C)** A wild type wing imaginal disc shifted to for 3 hours to 34ºC and stained for Flamingo. Corresponding E-cadherin image in Figure 15D. **(D)** A *shibire* mutant wing imaginal disc shifted to for 3 hours to 34ºC and stained for Flamingo. Corresponding E-cadherin image in Figure 15E. Alignment of Flamingo polarity between neighboring cells is not disturbed.

3.10. PCP mutants enhance epithelial disintegration caused by lack of Dynamin

Critical steps involving recycling of junctional components during remodeling are the initiation of a new junction from a four-fold vertex and the efficient expansion of an initiated junction. Failure of the junction initiation will cause accumulation of pentagons in the tissue; failure of junction expansion will result in irregular cell shapes (Figure 25). Both defects are characteristic for PCP mutant tissue. We therefore wondered whether PCP proteins might affect packing by influencing recycling of junctional components.

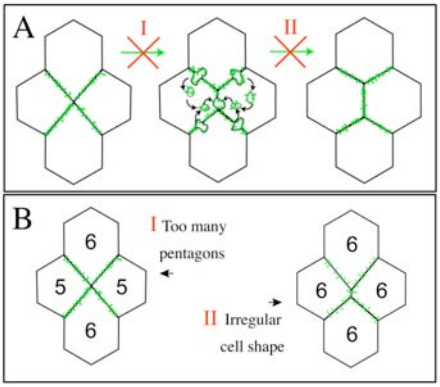

Figure 25 PCP packing defects may be caused by a deficiency in E-cadherin recycling

(A) There are two ways in which to fail to expand a new boundary during junctional remodeling. One possibility is to fail to initiate expansion of a new boundary from a four-way vertex (I). The other possibility is to fail to efficiently expand an initiated boundary (II). **(B)** The failure to initiate expansion of a new boundary from a four-way vertex results in the accumulation of cells with less than 6 neighbors (see Euler's formula in text to Figure 8) (I). A failure to efficiently expand new boundaries may give rise to short boundaries that translate into irregular cell shapes (II). Both packing defects I and II are observed in the PCP mutants.

Thus, we first asked whether PCP mutants enhanced the hole formation caused by *shibire* loss of function. We shifted *shibire*;*PCP* double mutant pupae to a sub-restrictive temperature that never causes holes to form in *shibire* mutants (Figure 26A) or in PCP mutants (not shown and Figure 26E,F). When *shibire* is combined with *dgo380*, *stbm6*, *stbm153*, *stbmD*, *stan3*, *pk-spl1* or *pk1*, hole formation occurs even under these mild conditions (Figure 26A). This raises the possibility that PCP proteins may worsen E-cadherin recycling defects in *dynamin* mutant cells. Consistent with this, gaps in E-cadherin arise more frequently in double *shi;pk1* (51gaps) or *shi; dgo380* (36 gaps) mutant wings than in wings mutant for *shibire* alone (20 gaps) (Figure 26B-F). This suggests that E-cadherin is recycled less efficiently in the absence of PCP proteins.

Intriguingly, the genetic interaction between *shibire* and PCP mutants also enhances hair polarity defects in PCP mutants (Figure 26G,H); again indicating that efficient Dynamin-dependent junctional remodeling is required for polarization and hair alignment. This result furthermore argues that hair polarity defects in the PCP mutants may only be due to a partial loss of PCP pathway function, which can be enhanced by interfering with E-cadherin trafficking and junctional remodeling. We cannot exclude though that the enhancement of polarity defects arises by other unrelated mechanisms.

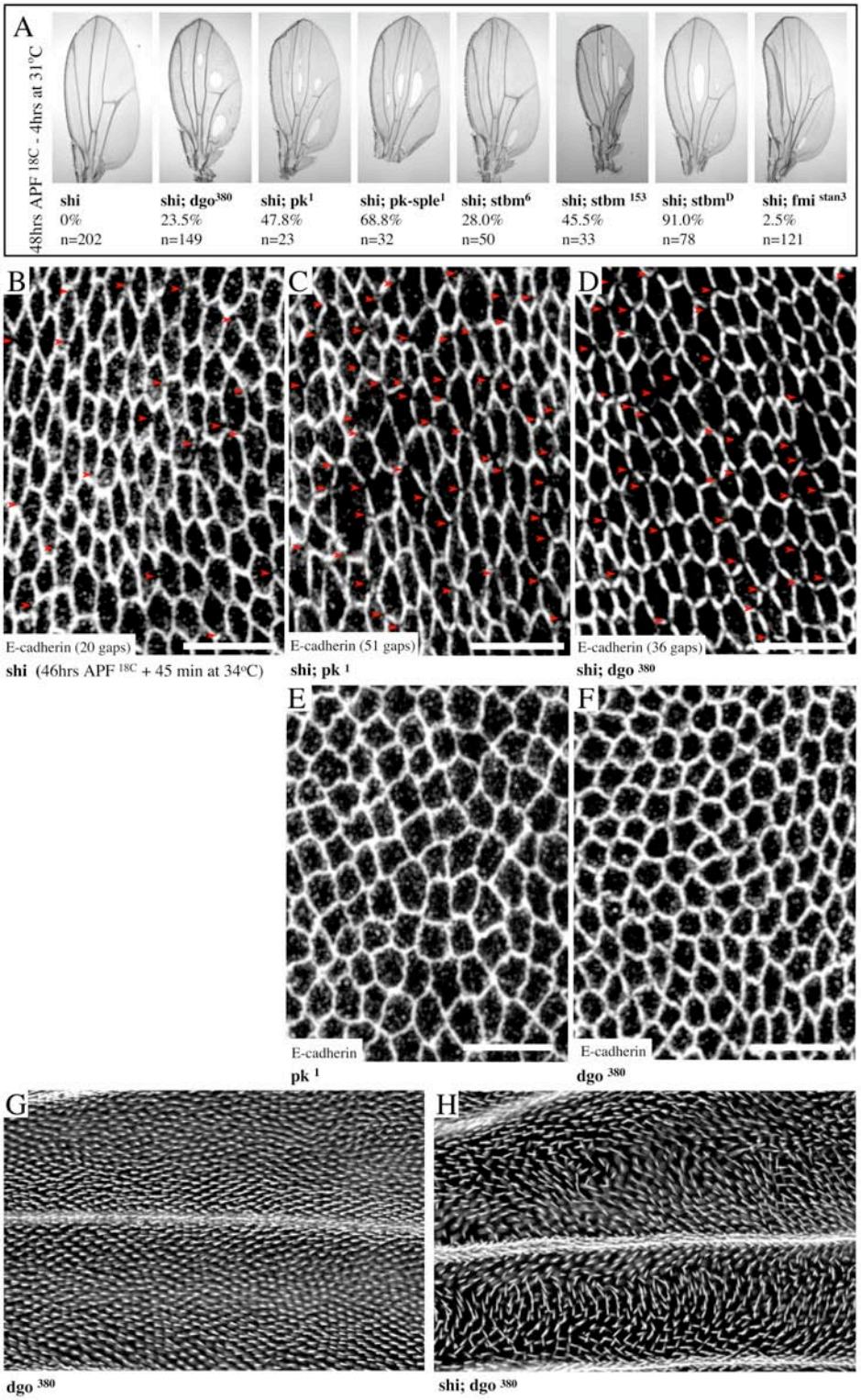

Figure 26 PCP mutations enhance E-cadherin recycling defects

(A) Wings of the indicated genotypes were shifted to 31ºC for 4 hours beginning at stage P2B. The percentage of adult wings with holes is shown. n indicates the number of wings analyzed. (B-F) Wings were shifted to 34ºC, stained for E-cadherin, and imaged in parallel under identical conditions. Arrows indicate gaps in junctional E-cadherin. **(B)** *shibire* mutant shifted to 34ºC for 45 minutes during P2B. **(C)** *shi;pk1* mutant wing shifted under the same conditions as in (B).

(D) *shi;dgo380* mutant wing shifted under the same conditions as in (B). **(E)** *pk1* mutant wing shifted under the same conditions as in (B). **(F)** A *dgo380* mutant wing shifted under the same conditions as in (B). **(G)** An adult *dgo380* mutant wing shifted to 31ºC for 4 hours beginning at stage P2B was imaged between L2 and L4, an area devoid of hair polarity defects. **(H)** An adult *shi;dgo380* mutant wing shifted to 31ºC for 4 hours beginning at stage P2B and imaged between L2 and L4 as in (G). Hairs show aberrant polarity.

Despite the enhancement of E-cadherin localization defects in *shibire;PCP* double mutants, no striking abnormalities in E-cadherin distribution were seen in most PCP mutants (Figure 27 and not shown). *fzP21* mutant cells sometimes show gaps in E-cadherin that are similar to, but much less frequent than, those of *shibire* mutants (Figure 27C). In *fmiE59* mutant cells, E-cadherin levels are elevated (Figure 27A,B), but no gaps in localization are observed.

These observations suggest that PCP proteins are not required per se for delivery of E-cadherin to cell contacts during remodeling. Nevertheless, the PCP mutants enhance E-cadherin recycling defects caused by loss of Dynamin. One model consistent with this is that PCP proteins bias E-cadherin recycling to specific places on the cortex. Reducing both the rate of recycling by Dynamin loss of function and reducing polarized delivery to particular sites in PCP mutants could exacerbate the failure of E-cadherin delivery to growing cell boundaries.

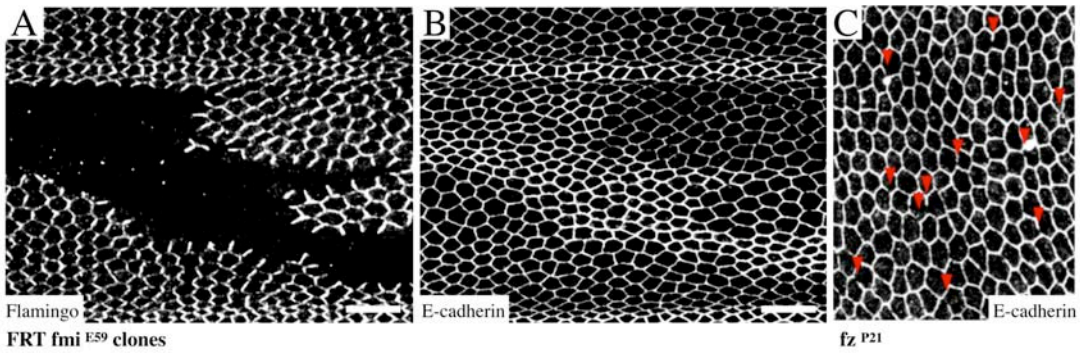

Figure 27 **Mild E-cadherin defects in PCP mutants**

(A,B) A wing containing a *fmiE59* mutant clone (indicated by loss of Flamingo staining in (A), stained for E-cadherin (B). **(C)** E-cadherin stained *fzP21* wing. Red arrows indicate gaps in junctional E-cadherin.

3.11. Flamingo recruits the exocyst component Sec5

Polarized delivery of membrane vesicles to the plasma membrane is known to be mediated by the exocyst complex. Some exocyst subunits create a binding patch at the plasma

membrane for targeting, docking and fusion of a complementary exocyst-marked vesicles. The exocyst coordinates **polarized** delivery of Golgi-derived vesicles to the growing bud tip in yeast. In epithelia, the exocyst promotes delivery of basolateral cargo to junction and, most importantly, directs the delivery of E-cadherin from recycling endosomes to junctions (Figure 6B-D).

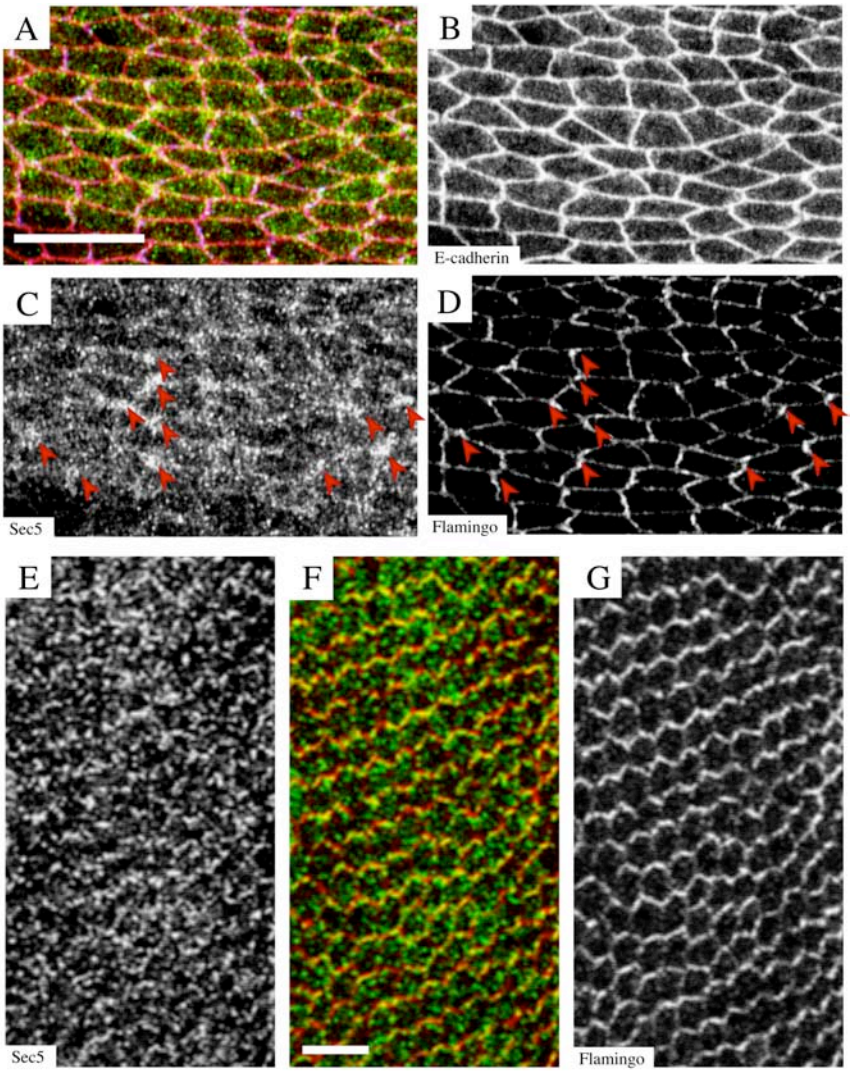

Figure 28 Sec5 polarizes with Flamingo

(A-D) Early pupal wing tissue undergoing repacking was stained for E-cadherin (B, red in A), Sec5 (C, green in A) and Flamingo (D, blue in A). Arrowheads indicate Sec5 accumulation near Flamingo-rich boundaries. **(I-K)** A hexagonally packed wing epithelium just before hair outgrowth was stained for Sec5 (I, green in J) and Flamingo (J, red in K).

Therefore, we wondered whether the PCP pathway may exploit polarized exocyst delivery to bias E-cadherin trafficking to certain sites at the cortex. To test whether exocyst components were polarized by PCP proteins, we examined Sec5 localization during repacking of the wing epithelium (Figure 28A-D). At this time, cell shapes are irregular and Flamingo polarity is not coherent between cells. Nevertheless, Flamingo accumulates preferentially on specific regions of the cortex (Figure 28D). Although Sec5 vesicles are seen throughout the cell, they are particularly enriched near Flamingo-positive cell boundaries (Figure 28C). Enrichment persists as Flamingo polarity becomes aligned (Figure 28E-G). In contrast, Sec6 and Sec15 are uniformly located at the cell junctions or within the cytoplasm, respectively (data not shown), indicating that not all exocyst components become polarized .

To test whether Flamingo played an active role in recruiting Sec5, we over-expressed Flamingo and examined Sec5 localization. Over-expressed Flamingo is present uniformly around the cortex and in large punctate structures within the cell (Figure 29A,D). Sec5 dramatically accumulates in cells over-expressing Flamingo and is recruited to sites of Flamingo localization (Figure 29A,C,D). Large internal structures positive for Flamingo and Sec5 also contain E-cadherin (Figure 29A,B). These observations indicate that Flamingo can recruit Sec5-positive vesicles containing E-cadherin, and suggest that PCP proteins may promote hexagonal packing by polarizing membrane trafficking.

To additionally test whether Flamingo was sufficient to recruit Sec5 we overexpressed other PCP proteins, such as Prickle (Figure 29E-H), Stbm and Fz (data not shown) and examined Sec5 localization. In all cases, we did not observe a dramatic accumulation of Sec5 in overexpressing cells. Rather Sec5 localization was always closely associated with Flamingo, also when Flamingo polarization was disturbed by misexpression of PCP components. This indicates that not the output of the PCP-pathway as a whole is required to recruit Sec5, rather Flamingo is one of the most downstream components able to determine Sec5 localization.

We suggest that the packing defects observed in the PCP mutants could be due to recruitment of E-cadherin containing Sec5 vesicles to aberrant cortical sites in PCP mutants marked by mispolarized Flamingo, leading to inefficient junction elongation, and, consequently, packing defects. Such a model (Figure 30) reconciles the different phenotypes in *shibire* and PCP mutants, since E-cadherin containing Sec5-vesicles never reach the junctions in initially normally polarized *shibire* tissue, giving rise to E-cadherin gaps.

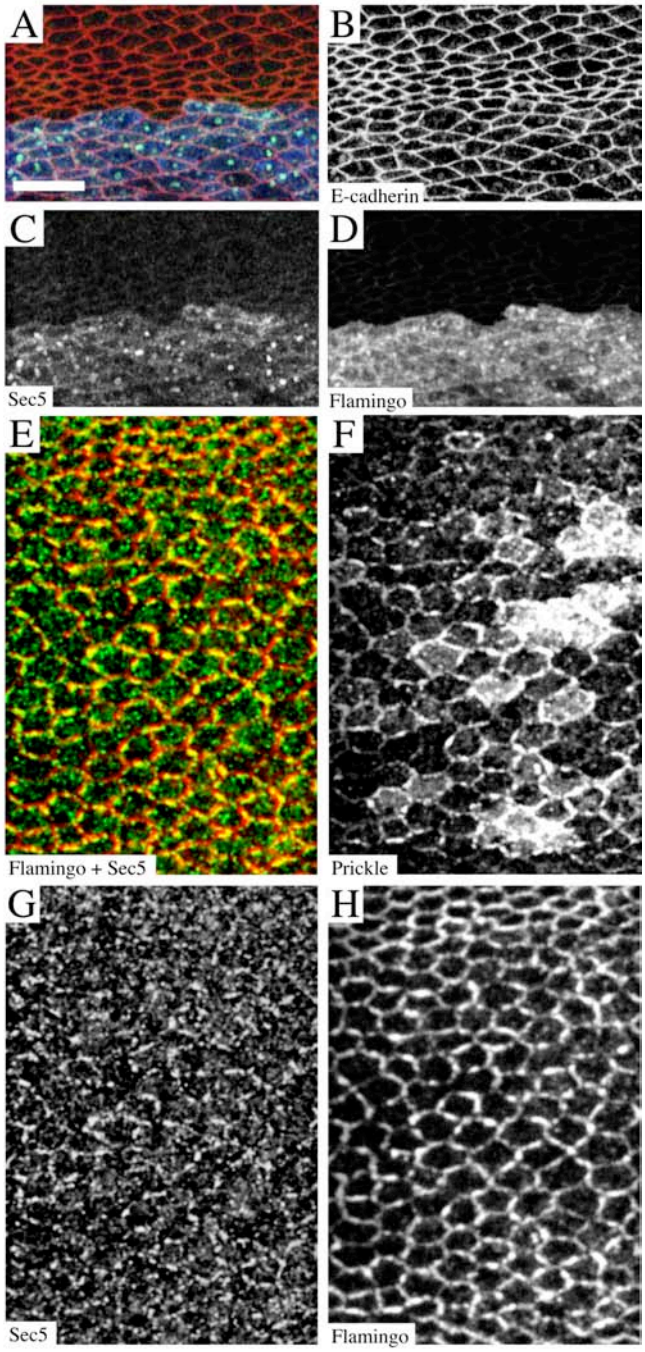

Figure 29 Sec5 is specifically recruited by Flamingo

(A-D) Pupal wing tissue undergoing repacking and over-expressing Flamingo (D, blue in A) at the AP boundary. Acquisition settings were adjusted so that over-expressed Flamingo was in the linear range, making endogenous Flamingo undetectable. Sec5 (C, green in A) accumulates with Flamingo at the cortex and on vesicles that also contain E-cadherin (B, red in A). **(E-F)** Pupal wing tissue undergoing repacking and over-expressing Prickle (F) at the AP boundary. Prickle overexpression causes Flamingo (H, red in E) to cluster at the cortex, where it colocalizes with Sec5 (G, green in E). Sec5 does not accumulate with Prickle in over-expressing cells.

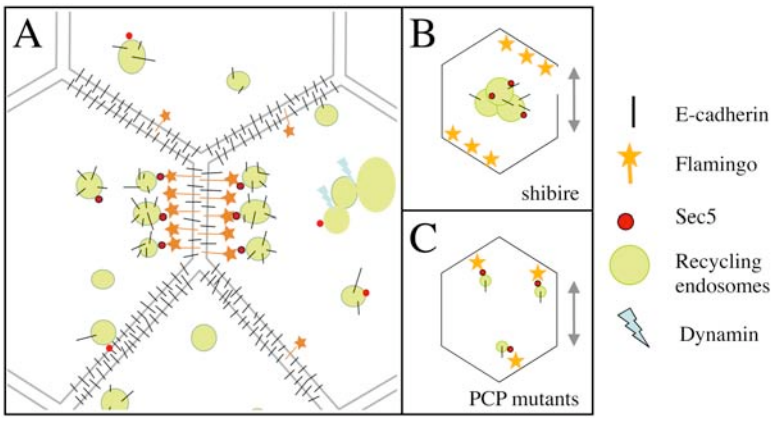

Figure 30 Recruitment of E-cadherin by Flamingo is mediated by the exocyst component Sec5

(A) Flamingo (orange) at the cortex recruits recycling endosome derived vesicles (green) that contain E-cadherin (black) and Sec 5 (red). As Flamingo is polarized in cortical domains, Sec5 vesicles are recruited to specific junctions. **(B)** Flamingo is still located in cortical domains in *shibire* wing tissue, but E-cadherin and Sec5 cannot be pinch off in vesicles from the recycling endosome. Therefore E-cadherin never reaches the cortex; this accounts for gaps in E-cadherin. **(C)** Flamingo is mispolarized in PCP mutants therefore E-cadherin containing Sec5 vesicles may be still recruited to boundaries, but inappropriate ones, accounting for lack of E-cadherin gaps in PCP mutants. However, both scenarios (B) and (C) will give rise to packing defects.

3.12. The cytoskeleton is highly polarized during junctional remodeling

During hair outgrowth PCP-signaling is known to direct the polarization of actin and microtubules into the growing hair. To ask whether PCP-signaling, in addition to biasing membrane trafficking, affects cytoskeletal organization during junctional remodeling we stained pupal wings at stage P2B for actin and Zipper (non-muscle myosin II heavy chain); and analyzed the localization of Spaghetti-squash:GFP (non-muscle myosin II light chain) (Barros et al 2003, Bertet et al 2004, Kiehart & Feghali 1986).

In *Drosophila* embryogenesis, Myosin II is reported to be specifically enriched in disassembling junctions during cell intercalations that occur in the context of convergent-extension (Bertet et al 2004). There, myosin II polarized distribution is required for the directionality of junction assembly and disassembly. We observed that throughout early pupal stages Zipper localizes to junctions rich in Flamingo (Figure 31A-C). Therefore, the localization of Zipper with Flamingo may depend on PCP-signaling. In contrast, Spaghetti-squash:GFP only polarized weakly with Flamingo. This may indicate that PCP-signaling in the pupal wing could direct junctional remodeling by also controlling the distribution of the actin motor myosin.

Especially during early stages of hexagonal repacking the actin cytoskeleton is highly polarized along anterior-posterior cell boundaries (Figure 31E). Actin forms long filament bundles interconnecting several cells. These filament bundles are easily visualized in vein cells and persist especially there up to the time of hair outgrowth (Figure 31F). To understand whether PCP-signaling affects the localization of actin during remodeling, we stained wings carrying *fmiE59* clones for actin. Surprisingly, actin accumulates at the *fmiE59* clone boundary (Figure 31G,H) and actin filament polarity is deviated at the interface between wild type and mutant cells (Figure 31I,J).

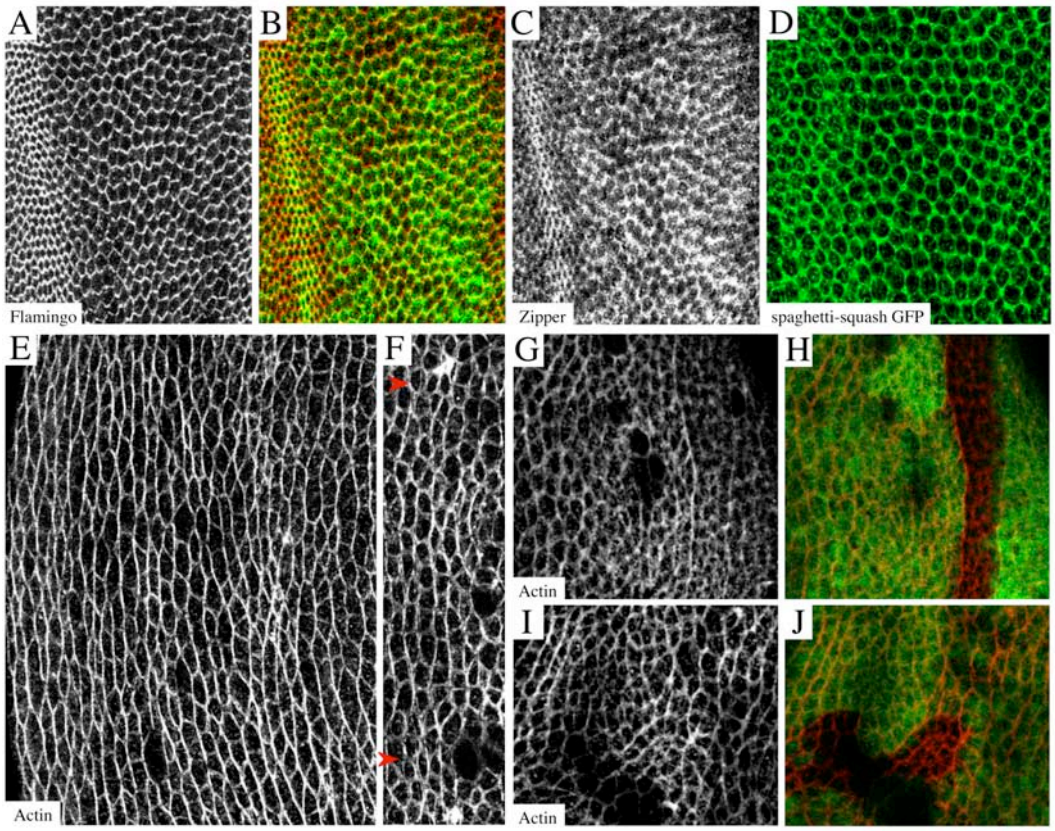

Figure 31 The cortical actin cytoskeleton is highly polarized during junction remodeling

(A-C) Early pupal wing during repacking stained for Flamingo (A, red in B) and for Zipper (C, green in B). Zipper accumulates with Flamingo near the cortex. **(D)** Early pupal wing during repacking expressing Spaghetti-squash:GFP. Sqh:GFP is not as highly polarized as Zipper. **(E-F)** Early pupal wing at the prepupal to pupal transition stained for actin. Actin is highly polarized along anterior-posterior boundaries (E) and appears to form long filament bundles interconnecting several cells that are easily visualized in vein cells (F). **(G-J)** Early pupal wing at stage P2A with *fmiE59* clones stained for actin (red in H,J). *fmiE59* clones in (G,I) are marked by absence of GFP (green). Clone boundaries accumulate actin (G,H) and deviate actin bundles from anterior posterior polarity (I,J). Anterior is left, posterior is right.

3.13. Hair polarity defects in PCP mutants do not depend on packing topology

During hair formation the polarized distribution of PCP proteins within a cell is thought to direct hair outgrowth to the distal side (Figure 32A), although they are not required for hair formation per se. The current view in the field is that in the absence of one of the PCP proteins all other remaining PCP proteins cannot polarize anymore. Then, the cortical site for hair outgrowth and local coordination of hair polarity must be determined by a presently unknown mechanism (Figure 32B).

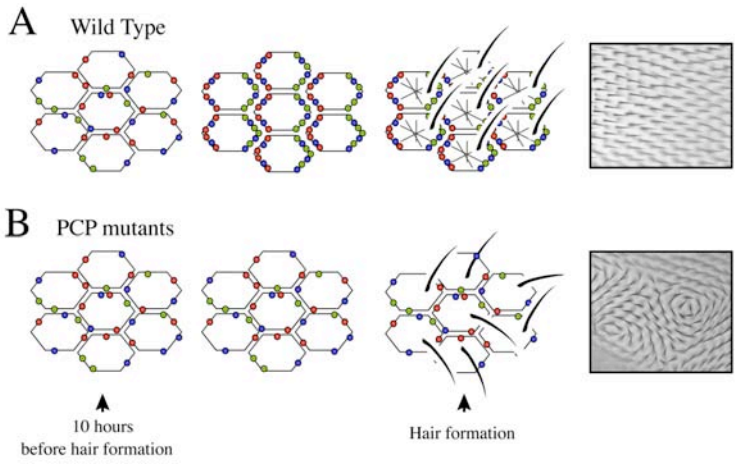

Figure 32 Establishment of hair polarity

(A) In wild type wing epithelial cells proximal and distal domains successfully polarize and subsequently organize hair outgrowth at the distal side. **(B)** The current view renders the remaining planar cell polarity proteins unable to polarize in the absence of one of them. Hair polarity is then organized and locally coordinated by another unknown mechanism. Note that both models assume that polarity is established from a uniform distribution of polarity proteins present at the prepupal-pupal transition.

Alignment of vertices in different packing topologies could provide an alternative cue for choosing the site of hair outgrowth (Figure 33A). We therefore wondered whether hair polarity defects in PCP mutants correlates with the occurrence with packing defects. However, we could not observe any correlation between the occurrence of packing defects and hair polarity defects when Cellenger images of pupal wings of PCP mutants at the time of hair outgrowth were overlaid with corresponding images visualizing hairs. Importantly, deviations from hexagonal packing occur even in regions of PCP mutant wings with normal hair polarity (Figure 33B,C).

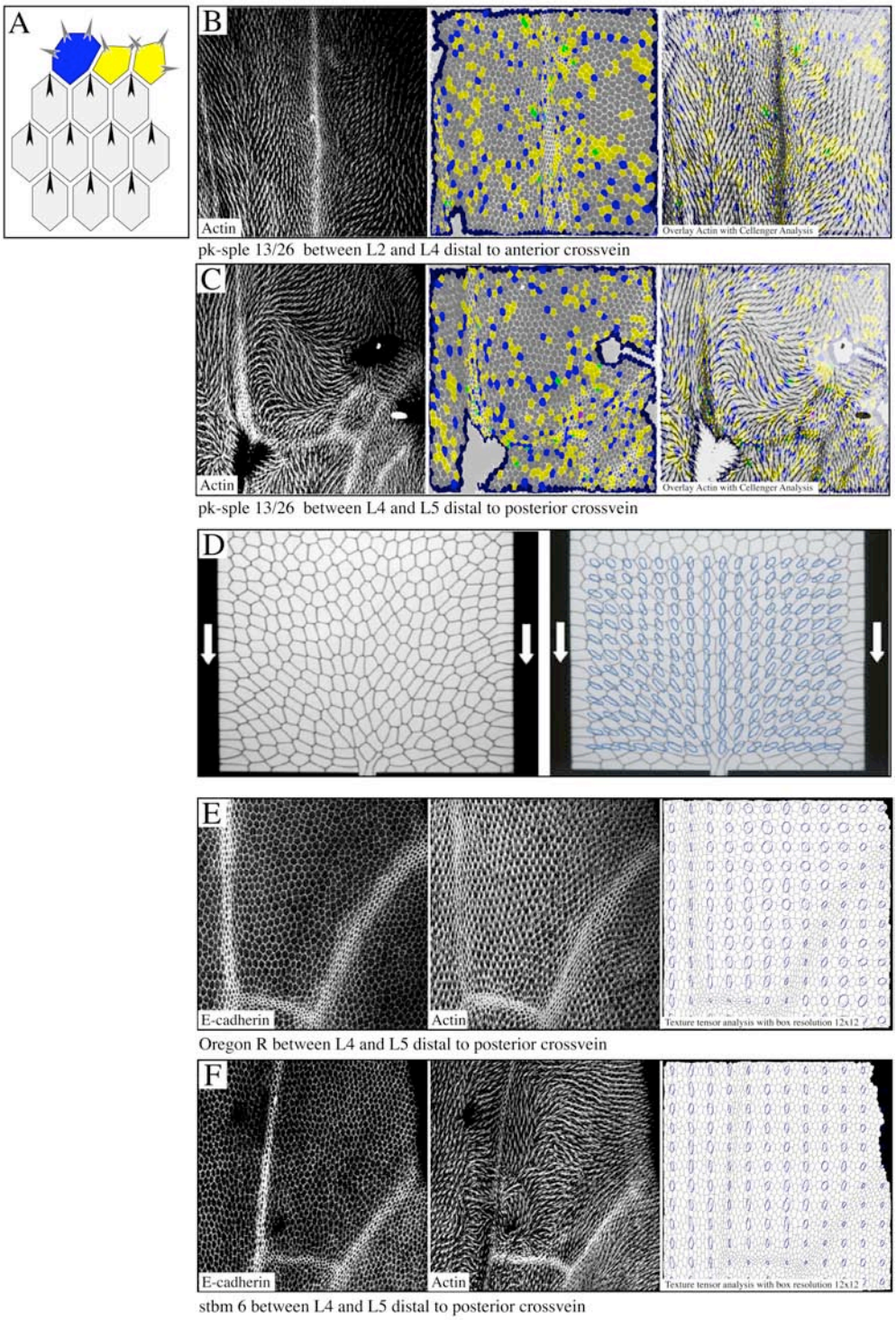

Figure 33 Hair polarity in PCP mutants is not determined by packing topology

Images (E-F) are based on a collaboration with Benjamin Dollet in the lab of Francois Graner (CNRS, Grenoble). **(A)** Hair initiation propagates as a wave from the distal to the proximal wing surface. In a simple scenario, hairs could be initiated at the opposite vertex of the next neighboring cell. This would align hairs well in a hexagonal lattice. However, the angle at which vertices lie in neighboring pentagons or heptagons would prevent alignment of hairs. Too many

pentagons in the PCP mutants may therefore cause hair polarity defects. **(B)** Distal *pk-sple13/26* mutant tissue at TP5 stained for actin to visualize hair outgrowth (left); an E-cadherin image of the same wing processed with Cellenger to visualize cell packing (middle) and an overlay of both (right). Even though the wing has many packing defects (clustered pentagons) there are no hair polarity defects in this region of the wing. **(C)** Posterior *pk-sple13/26* mutant tissue at TP5 stained for actin to visualize hair outgrowth (left); an E-cadherin image of the same wing processed with Cellenger to visualize cell packing (middle) and an overlay of both (right). This region of the wing exhibits some hair polarity defects, however they do not coincide with cell packing defects. **(D)** A two-dimensional foam forced to flow through a hole in the wall at the bottom of the image, giving rise to specific deformations of bubbles near the obstacle (left). Bubble deformation can be visualized by applying a tensor analysis (see text) to the image (right). **(E)** Posterior wild type tissue at TP5 stained for E-cadherin (left) and actin to visualize hair outgrowth (middle). The E-cadherin image was analyzed by Benjamin Dollet (CNRS, Grenoble) for cell deformation using the tensor analysis (right). The tensor ellipses are aligned with the polarity of the hairs. **(F)** Posterior *stbm6* mutant tissue at TP5 stained for E-cadherin (left), actin to visualize hair outgrowth (middle), and analyzed with tensor analysis (right). The tensors do not change in the region were hair polarity defects occur and appear to be coordinated similarly to wild type.

To understand if aspects of cell shape not solely described by polygon identity but by cell isometry or deformation were responsible for hair polarity defects in PCP mutants we performed a tensor analysis on images of PCP mutant tissues at hair outgrowth (Figure 33D-F, and not shown). The tensor analysis was developed to quantify local deformations of soap bubbles in order to describe strain in foams that are subjected to mechanical stress. The texture tensor is obtained by assigning bubble edges in a subregion of the image to a vector matrix, whose averaged eigenvalues are represented as a length and width of a tensor ellipse (Figure 33D). With this representation one can visualize geometrical intuition of bubble or cell deformation in any given image. The texture tensor ellipses in Figure 33F, however, reveal that the strain in cells close to hair polarity defects is not different to the strain experienced by cells in regions with normal polarity, or as in wild type cells (Figure 33E,F). Thus, hair polarity does not appear to be directly influenced by cell shape or packing topology in PCP mutants.

3.14. In PCP mutants Flamingo polarizes inefficiently but determines the site of hair outgrowth

What other mechanisms might misdirect hair polarity in these mutants? To understand which mechanisms organize local alignment of hairs in the PCP mutants we asked whether Flamingo and other PCP proteins may still be able to form residual cortical domains that could control hair outgrowth. A wide variety of studies have shown that clones of cells mutant for single

PCP proteins fail to polarize the distribution of remaining PCP proteins, although surrounding wild type cells have done so (Bastock et al 2003, Shimada et al 2001, Tree et al 2002b). On the other hand though, Flamingo has been observed to polarize to some extent when the entire wing is mutant for *diego*. In this case, Flamingo polarization occurs later than normal and along an abnormal axis (Feiguin et al 2001) indicating that a *diego* null mutant is not null for forming coupled proximal and distal domains (Figure 34). Furthermore, the different PCP mutants exhibit different stereotypical global hair patterns. However, if each PCP mutant entirely inhibited organization of hair polarity and only depended on the same unknown mechanism of locally aligning hairs, then all PCP mutants should exhibit the same hair pattern of whorls. Furthermore, the enhancement of polarity defects in PCP mutants by *shibire* (Figure 26G,H) could be explained by the enhancement of inefficient polarization in the context of junctional remodeling in a residually polarizing background.

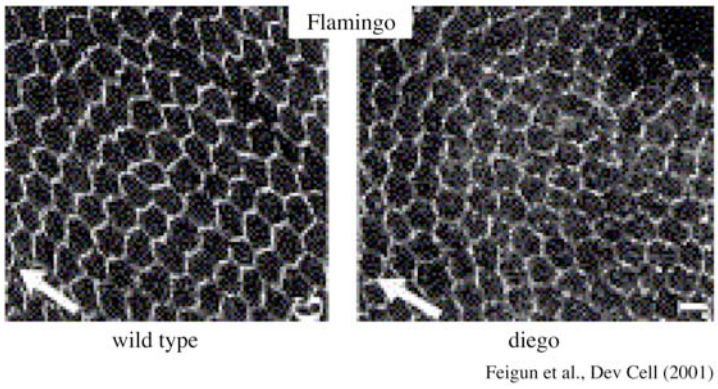

Figure 34 Flamingo polarizes incorrectly in the PCP mutant *diego*

Both images are wing epithelia stained for Flamingo before hair formation and imaged between veins 4 and 5. Wild type tissue is on the left, a *diego380* mutant wing on the right. There, Flamingo is abnormally polarized in whorls (Feiguin et al 2001).

To understand whether PCP mutants other than *diego* are also able to polarize cortical domains, albeit inefficiently, we stained several PCP mutant wings at the time of hair outgrowth for Flamingo as a marker for coupled cortical domains. While Flamingo polarization was clearly less complete than in wild type wings, residual Flamingo polarity was observed in many regions of *pk1*, *pk30*, *stbm6* and *stbm153* mutant wings. However, the axis along which Flamingo polarized was often defective (Figure 35 and not shown). To see whether altered Flamingo polarity presaged hair misorientation, we stained *pk30* pupal wings with phalloidin to detect filamentous actin. Figure 35A and D show that hair orientation is predicted by the polarity of Flamingo localization, whether it is normal (Figure 35E) or abnormal (Figure 35B).

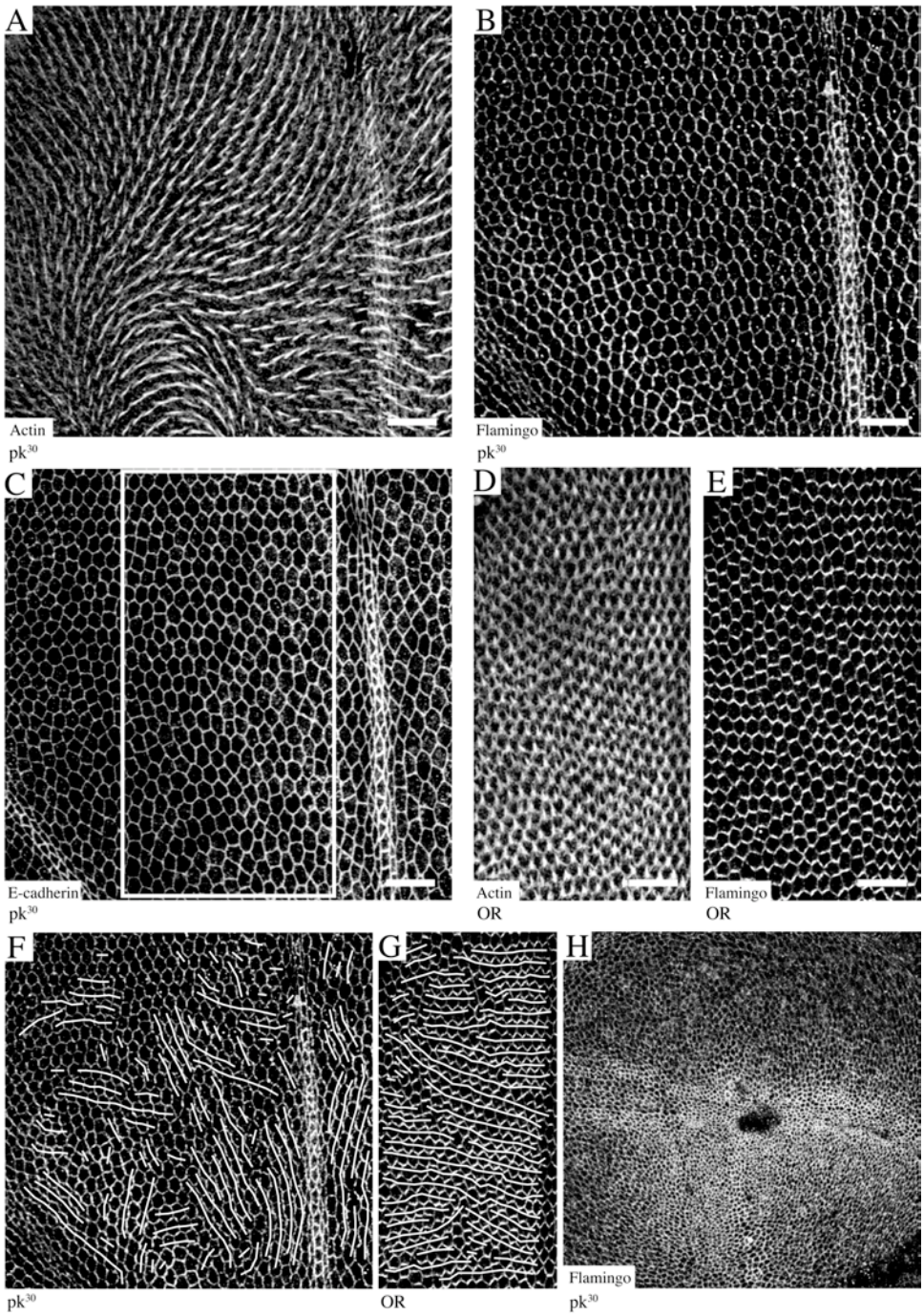

Figure 35 Incorrect Flamingo polarity in *pk30/ pk30* wings presages hair misorientation

(A-C) *pk30/pk30* mutant pupal wing at hair outgrowth stained for Actin (A), Flamingo (B) and E-cadherin (C). **(D,E)** Wild type wing in the same region as outlined by the box in (C) stained for Actin (D) and Flamingo (E). **(F,G)** Regions of coherent Flamingo polarity are connected by white lines drawn through boundaries lacking Flamingo to better visualize incorrect polarization in *pk30/pk30* wings (F) compared to wild-type (G). **(H)** A *pk30* mutant wing imaginal disc stain for Flamingo. Early polarity is disturbed (enlarged in Appendix I L, compare with Appendix I A,J).

Thus, two conclusions can be drawn: interfering with the function of one PCP protein does not prevent other PCP-proteins from polarizing, although they do so inefficiently. This suggests that in PCP mutant tissue the machinery that directs cortical domain polarity shows evidence of residual function. Most importantly, though, incorrectly polarized cortical domains may still direct hair outgrowth in PCP mutant wings.

Because the long-range alignment of cortical polarity and junction remodeling at the time of hexagonal packing appear to be interdependent events, one may suggest that failure of these mutants to complete junction remodeling interferes with normal alignment of the remaining members of the PCP cassette and misdirects hair outgrowth. We observed, however, that Flamingo polarity is already abnormal in PCP mutant wing imaginal discs (Figure 35H, Appendix I L). Flamingo localizes in a punctate pattern at the junctions of PCP-mutant disc cells; no coordination of Flamingo polarity between neighboring cells can be perceived. Early PCP-signaling appears to be important for determining hair polarity later on, therefore we cannot exclude that these early polarity defects solely underlie hair polarity defects in PCP mutants.

3.15. An endocytic compartment moves into the hair

We wondered whether the ability of Flamingo to bias membrane trafficking by recruiting Sec5-containing exocyst vesicles may also be utilized by cortical domains to coordinate hair outgrowth at the distal side of the cell. It is known that during hair outgrowth the apical microtubule and actin cytoskeleton polarizes towards the distal side of the cell and eventually fills the forming hair. Further observations suggest that also a endocytic membrane compartment enters the emerging hair (Figure 36A). Recycling endosomes labeled by DiI(C18) move into the hair (Suzanne Eaton, personal communication; Figure 36B,C).

Rab11:YFP endosomes become positioned at the base of the newly forming hair (Figure 36E), much in the same location where centrosomes localize at hair outgrowth (Heather Thompson, personal communcication). In many cells the recycling compartment is found close to the pericentriolar MTOC; and export to the cell surface depends on microtubules and kinesin (Apodaca 2001, Lin et al 2002). This may suggest that centrosome and Rab11 positioning at the base of the forming hair may be functionally linked. During later stages of hair outgrowth Rab11:YFP is found in punctate structures within the hair (not shown). Intriguingly, in pupal wings Sec5 strongly localizes to the forming hair (Figure 36D). We suggest that Sec5 localization in the emerging hair depends on the recruitment of Sec5 vesicles to the distal boundary and into the hair by Flamingo.

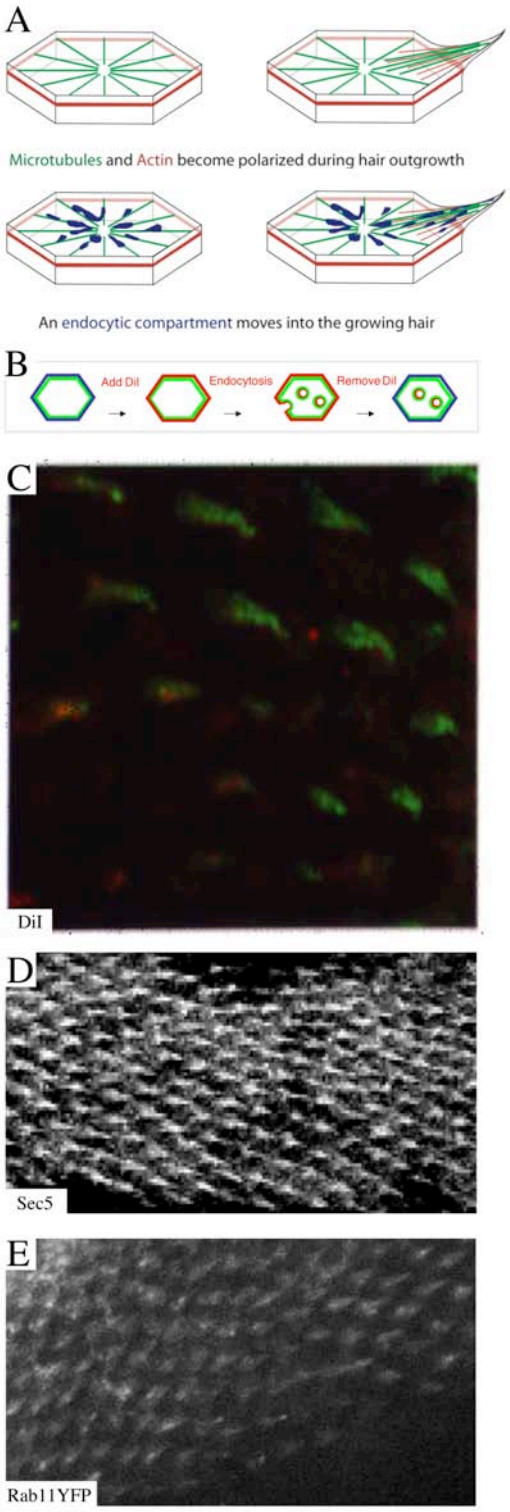

Figure 36 An endocytic compartment moves into hairs

(A) The microtubule (green) and actin (red) cytoskeleton polarizes at the distal side of the cell during hair outgrowth and polymerizes in the forming hair. A population of membrane vesicles derived from the endocytosis of plasma membrane moves into the forming hair. **(B)** The membrane dye DiI(C:18) is applied to live pupal wings at the time of hair outgrowth. The dye inserts into the outer leaflet of the plasma membrane and will be taken up quickly into the cell by

endocytosis. Dye remaining in the plasma membrane is washed off and then the fate of only endocytosed DiI(C18) labeled membrane can be visualized. **(C)** A pupal wing treated with DiI(C18) as in (B) at the time of hair outgrowth. Recycled DiI(C18) positive vesicles (green) move into forming hairs. **(D)** A pupal wing stained at the time of hair outgrowth for Sec5. **(E)** A live pupal wing expressing Rab11:YFP at the time of hair outgrowth. Rab11-positive endosomes become located at the base of the hair and move into the forming hair.

3.16. Membrane traffic supports hair outgrowth

To ask whether membrane traffic and exocyst function is required for hair outgrowth we examined hair morphology in *sec5, sec15* and in *shibire* mutant cells. Adult wings with clones of $sec5^{E13}$ or *sec15* mutant alleles display patches of short and stunted hairs (Figure 37A). This is not due to defects in actin polymerization in the forming hair (Figure 37B,C). Adult wings of *shibire* mutant animals shifted for 6 hours to 34ºC at the time of hair formation have short and stunted hairs (Figure 37D,E). This data indicates that exocyst and Dynamin-dependent membrane trafficking is required to support hair outgrowth potentially by delivering the membrane material that envelops the hair.

Based on these observations we suggest that PCP proteins affect cell packing and hair outgrowth independently but they may do so by the same mechanism: polarizing membrane traffic.

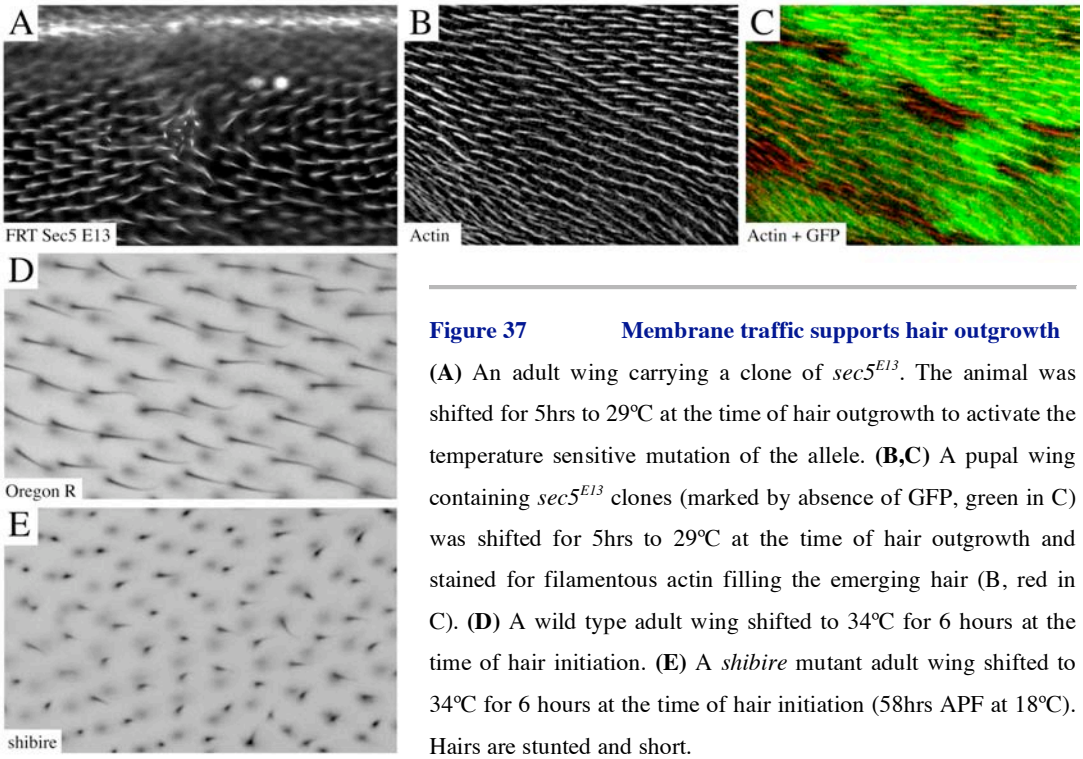

Figure 37 Membrane traffic supports hair outgrowth

(A) An adult wing carrying a clone of $sec5^{E13}$. The animal was shifted for 5hrs to 29ºC at the time of hair outgrowth to activate the temperature sensitive mutation of the allele. **(B,C)** A pupal wing containing $sec5^{E13}$ clones (marked by absence of GFP, green in C) was shifted for 5hrs to 29ºC at the time of hair outgrowth and stained for filamentous actin filling the emerging hair (B, red in C). **(D)** A wild type adult wing shifted to 34ºC for 6 hours at the time of hair initiation. **(E)** A *shibire* mutant adult wing shifted to 34ºC for 6 hours at the time of hair initiation (58hrs APF at 18ºC). Hairs are stunted and short.

4. Discussion

4.1. Junctional remodeling and polarized membrane traffic

Although a precise cell packing geometry is critical to the function of many tissues, the mechanisms that control cell packing are only beginning to be studied. Our data show the wing epithelium is irregularly packed throughout larval and pre-pupal development and is repacked into a quasi-hexagonal array shortly before hair outgrowth. We observe that during the process of hexagonal repacking cellular junctions are actively remodeled; they dynamically grow and shrink resulting in local neighbor exchanges. These events are able to mediate the changes in packing topology observed during hexagonal repacking.

Our data suggests that remodeling of junction and concurrent hexagonal packing in the pupal wing depends on cellular mechanisms that regulates the dynamic endocytic trafficking of E-cadherin. The loss of Dynamin or Rab11 function causes adherens junction components to rapidly disappear from the cortical region near cell vertices. Loss of E-cadherin occurs specifically when recycling and Dynamin-function is prevented during hexagonal repacking and not during earlier larval stages, suggesting that the requirement for E-cadherin recycling is particularly acute during pupal stages. Loss of E-cadherin is likely to reflect a direct effect on the trafficking of E-cadherin, because it occurs before cells enter apoptosis. Furthermore, E-cadherin is endocytosed rapidly by pupal wing cells, and can be found in Rab11-positive recycling endosomes. Consistent with this, E-cadherin is delivered to the cell surface via recycling endosomes in cultured epithelial cells (Lock & Stow 2005). We suggest that defects in E-cadherin localization in *dynamin* and Rab11 mutant cells reflects a failure to deliver E-cadherin from recycling endosomes to newly expanding junctions.

The fact that loss of Dynamin function and interfering with E-cadherin:α-catenin dissociation concomitantly perturbs the packing of the wing epithelial cells suggests that efficient endocytosis and recycling are necessary for successful remodeling of epithelial contacts.

We furthermore suggest that planar cell polarity proteins comprise an essential part of the cellular mechanism that dynamically disassembles and reassembles junctional complexes to achieve hexagonal packing. PCP proteins are required to develop hexagonal packing, and are non-uniformly distributed at junctions during remodeling. Final alignment of PCP proteins occurs at precisely the same time when epithelial packing is reorganized and E-cadherin recycling is needed for junctional remodeling. Our data raise the possibility that PCP proteins polarize trafficking of E-cadherin to specific sites at the cell cortex. The importance of PCP proteins in facilitating Dynamin-dependent E-cadherin trafficking first emerged when it became apparent that mutants in the PCP pathway strongly enhance E-cadherin recycling defects in the *shibire*-background.

We wondered whether PCP proteins may help to target E-cadherin-containing recycling endosomes to assembling junctions where they are needed to deliver E-cadherin. Consistent with this, it was previously reported that Strabismus cooperates with Z0-1 to deliver membrane to growing cellularization furrows during embryogenesis (Lee et al 2003) – a process that is known to involve trafficking through recycling endosomes (Pelissier et al 2003). Interestingly, we found that Sec5 positive vesicles concentrate near cortical regions rich in the PCP protein Flamingo at this time, and Flamingo over-expression recruits Sec5. Sec5 is part of the multiprotein exocyst complex that mediates polarized membrane delivery in a wide variety of contexts (Lipschutz & Mostov 2002). In the thorax, the exocyst promotes delivery of E-cadherin from recycling endosomes to the zonula adherens (Langevin et al 2005). An intriguing possibility is that PCP proteins, and particularly Flamingo, specify delivery of E-cadherin containing Sec5-vesicles to specific subregions of the zonula adherens where they are enriched.

Yet, we cannot rule out the alternative possibility that PCP proteins regulate endocytosis of junctional components. In the oocyte, Sec5 has been found to associate very early with Clathrin-coated pits and Yolkless-containing endosomes destined for recycling (Sommer et al 2005), therefore accumulation of Sec5 need not reflect delivery to the plasma membrane. However, only very few Rab5:CFP-positive endosomes co-localize with Sec5 in the pupal wing (not shown) indicating that, here, Sec5 may not function primarily at early endosomes.

We have not yet determined whether Sec5 is recruited to one or both sides of PCP boundaries and the mechanism by which PCP proteins recruit Sec5 vesicles remains to be addressed. Flamingo appears to be the most direct Sec5 recruitment regulator in the PCP machinery that we were able to identify. Flamingo localizes to both distal and proximal domains, thereby Sec5

could potentially be recruited to both. One possibility is that recruitment is mediated by activating Rho, a downstream effector of the PCP pathway (Winter et al 2001); in yeast, Rho1 and Rho3 interact directly with components of the exocyst and affect polarized delivery of vesicles to the bud and docking at the plasma membrane. Alternatively, PCP proteins, or Flamingo specifically, might recruit Sec5 simply by polarizing the actin cytoskeleton; exocyst vesicles travel to the yeast bud tip on polarized actin cables using myosin motors (Pruyne et al 1998). We show that the non-muscle myosin Zipper accumulates near PCP domains. Physical interaction between Flamingo and Sec5, or a role for Flamingo's suspected ability to signal through heterotrimeric G-proteins, should also be addressed in the future.

An intriguing speculation is that Flamingo polarizes exocyst-dependent membrane trafficking during hair outgrowth, too. PCP proteins appear to affect junctional remodeling and hair outgrowth independently, but they may do so by polarizing membrane traffic (Figure 37). We find that the Flamingo-target Sec5 and Rab11 move into emerging hairs. Furthermore, membrane traffic is clearly required to support hair outgrowth; *dynamin* and *Sec5*/*Sec15* mutant cells give rise to short and stunted hairs. We suggest that Flamingo and PCP proteins in addition to regulating actin and microtubule organization during hair formation may recruit Sec5-vesicles to the distal side of the cell to efficiently support hair outgrowth.

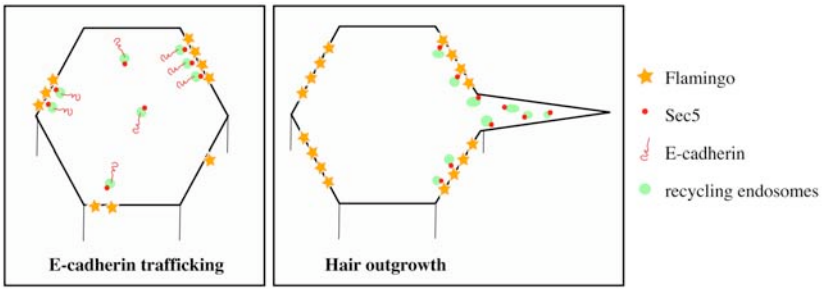

Figure 37 **Polarized membrane traffic is a new effector of PCP signaling in the *Drosophila* wing**

Flamingo recruits Sec5 containing membrane vesicle to cortical domains to regulate E-cadherin trafficking during junctional remodeling and hexagonal repacking. At a temporally separate context Flamingo may recruit Sec5 containing membrane vesicles to regulate membrane trafficking that supports hair outgrowth.

How exocyst recruitment is restricted to the distal side of the cell during hair outgrowth needs to be determined. Furthermore, whether hair membrane is derived exclusively from recycling endosomes or whether also post-Golgi membrane contributes to hair outgrowth can be easily

addressed. It will be interesting to analyze how hair outgrowth PCP mutant cells that form hairs in the cell center (*frizzled* and *flamingo*) regulate membrane trafficking and whether it is as efficient as at the distal cell cortex. However, actin filament formation in *flamingo* mutant cells is less successful (not shown). Membrane traffic depends on a functional actin cytoskeleton, therefore primary defects in membrane traffic may be difficult to distinguish from defects downstream of actin.

The conserved cassette of PCP proteins control a variety of seemingly different developmental processes, and no common cell biological mechanism has ever been proposed for their action (Copp et al 2003, Maurus & Kuhl 2004, McNeill 2002, Mlodzik 2002, Strutt 2003, Veeman et al 2003). Here we suggest that polarized membrane traffic may be a new and universal downstream effector of the PCP-signaling pathway. Polarizing membrane trafficking by recruiting Sec5 is a basic function that could be utilized in many different contexts, and may help explain the requirement of PCP proteins in a divergent set of processes. Rotation of photoreceptor clusters (McNeill 2002, Strutt & Strutt 2002b), convergent extension movements (Copp et al 2003, Maurus & Kuhl 2004), and development of the inner ear neuroepithelium (Wang et al 2005) depend on the ability of cells to make and break intercellular contacts, as they do during hexagonal packing in the wing (Figure 38); polarized membrane traffic may contribute to effectively remodel contacts. Consistent with this, Silberblick (Wnt-11) acts through the PCP pathway and also appears to affect endocytic trafficking of Cadherin during Zebrafish gastrulation (Ulrich et al 2005).

Furthermore, we suggest that an exocyst-dependent membrane pool may be recruited by PCP-proteins into the emerging hair to support outgrowth. This exocyst function would be independent of the role in remodeling of adhesion a few hours before hair outgrowth (Figure 37). Recruitment of exocyst components might also be a plausible mechanism to explain the ability of PCP proteins to bias Notch Delta signaling between R3 and R4 photoreceptors, since Delta delivery is dependent on the exocyst (Jafar-Nejad et al 2005). In future, identifying the chain of events that lead from PCP protein localization to exocyst recruitment may increase our understanding of these important processes.

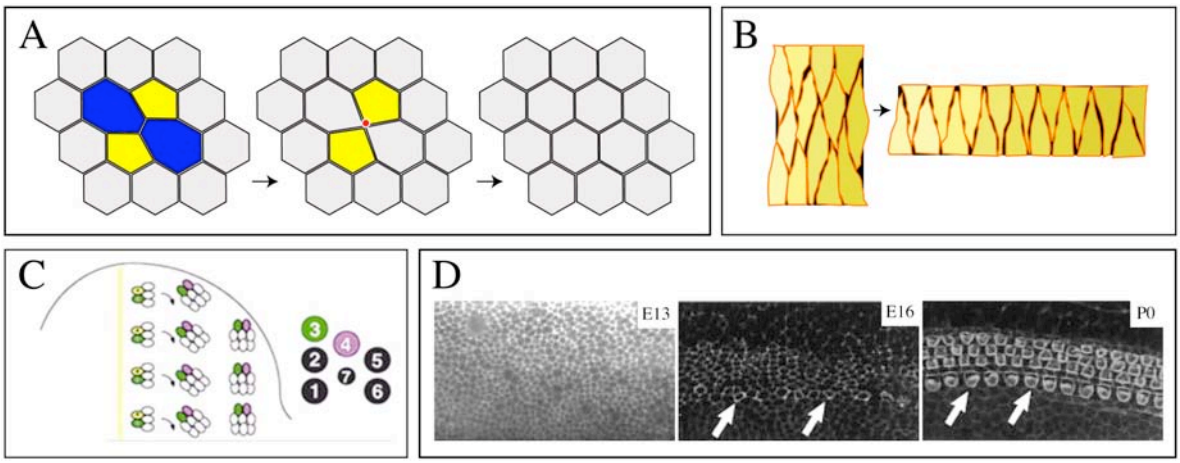

Figure 38 Dynamic modulation of intercellular contacts and the biasing of membrane trafficking via the exocyst complex may be the common cellular mechanism of PCP function

All examples in (A-D) rely on the function of the PCP proteins and remodeling of intercellular contacts for proper morphogenesis. The ability to polarize membrane traffic by PCP proteins may assist proper remodeling. **(A)** Junctional remodeling in the *Drosophila* pupal wing epithelium. **(B)** Convergent-extension during vertebrate gastrulation. **(C)** Ommatidial rotation in the *Drosophila* eye. Additionally, biasing Notch-signaling by biasing membrane trafficking may be important. **(D)** Mouse inner ear neuroepithelium morphogenesis. The cochlea extends using convergent-extension-like cell intercalation, after which the tissue is patterned by local cell rearrangements (adapted from McKenzie et al 2004).

4.2. Junctional remodeling and the establishment of polarity

The mechanisms that polarize the localization of proximal and distal PCP proteins to form coupled cortical domains, and the mechanisms that align PCP polarity within a field of cells have been the subject of intense investigation. Intracellular polarization of core PCP proteins appears to depend on a feedback loop in which the cortical accumulation of the proximal protein Prickle inhibits accumulation of the distal proteins Dishevelled and Frizzled. The loop is reinforced as Frizzled localized to distal membranes promotes the accumulation of Prickle on the boundary of the adjacent cell (Tree et al 2002b).

The mechanisms that determine the axis of global polarity across the wing have been more obscure. The atypical Cadherins Fat and Dachsous play crucial role in this process by impinging on *fz*/PCP signaling in a yet not well-understood way. It is clear that Dachsous and the Frizzled pathway must be active during late larval or prepupal stages to correctly specify the axis of cortical domain polarity, but cortical domains are not thought to actually polarize until much later during pupal development. Our data resolve this anomaly by showing that cortical domains do indeed polarize much earlier, at a time consistent with genetic requirements for Frizzled and Dachsous.

We show that PCP proteins are polarized during late larval and prepupal stages; their axis of polarity varies in different parts of the wing and is aligned between adjacent cells over much shorter distances than in the pupal wing. Specifically long-range alignment of cortical domains only occurs during pupal stages. We suggest that the feedback mechanism that acts between two neighboring cells to organize cortical polarity during pupal stages (Amonlirdviman et al 2005, Tree et al 2002b) probably operates also much earlier.

For future investigations our results will refocus the attention on identifying the polarity signal or "Factor X". It is clear that the first polarizing and axis-determining cue has to already signal during larval development. Since PCP-proteins are polarized even in very early wing imaginal discs (data not shown) the axis of polarity may be determined very early in development. Intriguingly, one modeling study (Le Garrec et al 2006) suggests that a global gradient that induces polarity should be relatively weak and short-lived; once a global polarity axis is established local coupling of cortical domain is sufficient to maintain it. It is fascinating to speculate that an early polarity axis could be retained throughout growth of the imaginal disc solely via local coupling between cells. Excitingly, a very recent paper describes polarization of PCP proteins in embryonic denticle belts where polarity establishment appears to require canonical Wingless and Hedgehog signaling (Price et al 2006). Furthermore, several studies have identified PCP signaling to be required for oriented cell division during organ growth and oriented reintegration of dividing cells both in vertebrate and *Drosophila* tissues (Baena-Lopez et al 2005, Ciruna et al 2006, Gong et al 2004). Based on these observations we suggest that a global polarity axis is established during embryonic development by transient signaling of classical morphogen pathways between segments and subsequently inherited throughout epidermal development into the wing primordium by local cortical coupling. The pathway could be critically required to spatially bias tissue growth and morphogenesis until pupal stages and, thus, determine adult organ shape.

Our data indicates that during pupal stages junctional remodeling and long-range alignment of polarized cortical domains occur at the same time and may be mechanistically related. When junctional remodeling is prevented by blocking Dynamin function, wing cells fail to align Flamingo polarity coherently and polarity defects in PCP mutants are enhanced. However, junctional remodeling does not appear to be required per se to establish polarized cortical domains. We show that partial cortical polarity is already established in imaginal discs, which do not appear to undergo junctional remodeling. Furthermore, individual *shibire* mutant cells are still polarized after a shift to the restrictive temperature; rather the alignment with polarized domains in neighboring cells is disrupted. We therefore suggest that junctional remodeling in the pupal wing is

needed to establish long-range coherence of cortical domain polarity. Conversely, cortical domain polarity may be directly instructive for junctional remodeling and hexagonal packing. Not only are PCP mutant cells mispacked, but also wild type cells whose proximal-distal polarity alignment has been disrupted by a proximal *frizzled*-clone imposing domineering non-autonomy effects.

PCP mutant cells were believed to not construct polarized cortical domains. Remaining PCP-proteins were reported to assume a uniform cortical distribution; therefore stereotypical hair polarity patterns in mutant wings were thought to be controlled by PCP-independent mechanisms. Is it then that defects in packing geometry directly perturb hair polarity in PCP mutant wings? Our data do not support this idea; we searched assiduously but without success for correlations between regions of irregular packing and hair polarity defects. Rather, we suggest that hair outgrowth in PCP mutants is directly misoriented by the residual activity of the PCP proteins themselves. We observe that the subcellular distribution of Flamingo is partially polarized in many PCP mutant backgrounds, although its polarity is often along an abnormal axis. Strikingly, this axis presages the alteration in hair orientation.

We cannot yet deduce the relationship between inefficient junctional remodeling and aberrant polarity in PCP mutant backgrounds. PCP mutants exhibit aberrant polarity in discs, potentially affecting the axis of polarity at later stages during hair outgrowth. Nevertheless, *shibire* enhances hair polarity defects in PCP mutants, suggesting that PCP mutants may rely as well on junctional remodeling for optimizing and aligning residual polarity, even along an aberrant axis.

4.3. Junctional remodeling and cellular mechanisms driving repacking

Our work presented in this thesis suggests that planar cell polarity proteins comprise an essential part of a molecular mechanism that dynamically traffics adhesion molecules to achieve hexagonal packing. Yet, what are the forces and signals that guide remodeling into a highly ordered array of hexagons at a very specific developmental stage?

Acquisition of a hexagonal packing geometry suggests forces that promote surface area minimization may influence packing geometry as they appear to do in the retina (Hayashi & Carthew 2004). Hexagonal packing represents the global energy minimum in cell packing systems where surface energy is directly proportional to surface area. This is true for bubbles in a two-dimensional foam; their surface area is minimized when the bubbles are packed as regular hexagons (Hales 2000). It is clear that epithelial cells with a complex biological architecture are not

simple bubbles and will not behave as such. However, under certain circumstances physical principles of foam behavior that are discussed below may guide the behavior of epithelial cells during junctional remodeling.

Hexagonal packing is only a low-energy configuration in an infinite array of close-packed cells. Quasi-hexagonal packing, as achieved during repacking in the pupal wing, represents the lowest energy state when fixed boundaries exist or where bubbles are not of identical sizes (Graner et al 2001); thus, the packing of intervein cells in the pupal wing may be the lowest energy arrangement when boundaries, such as veins and wing margin, and cell area variation are considered.

Even if hexagonal packing represented a global energy minimum, cells can only alter their packing geometry to conform to it if they are able to dynamically remodel their cell contacts and change neighbors. We observed that epithelial repacking occurs by growth and shrinkage of individual cell contacts that sometimes result in local neighbor exchanges after formation of a four-way vertex. This is not a trivial task. Like epithelial cells, bubbles change their neighbors by transient formation of a four-way vertex (see Figure 39) and the surface energy of this intermediate is always higher than either pair of three-fold vertices (Figure 39D-F). This means that soap bubbles, once irregularly packed, cannot reform into an hexagonal array without an input of energy (Figure 39G,H). Thus, cellular mechanisms may exist in the pupal wing to actively shrink and expand cell boundaries to drive the formation of 4-way vertices between cells. Live imaging suggests that the length of individual cell boundaries fluctuates. One role for these fluctuations might be to promote the transient formation of four-fold vertices and provide an opportunity for neighbor rearrangements to occur. The choice of a particular neighbor pair into which a four-fold vertex resolves might depend on which packing energy was more favorable; in foams, four-way vertices resolve quickly into one of an alternative pair of three-way vertices, depending on which pair represents the lowest energy configuration (Figure 39G,H) (Elias 1999). In the wing epithelium, however, numerous four-way vertices are observed in fixed and stained samples, and time-lapse imaging suggests that cells spend several minutes in this configuration before initiating the formation of new cell contacts (data not shown), suggesting that wing epithelial cells may not immediately approach local energy attractors by default.

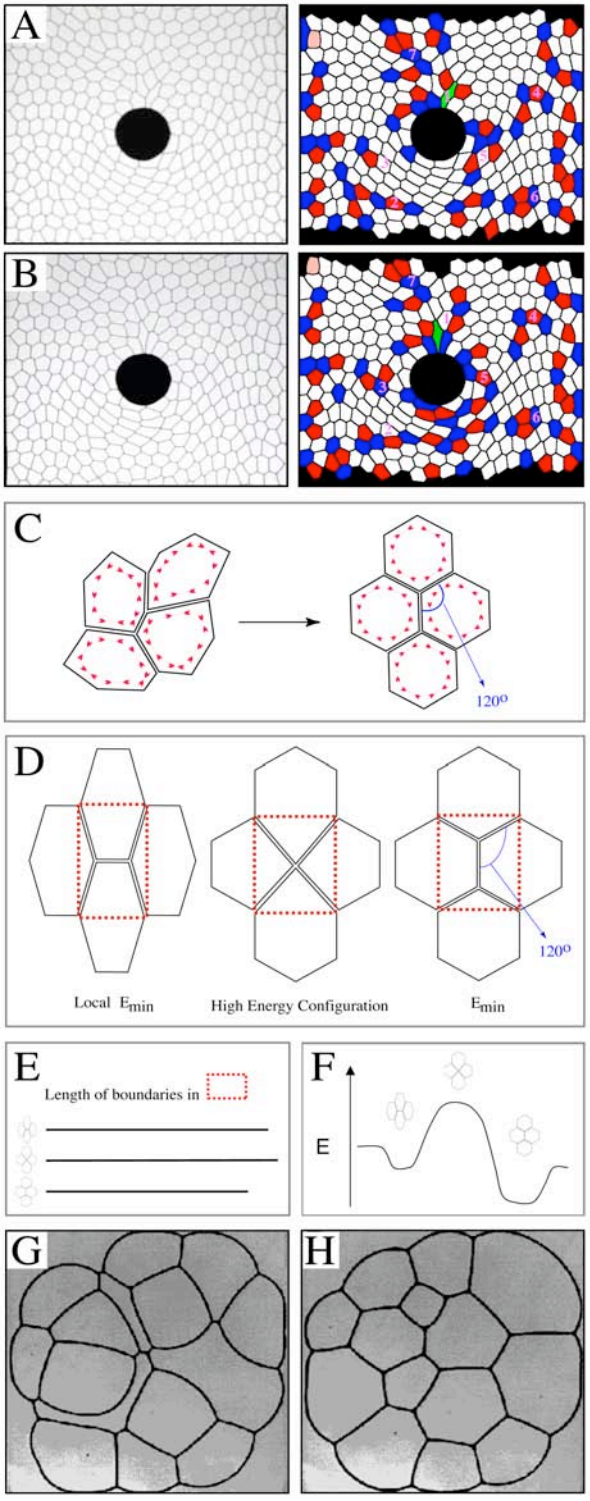

Figure 39 Physical principles governing behavior of two-dimensional foams

Images (A,B,G,H) are work of the group of Francois Graner (CNRS, Grenoble) and are accessible at this website: http://www-lsp.ujf-grenoble.fr/recherche/a3t2/a3t2a1/mousses2d3d.htm **(A,B)** Still images taken from a movie of a foam flowing past the round black obstacle in the middle (left panels). Images were analyzed for packing topology using

Mathlab (tetragon-green, pentagon-red, hexagon-white, heptagon-blue). Same bubbles are numbered in (A) and (B) to illustrate change in position and topology. When exposed to mechanical stress such as shear, the cells in the foam lattice will rearrange to find other local energy minima. This is mediated by neighbor exchanges, whereby the boundary between two threefold vertices shrinks to an unstable fourfold vertex that eventually decays into a new boundary lying perpendicular to the original boundary. Physical strain and topological defects induced by foam deformation are removed by such rearrangements that can travel over long distances through the lattice (Graner et al, 2001 and http://math.lanl.gov/~yi/foam.html). **(C)** Surface area of bubbles is proportional to the surface energy. If foams are not subjected to mechanical deformation then surface tension causes bubbles in an infinite lattice to meet at vertices with angles of 120° (Plateau's Rule). This means bubbles will pack as hexagons, the minimal energy configuration (Honeycomb conjecture recently proven by Hales, 2000). **(D-F**) Neighbor exchanges occur to find a minimal energy configuration. **(D)** Different close packing configurations of 4 bubbles are shown. The energy used to make contact between these 4 bubbles is proportional to the boundary length they share between them (F, red box in E). For the four bubbles to become packed in the absolute global energy minimum where all edges meet at 120° they have to rearrange their neighbors by side swapping. A transient four-way vertex mediates neighbor exchange. However, in this configuration cells share an even longer boundary with each other requiring energy to be provided for the formation of this configuration. A four-way vertex is intrinsically unstable and will quickly decay into the absolute minimal energy configuration where edges meet at 120ºC. Images (G,H) illustrate this mechanism. **(E)** The length of the lines are proportional to the boundary length the bubbles share between them in the different configuration. **(F)** Graphical representation of the energy stored in the different bubble configurations. **(G)** A stable disordered cluster of bubbles trapped in a local energy minimum with irregular cell shapes and high wall curvature. Energy is provided to the system to form transient four-way vertices to reach a lower energy minimum **(H)** by magnetic manipulation of vertices.

This may be due to the fact that although surface energy minimization might be the driving force behind remodeling and neighbor choice, it cannot act directly by simply causing cells to slip past each other. Rather, it must impinge on cellular mechanisms, such as cortical contraction, endocytosis or membrane recycling, to regulate the assembly and disassembly of cell contacts. Consistent with this, we find that recycling E-cadherin is required to support hexagonal packing. Intriguingly, accumulation of four-way vertices in *pk*, *pk-sple*, and *stbm* mutants suggests that recruitment of the required machinery for junction assembly at a four-way vertex is perturbed.

What other cellular and molecular mechanisms beside polarized endocytic trafficking might support assembly or disassembly of specific cell contacts? During *Drosophila* gastrulation, shrinkage of individual cell contacts depends on localized activity of the actin-motor myosin (Bertet et al 2004). We now show that MyosinII (Zipper) accumulates near Flamingo-rich cortical domains indicating that Myosin may be localized to specific junctions by PCP-proteins. There, Myosin II may mediate shrinkage or growth of junctions by impinging on the actin cytoskeleton. We furthermore observe polarized actin filament localization during early stages of remodeling;

this localization may indirectly depend on the activity of the PCP pathway. Rho, Rho-kinase and Myosin II are downstream targets of PCP proteins regulating actin dynamics during hair outgrowth (Winter et al 2001). The PCP-pathway may target these same molecules a few hours earlier during remodeling to regulate contractility at specific junctions, which are marked by asymmetric distribution of cortical domain. Interestingly, cortical actin-myosin driven contractility is also required for the endocytosis of E-cadherin in cultured epithelial cells (Sahai & Marshall 2002), suggesting that the two processes may be coordinated.

In summary, it is clear that the elements contributing to the surface energy of cells in tissue are extremely complex; intercellular adhesion, cortical contractility and volume constraints must all be considered. These forces may act in opposition to each other and may work within a tight equilibrium. Furthermore, adhesion and contractility may have different strengths at different junctions within an individual cell. A certain type of epithelial packing topology is likely to reflect the relative strengths of all of these contributing forces. A hexagonal epithelial packing geometry might represent an energy minimum only when forces that would tend to minimize the perimeter of individual cells (such as cortical contractility) become dominant. Since hexagonal packing only occurs during pupal stages it may be possible that cortical contractility specifically increase during this time. Interestingly, Waddington observes that the area of the wing contracts at the beginning of the pupal stage (Waddington 1941). During larval and prepupal stages other forces, such as differential adhesion between cells, may make competing contributions to surface energy creating irregular packing geometries.

In the future, it will be exciting to try to understand the nature of the signal that over several hours and specifically during pupal stages induces the cellular machinery for junctional remodeling and hexagonal packing to occur. The fact that planar cell polarity proteins already polarize during less dynamic wing imaginal disc stages (see below) suggests that such a signal may not be directly part of core PCP-signaling. Rather, initiation of mass junctional remodeling may require additional upstream Frizzled-independent signals.

5. Conclusion

The research undertaken during this thesis has provided important insight into the functional mechanism of planar cell polarity signaling that is essential for many different developmental processes. So far, it was not clear how outgrowth of a polarized structure in the *Drosophila* wing and convergent-extension movements during vertebrate gastrulation could be regulated by the same signaling pathway.

We show here that the planar cell polarity pathway is required to modulate intercellular adhesive contacts in the *Drosophila* wing epithelium. Modulation of cell adhesion is at the heart of hexagonal repacking, photoreceptor rotation, convergent extension and inner ear development. Therefore one of the basic cellular functions of planar cell polarity signaling may be the regulation of dynamic cell adhesion. In some contexts the PCP machinery may contribute to the development of regular tissue geometry.

Importantly, we identify polarized exocyst-dependent membrane traffic as the first basic cellular mechanism that can explain the role of PCP proteins in different developmental systems. Polarized membrane traffic can mediate trafficking of adhesion molecules during junctional remodeling, deliver membrane during hair outgrowth and bias notch-delta signaling during photoreceptor development.

6. Material and Methods

6.1. Fly Stocks

Fly Stocks	Kindly provided by:
Wild type Orgeon R flies	Bloomington
ptcGAL4	Bloomington
hs-flipase	Bloomington
FRT18 ubiP:GFP/FM7	Bloomington
FRT40 ubiP:GFP/bcg	Bloomington
FRT42 ubiP:GFP/Cyo	Bloomington
FRT80 ubiP:GFP/TM6b	Bloomington
FRT82 ubiP:GFP/TM6b	Bloomington
FRT18 *shi(1)ts* /FM7	Bloomington
FRT42 *fmi E59*	T. Uemura
FRT80 *fz P21*/TM6b	D. Strutt
FRT80 *fz R52*/TM6b	D. Strutt
FRT40 *sec5 E13* and FRT40 *sec5 E10*	S. Munro
FRT82 *sec15 1* and FRT83 *sec15 2*	H. Belen
UAS E-cad:a-Cat	U. Tepass
UAS< HcRed >Rab11SN	E. Marois
UbiP:E-cadherin:GFP	S. Tsukita
ArmP:Fz:GFP	D. Strutt
Squ:GFP	A. Brand
tubP:Rab5:CFP	S. Eaton lab
tubP:Rab11:YFP	S. Eaton lab
shibire ^{ts}	Bloomington
dgo380	S. Eaton lab

pk-sple1	Bloomington
pk-sple 13/26	D. Gubb
pk1	Bloomington
pk30	D. Gubb
stan3	P. Adler
stbm153	Bloomington
stbm6	Bloomington

6.2. Antibodies

Animal/Antigen	Dilution	Kindly provided by:	
Rat α-DE-cadherin	(1:100)	S. Tsukita	(Oda et al 1994)
Mouse α-Armadillo	(1:1000)	E. Wieschaus	(Riggleman et al 1990)
Guinea Pig α-Coracle	(1:3000)	R. Fehon	(Fehon et al 1994)
Mouse α-Flamingo	(1:20)	T. Uemura	(Usui et al 1999)
Rabbit α-Zipper	(1:500)	D. Kiehart	(Kiehart & Feghali 1986)
Rat α-Dsh	(1:1000)	J. Axelrod	(R. Nusse)
Rabbit α-Stbm	(1:500)	T. Wolff	(Rawls & Wolff 2003)
Rabbit α-Sec5	(1:1000)	S. Munroe	(Sommer et al 2005)
Guinea pig α-Sec6	(1:1000)	U. Tepass	(Beronja et al 2005)
Guinea pig α-Sec15	(1:2000)	H. Belen	(Jafar-Nejad et al 2005)

6.3. Reagents

Most reagents are standard products. More specific reagents are listed here:

Product	Supplier
Sodium Cacodylate	Sigma (Cat.: C0250)
Normal Goat Serum	GibcoBRL (Cat.: 16210-072)
Prolong Gold Antifade Mounting Medium	Molecular Probes (Cat.: P36934)

α-Tocopherol	Sigma (Cat.: T32510)
Ascorbic acid	Sigma (Cat.: A4544)
DiC18	Molecular Probes (Cat.: D7779)
FM4-64	Molecular Probes (Cat.: T3166)
Forceps 55	Fine Science Tools/Dumont
Microwell Minitrays 60 well/lid	Nunc (Cat.: 439225)

6.4. Methods

6.4.1. Immunofluorescence Microscopy

Pupal wings were dissected in fixative (8% (w/v) PFA, 200mM Sodium Cacodylate, 100mM Sucrose, 40mM Potassium Acetate, 10mM Sodium Acetate, 10mM EGTA) and washed in SPT (0.02% (w/v) Saponin + 0.02% (w/v) TritonX-100/PBS). Four pupae were dissected in parallel to allow for sufficient fixing in between dissection steps (takes 30 min). Dissection step 1: Front lid in pupal case was taken off and a little hole in the head cuticle was made. Step 2: Thoracic and abdominal interior was taken out though head region while pupae was still in pupal case. Special care was taken to remove larval salivary glands and gut. Step 3: The pupae was pulled out of pupal case holding on to the thoracic cuticle. Step 4: In a fresh drop of fixation a small opening into hinge cuticle was made to allow access of fixation to wing tissue. Wing tissue was allowed to fix in case for 5 min. Step 6: Wing was removed through opening by holding on to the hinge. Wing imaginal discs were dissected in PBS and fixed in 4%PFA/PBS for 20 min. Wing tissues were permeabilized for 30 min in PBT (0.1% (w/v) TritonX-100/PBS), washed in SPT, and then blocked for 30 min in SPN (SPT + 5% (w/v) normal goat serum). Wings were transferred to microtitre plates (Nalge Nunc) with 3-4 wings per well. Primary antibodies/SPN (see antibodies section) were incubated @ 4°C overnight, washed in SPT, blocked in SPN and incubated with secondary antibodies in SPN for 3 hours at RT, then mounted (ProLong Antifade) and imaged on a Zeiss Confocal Microscope.

6.4.2. Live Imaging

Pupal wings were dissected out of the pupal case but retained in pupal cuticle. Wing imaginal discs were dissected away from larval cuticle. Wings were mounted in imaging flow chambers built from

double-stick tape. Grace's or Schneiders medium with or without FM4-64, and with 10 μM -tocopherol (Vitamine E) and 1 mM ascorbic acid (Vitamine C) was used as a imaging medium.

6.4.3. Automated image analysis

Cell neighborhood analysis was performed using Cellenger software (Definiens AG, Munich) with a specifically developed ruleset for the packing analysis. Briefly, Cellenger uses hierarchical classification to selectively combine small groups of pixels into larger objects such as cells, borders, and junctions. First, the algorithm classified "seed" regions in the center of each cell, defined as local regions of lowest pixel intensity. Seeds were expanded by iteratively adding pixels, which bordered the seed, first adding darker and then lighter pixels. Simultaneous growth of all seeds in this manner resulted in good general convergence of seed perimeters with cell boundaries; which were finally optimized by edge smoothing. In their fully-grown state the seeds were classified as cells. All images were closely checked visually for mistakes in boundary recognition. If image contrast was poor, manual clean up of cell boundaries was required.
The algorithm then quantified neighbor number by counting cells in direct contact with each cell in the image. A boundary had to be at least 4 pixels long to be considered as the side of a cell. Below 4 pixels, the boundary was classified as a four-fold vertex. Cells, which were only partly contained at the edge of the image, were completely excluded from analysis. The outermost perimeter of cells completely contained within the image were classified as "edge" cells. Edge cells were counted as the neighbors of other cells, but the number of neighbors for edge cells was not counted.
Cell borders and vertices were classified in the following manner. For each cell a perimeter 2 pixels deep was reclassified as "border". The border pixels from all cells were combined into a single object having the appearance of a meshwork. Intersection points were identified by attempting to overlay the meshwork with a variety of branched patterns. Those places where a branching pattern could be completely fit within the border meshwork were re-classified as "vertex". Vertices were further classified as three-fold or four-fold vertices according to the number of cells they contacted. Border pixels between vertices retained the classification "border"; with each border now representing the common boundary between two cells. All images were closely checked visually for mistakes in vertex and border recognition. Images were cleaned up manually if required.
Statistical data about the number of neighbor classes, cell perimeter, cell area and individual boundary length between two vertices was provided by the Cellenger algorithm.

6.4.4. Data processing and statistics

Raw data output from Cellenger was further processed and analyzed using Microsoft Excel software.

Output 1 - Cell objects and Polygon identity

1. Objects not designated as "3er,4er,5er,6er,7er,8er" polygons but "cells" were deleted – "cells" were 3-5 badly identified cell objects per image and were thus neglected (~ 0.005% error)
2. Objects were sorted according to "existence of vein super-object" :
   1 = vein cell
   0 = intervein cell
3. The total number of only intervein cells were considered a 100% and further analyzed for percentage of different polygon classes, perimeter and area of all cells and perimeter and area within individual polygon classes.

Output 2 – Cell-cell contacts and vertex identity

Output was separated into cell-cell contact data ("border") and vertex data ("3er" and "4er").

For vertex data

1. Vertex data was sorted and split into "3er" and "4er" vertices
2. Erroneous vertex data was often generated in edge regions of the image and needed to be filtered out. Therefore, the total sum of neighbors for each vertex was identified by adding up values in "number of neighbors"-columns and data was then sorted ascending/descending to the total sum (0 = no neighbor; > 0 = number of neighbors). Advantageously, vein cells at this stage have lost their polygon class identity hence they would not be considered twice in this analysis.
   Number of total neighbors had to correspond to vertex identity of "3er" (=3) or "4er" (=4) for the vertex to be included in analysis. For reasons of pixel assignments by Cellenger during border identification also "3er" vertices with 2 neighbors and "4er" vertices with 3 neighbors were included.
3. Then the columns "Number of vein cell" neighbors and "Number of edge" neighbors were summed up for each vertex and data was then sorted ascending/descending to the sum.

4. The sum of these two columns had to be at least 2 for 3er and 3 for 4er vertices or 'Total number of all neighbors –1' for them to be included in the analysis – other vertices either lied in vein or edge regions.
5. Sum of the now remaining vertices in "3er" and "4er" class were counted as 100%.

For cell-cell contact ("border") data

1. Erroneous "border" data was often generated in edge regions of the image and needed to be filtered out. Therefore, the total sum of neighbors for each border was identified by adding up values in "number of neighbors"-columns and data was then sorted ascending/descending to the total sum (0 = no neighbor; > 0 = number of neighbors).
2. Since each cell-cell contact or "border" should only have two neighbors, all "borders" having more than 2 neighbors were omitted from further analysis.
   Then the columns "Number of vein cell" neighbors and "Number of edge" neighbors were summed up for each "border" and data was then sorted ascending/descending to the sum. The sum of these two columns had to be at least 1 for borders to be included in the analysis – other borders either lied in vein or edge regions.
3. Remaining borders, which did not have a vein or edge neighbor were counted twice because both neighboring intervein cells were included in polygon analysis – this accounts for the fact that "borders" to vein or edge cells technically only contribute one 'side' to the analysis.
4. To determine the length of each cell contact the "perimeter" of each "border" was divided by 2; this is giving the "border" length relative to the pixel dimensions of the image.

Calculation of cell-cell contact length variation in mutant background as percentage relative to wild type

Variation was calculated using following equation:

{(Standard deviation of average junction length / average junction length) $_{mutant}$ / (Standard deviation of average cell perimeter / average cell perimeter) $_{mutant}$} / {(Standard deviation of average junction length / average junction length) $_{wild\ type}$ / (Standard deviation of average cell perimeter / average cell perimeter) $_{wild\ type}$} x 100

7. References

Adler PN. 2002. Planar signaling and morphogenesis in Drosophila. *Dev Cell* 2: 525-35

Adler PN, Charlton J, Jones KH, Liu J. 1994. The cold-sensitive period for frizzled in the development of wing hair polarity ends prior to the start of hair morphogenesis. *Mech Dev* 46: 101-7

Adler PN, Krasnow RE, Liu J. 1997. Tissue polarity points from cells that have higher Frizzled levels towards cells that have lower Frizzled levels. *Curr Biol* 7: 940-9

Adler PN, Zhu C, Stone D. 2004. Inturned localizes to the proximal side of wing cells under the instruction of upstream planar polarity proteins. *Curr Biol* 14: 2046-51

Amonlirdviman K, Khare NA, Tree DR, Chen WS, Axelrod JD, Tomlin CJ. 2005. Mathematical modeling of planar cell polarity to understand domineering nonautonomy. *Science* 307: 423-6

Ang AL, Taguchi T, Francis S, Folsch H, Murrells LJ, et al. 2004. Recycling endosomes can serve as intermediates during transport from the Golgi to the plasma membrane of MDCK cells. *J Cell Biol* 167: 531-43

Apodaca G. 2001. Endocytic traffic in polarized epithelial cells: role of the actin and microtubule cytoskeleton. *Traffic* 2: 149-59

Axelrod JD, Miller JR, Shulman JM, Moon RT, Perrimon N. 1998. Differential recruitment of Dishevelled provides signaling specificity in the planar cell polarity and Wingless signaling pathways. *Genes Dev* 12: 2610-22

Baena-Lopez LA, Baonza A, Garcia-Bellido A. 2005. The orientation of cell divisions determines the shape of Drosophila organs. *Curr Biol* 15: 1640-4

Barros CS, Phelps CB, Brand AH. 2003. Drosophila nonmuscle myosin II promotes the asymmetric segregation of cell fate determinants by cortical exclusion rather than active transport. *Dev Cell* 5: 829-40

Bastock R, Strutt H, Strutt D. 2003. Strabismus is asymmetrically localised and binds to Prickle and Dishevelled during Drosophila planar polarity patterning. *Development* 130: 3007-14

Beronja S, Laprise P, Papoulas O, Pellikka M, Sisson J, Tepass U. 2005. Essential function of Drosophila Sec6 in apical exocytosis of epithelial photoreceptor cells. *J Cell Biol* 169: 635-46

Bertet C, Sulak L, Lecuit T. 2004. Myosin-dependent junction remodelling controls planar cell intercalation and axis elongation. *Nature* 429: 667-71

Bloor JW, Kiehart DP. 2002. Drosophila RhoA regulates the cytoskeleton and cell-cell adhesion in the developing epidermis. *Development* 129: 3173-83

Boutros M, Mlodzik M. 1999. Dishevelled: at the crossroads of divergent intracellular signaling pathways. *Mech Dev* 83: 27-37

Braga VM. 2002. Cell-cell adhesion and signalling. *Curr Opin Cell Biol* 14: 546-56

Brodsky MH, Steller H. 1996. Positional information along the dorsal-ventral axis of the Drosophila eye: graded expression of the four-jointed gene. *Dev Biol* 173: 428-46

Bryant DM, Stow JL. 2004. The ins and outs of E-cadherin trafficking. *Trends Cell Biol* 14: 427-34

Cantalupo G, Alifano P, Roberti V, Bruni CB, Bucci C. 2001. Rab-interacting lysosomal protein (RILP): the Rab7 effector required for transport to lysosomes. *Embo J* 20: 683-93

Carreira-Barbosa F, Concha ML, Takeuchi M, Ueno N, Wilson SW, Tada M. 2003. Prickle 1 regulates cell movements during gastrulation and neuronal migration in zebrafish. *Development* 130: 4037-46

Chen W, ten Berge D, Brown J, Ahn S, Hu LA, et al. 2003. Dishevelled 2 recruits beta-arrestin 2 to mediate Wnt5A-stimulated endocytosis of Frizzled 4. *Science* 301: 1391-4

Chen YT, Stewart DB, Nelson WJ. 1999. Coupling assembly of the E-cadherin/beta-catenin complex to efficient endoplasmic reticulum exit and basal-lateral membrane targeting of E-cadherin in polarized MDCK cells. *J Cell Biol* 144: 687-99

Cho E, Irvine KD. 2004. Action of fat, four-jointed, dachsous and dachs in distal-to-proximal wing signaling. *Development* 131: 4489-500

Christoforidis S, McBride HM, Burgoyne RD, Zerial M. 1999. The Rab5 effector EEA1 is a core component of endosome docking. *Nature* 397: 621-5

Ciruna B, Jenny A, Lee D, Mlodzik M, Schier AF. 2006. Planar cell polarity signalling couples cell division and morphogenesis during neurulation. *Nature* 439: 220-4

Clark HF, Brentrup D, Schneitz K, Bieber A, Goodman C, Noll M. 1995. Dachsous encodes a member of the cadherin superfamily that controls imaginal disc morphogenesis in Drosophila. *Genes Dev* 9: 1530-42

Collier S, Lee H, Burgess R, Adler P. 2005. The WD40 repeat protein Fritz links cytoskeletal planar polarity to Frizzled subcellular localization in the Drosophila epidermis. *Genetics*

Cong F, Schweizer L, Varmus H. 2004. Casein kinase Iepsilon modulates the signaling specificities of dishevelled. *Mol Cell Biol* 24: 2000-11

Copp AJ, Greene ND, Murdoch JN. 2003. The genetic basis of mammalian neurulation. *Nat Rev Genet* 4: 784-93

Daniel JM, Reynolds AB. 1997. Tyrosine phosphorylation and cadherin/catenin function. *Bioessays* 19: 883-91

Das G, Jenny A, Klein TJ, Eaton S, Mlodzik M. 2004. Diego interacts with Prickle and Strabismus/Van Gogh to localize planar cell polarity complexes. *Development* 131: 4467-76

Das G, Reynolds-Kenneally J, Mlodzik M. 2002. The atypical cadherin Flamingo links Frizzled and Notch signaling in planar polarity establishment in the Drosophila eye. *Dev Cell* 2: 655-66

Deneka M, Neeft M, van der Sluijs P. 2003. Regulation of membrane transport by rab GTPases. *Crit Rev Biochem Mol Biol* 38: 121-42

Djiane A, Riou J, Umbhauer M, Boucaut J, Shi D. 2000. Role of frizzled 7 in the regulation of convergent extension movements during gastrulation in Xenopus laevis. *Development* 127: 3091-100

Eaton S. 2003. Cell biology of planar polarity transmission in the Drosophila wing. *Mech Dev* 120: 1257-64

Eaton S, Wepf R, Simons K. 1996. Roles for Rac1 and Cdc42 in planar polarization and hair outgrowth in the wing of Drosophila. *J Cell Biol* 135: 1277-89

Elias F, Flament, C., Glazier, J., Graner, R. and Y. Jiang. 1999. Foams out of stable equilibrium: cell elongation and side swapping. *Phil. Mag*. 5: 729-51

Fanto M, Clayton L, Meredith J, Hardiman K, Charroux B, et al. 2003. The tumor-suppressor and cell adhesion molecule Fat controls planar polarity via physical interactions with Atrophin, a transcriptional co-repressor. *Development* 130: 763-74

Fanto M, Mayes CA, Mlodzik M. 1998. Linking cell-fate specification to planar polarity: determination of the R3/R4 photoreceptors is a prerequisite for the interpretation of the Frizzled mediated polarity signal. *Mech Dev* 74: 51-8

Fanto M, Mlodzik M. 1999. Asymmetric Notch activation specifies photoreceptors R3 and R4 and planar polarity in the Drosophila eye. *Nature* 397: 523-6

Fanto M, Weber U, Strutt DI, Mlodzik M. 2000. Nuclear signaling by Rac and Rho GTPases is required in the establishment of epithelial planar polarity in the Drosophila eye. *Curr Biol* 10: 979-88

Fehon R, Dawson I, Artavnis-Tsakonas S. 1994. A *Drosophla* homologue of membrane-skeleton protein 4.1 is associated with septate junctions and is encoded by the *coracle* gene. *Development* 120: 545-57

Feiguin F, Hannus M, Mlodzik M, Eaton S. 2001. The ankyrin repeat protein Diego mediates Frizzled-dependent planar polarization. *Dev Cell* 1: 93-101

Fielding AB, Schonteich E, Matheson J, Wilson G, Yu X, et al. 2005. Rab11-FIP3 and FIP4 interact with Arf6 and the exocyst to control membrane traffic in cytokinesis. *Embo J* 24: 3389-99

Fischer E, Legue E, Doyen A, Nato F, Nicolas JF, et al. 2006. Defective planar cell polarity in polycystic kidney disease. *Nat Genet* 38: 21-3

Fristrom D. 1988. The cellular basis of epithelial morphogenesis. A review. *Tissue Cell* 20: 645-90

Fristrom DK. 1982. Septate junctions in imaginal disks of Drosophila: a model for the redistribution of septa during cell rearrangement. *J Cell Biol* 94: 77-87

Fujita Y, Krause G, Scheffner M, Zechner D, Leddy HE, et al. 2002. Hakai, a c-Cbl-like protein, ubiquitinates and induces endocytosis of the E-cadherin complex. *Nat Cell Biol* 4: 222-31

Fukata M, Nakagawa M, Kaibuchi K. 2003. Roles of Rho-family GTPases in cell polarisation and directional migration. *Curr Opin Cell Biol* 15: 590-7

Garriock RJ, D'Agostino SL, Pilcher KC, Krieg PA. 2005. Wnt11-R, a protein closely related to mammalian Wnt11, is required for heart morphogenesis in Xenopus. *Dev Biol* 279: 179-92

Gates J, Peifer M. 2005. Can 1000 reviews be wrong? Actin, alpha-Catenin, and adherens junctions. *Cell* 123: 769-72

Gaullier JM, Simonsen A, D'Arrigo A, Bremnes B, Stenmark H. 1999. FYVE finger proteins as effectors of phosphatidylinositol 3-phosphate. *Chem Phys Lipids* 98: 87-94

Gong Y, Mo C, Fraser SE. 2004. Planar cell polarity signalling controls cell division orientation during zebrafish gastrulation. *Nature* 430: 689-93

Graner F, Jiang Y, Janiaud E, Flament C. 2001. Equilibrium states and ground state of two-dimensional fluid foams. *Phys Rev E Stat Nonlin Soft Matter Phys* 63: 011402

Grindstaff KK, Yeaman C, Anandasabapathy N, Hsu SC, Rodriguez-Boulan E, et al. 1998. Sec6/8 complex is recruited to cell-cell contacts and specifies transport vesicle delivery to the basal-lateral membrane in epithelial cells. *Cell* 93: 731-40

Gruenberg J. 2001. The endocytic pathway: a mosaic of domains. *Nat Rev Mol Cell Biol* 2: 721-30

Gubb D. 1993. Genes controlling cellular polarity in Drosophila. *Dev Suppl*: 269-77

Gubb D, Garcia-Bellido A. 1982. A genetic analysis of the determination of cuticular polarity during development in Drosophila melanogaster. *J Embryol Exp Morphol* 68: 37-57

Gubb D, Green C, Huen D, Coulson D, Johnson G, et al. 1999. The balance between isoforms of the prickle LIM domain protein is critical for planar polarity in Drosophila imaginal discs. *Genes Dev* 13: 2315-27

Gumbiner BM. 2000. Regulation of cadherin adhesive activity. *J Cell Biol* 148: 399-404

Gumbiner BM. 2005. Regulation of cadherin-mediated adhesion in morphogenesis. *Nat Rev Mol Cell Biol* 6: 622-34

Guo N, Hawkins C, Nathans J. 2004. Frizzled6 controls hair patterning in mice. *Proc Natl Acad Sci U S A* 101: 9277-81

Habas R, Kato Y, He X. 2001. Wnt/Frizzled activation of Rho regulates vertebrate gastrulation and requires a novel Formin homology protein Daam1. *Cell* 107: 843-54

Hales TC. 2000. The honeycomb conjecture. *http://xxx.lanl.gov/abs/math.MG/9906042*

Hannus M, Feiguin F, Heisenberg CP, Eaton S. 2002. Planar cell polarization requires Widerborst, a B' regulatory subunit of protein phosphatase 2A. *Development* 129: 3493-503

Hawkins RD, Lovett M. 2004. The developmental genetics of auditory hair cells. *Hum Mol Genet* 13 Spec No 2: R289-96

Hayashi T, Carthew RW. 2004. Surface mechanics mediate pattern formation in the developing retina. *Nature* 431: 647-52

Heisenberg CP, Tada M, Rauch GJ, Saude L, Concha ML, et al. 2000. Silberblick/Wnt11 mediates convergent extension movements during zebrafish gastrulation. *Nature* 405: 76-81

Henderson DJ, Phillips HM, Chaudhry B. 2006. Vang-like 2 and noncanonical Wnt signaling in outflow tract development. *Trends Cardiovasc Med* 16: 38-45

Hicke L, Riezman H. 1996. Ubiquitination of a yeast plasma membrane receptor signals its ligand-stimulated endocytosis. *Cell* 84: 277-87

Hinshaw JE. 2000. Dynamin and its role in membrane fission. *Annu Rev Cell Dev Biol* 16: 483-519

Hoekstra D, Tyteca D, van ISC. 2004. The subapical compartment: a traffic center in membrane polarity development. *J Cell Sci* 117: 2183-92

Honda H, Ogita Y, Higuchi S, Kani K. 1982. Cell movements in a living mammalian tissue: long-term observation of individual cells in wounded corneal endothelia of cats. *J Morphol* 174: 25-39

Hull BE, Staehelin LA. 1976. Functional significance of the variations in the geometrical organization of tight junction networks. *J Cell Biol* 68: 688-704

Itoh K, Antipova A, Ratcliffe MJ, Sokol S. 2000. Interaction of dishevelled and Xenopus axin-related protein is required for wnt signal transduction. *Mol Cell Biol* 20: 2228-38

Ivanov AI, McCall IC, Parkos CA, Nusrat A. 2004a. Role for actin filament turnover and a myosin II motor in cytoskeleton-driven disassembly of the epithelial apical junctional complex. *Mol Biol Cell* 15: 2639-51

Ivanov AI, Nusrat A, Parkos CA. 2004b. Endocytosis of epithelial apical junctional proteins by a clathrin-mediated pathway into a unique storage compartment. *Mol Biol Cell* 15: 176-88

Jacinto A, Martinez-Arias A, Martin P. 2001. Mechanisms of epithelial fusion and repair. *Nat Cell Biol* 3: E117-23

Jafar-Nejad H, Andrews H, Acar M, Bayat V, Wirtz-Peitz f, et al. 2005. Sec15, a component of the exocyst, promotes Notch signaling during asymmetric division of Drosophila sensory organ precursors. *Dev. Cell* in press

Jeffers M, Taylor GA, Weidner KM, Omura S, Vande Woude GF. 1997. Degradation of the Met tyrosine kinase receptor by the ubiquitin-proteasome pathway. *Mol Cell Biol* 17: 799-808

Jenny A, Reynolds-Kenneally J, Das G, Burnett M, Mlodzik M. 2005. Diego and Prickle regulate Frizzled planar cell polarity signalling by competing for Dishevelled binding. *Nat Cell Biol*

Jiang D, Munro EM, Smith WC. 2005. Ascidian prickle regulates both mediolateral and anterior-posterior cell polarity of notochord cells. *Curr Biol* 15: 79-85

Kaibuchi K, Kuroda S, Fukata M, Nakagawa M. 1999. Regulation of cadherin-mediated cell-cell adhesion by the Rho family GTPases. *Curr Opin Cell Biol* 11: 591-6

Kamei T, Matozaki T, Sakisaka T, Kodama A, Yokoyama S, et al. 1999. Coendocytosis of cadherin and c-Met coupled to disruption of cell-cell adhesion in MDCK cells--regulation by Rho, Rac and Rab small G proteins. *Oncogene* 18: 6776-84

Katanaev VL, Ponzielli R, Semeriva M, Tomlinson A. 2005. Trimeric G protein-dependent frizzled signaling in Drosophila. *Cell* 120: 111-22

Katoh M. 2005. Epithelial-mesenchymal transition in gastric cancer (Review). *Int J Oncol* 27: 1677-83

Kiehart DP, Feghali R. 1986. Cytoplasmic myosin from Drosophila melanogaster. *J Cell Biol* 103: 1517-25

Kilian B, Mansukoski H, Barbosa FC, Ulrich F, Tada M, Heisenberg CP. 2003. The role of Ppt/Wnt5 in regulating cell shape and movement during zebrafish gastrulation. *Mech Dev* 120: 467-76

Kim GH, Han JK. 2005. JNK and ROKalpha function in the noncanonical Wnt/RhoA signaling pathway to regulate Xenopus convergent extension movements. *Dev Dyn* 232: 958-68

Kishida S, Yamamoto H, Hino S, Ikeda S, Kishida M, Kikuchi A. 1999. DIX domains of Dvl and axin are necessary for protein interactions and their ability to regulate beta-catenin stability. *Mol Cell Biol* 19: 4414-22

Langevin J, Morgan M, Rosse C, Racine V, Sibarita J, et al. 2005. Drosophila Exocyst components Sec5, Sec6, and Sec15 regulate DE-Cadherin trafficking from recycling endosomes to the plasma membrane. *Dev Cell* 9: 1-12

Lawrence PA, Casal J, Struhl G. 2002. Towards a model of the organisation of planar polarity and pattern in the Drosophila abdomen. *Development* 129: 2749-60

Le Bivic A. 2005. E-cadherin-mediated adhesion is not the founding event of epithelial cell polarity in Drosophila. *Trends Cell Biol* 15: 237-40

Le Garrec JF, Lopez P, Kerszberg M. 2006. Establishment and maintenance of planar epithelial cell polarity by asymmetric cadherin bridges: a computer model. *Dev Dyn* 235: 235-46

Le TL, Joseph SR, Yap AS, Stow JL. 2002. Protein kinase C regulates endocytosis and recycling of E-cadherin. *Am J Physiol Cell Physiol* 283: C489-99

Le TL, Yap AS, Stow JL. 1999. Recycling of E-cadherin: a potential mechanism for regulating cadherin dynamics. *J Cell Biol* 146: 219-32

Lecuit T, Wieschaus E. 2002. Junctions as organizing centers in epithelial cells? A fly perspective. *Traffic* 3: 92-7

Lee H, Adler PN. 2002. The function of the frizzled pathway in the Drosophila wing is dependent on inturned and fuzzy. *Genetics* 160: 1535-47

Lee H, Adler PN. 2004. The grainy head transcription factor is essential for the function of the frizzled pathway in the Drosophila wing. *Mech Dev* 121: 37-49

Lee OK, Frese KK, James JS, Chadda D, Chen ZH, et al. 2003. Discs-Large and Strabismus are functionally linked to plasma membrane formation. *Nat Cell Biol* 5: 987-93

Lee S, Kolodziej PA. 2002. The plakin Short Stop and the RhoA GTPase are required for E-cadherin-dependent apical surface remodeling during tracheal tube fusion. *Development* 129: 1509-20

Lilien J, Balsamo J. 2005. The regulation of cadherin-mediated adhesion by tyrosine phosphorylation/dephosphorylation of beta-catenin. *Curr Opin Cell Biol* 17: 459-65

Lim J, Norga KK, Chen Z, Choi KW. 2005. Control of planar cell polarity by interaction of DWnt4 and four-jointed. *Genesis* 42: 150-61

Lin SX, Gundersen GG, Maxfield FR. 2002. Export from pericentriolar endocytic recycling compartment to cell surface depends on stable, detyrosinated (glu) microtubules and kinesin. *Mol Biol Cell* 13: 96-109

Lipschutz JH, Mostov KE. 2002. Exocytosis: the many masters of the exocyst. *Curr Biol* 12: R212-4

Liu G, Bafico A, Aaronson SA. 2005. The mechanism of endogenous receptor activation functionally distinguishes prototype canonical and noncanonical Wnts. *Mol Cell Biol* 25: 3475-82

Lock JG, Stow JL. 2005. Rab11 in recycling endosomes regulates the sorting and basolateral transport of E-cadherin. *Mol Biol Cell* 16: 1744-55

Ma D, Yang CH, McNeill H, Simon MA, Axelrod JD. 2003. Fidelity in planar cell polarity signalling. *Nature* 421: 543-7

Magie CR, Pinto-Santini D, Parkhurst SM. 2002. Rho1 interacts with p120ctn and alpha-catenin, and regulates cadherin-based adherens junction components in Drosophila. *Development* 129: 3771-82

Marois E, Mahmoud A, Eaton S. 2006. The endocytic pathway and formation of the Wingless morphogen gradient. *Development* 133: 307-17

Matakatsu H, Blair SS. 2004. Interactions between Fat and Dachsous and the regulation of planar cell polarity in the Drosophila wing. *Development* 131: 3785-94

Matusek T, Djiane A, Jankovics F, Brunner D, Mlodzik M, Mihaly J. 2006. The Drosophila formin DAAM regulates the tracheal cuticle pattern through organizing the actin cytoskeleton. *Development* 133: 957-66

Maurus D, Kuhl M. 2004. Getting an embryo into shape. *Bioessays* 26: 1272-5

Maxfield FR, McGraw TE. 2004. Endocytic recycling. *Nat Rev Mol Cell Biol* 5: 121-32

McGuire SE, Mao Z, Davis RL. 2004. Spatiotemporal gene expression targeting with the TARGET and gene-switch systems in Drosophila. *Sci STKE* 2004: pl6

McKenzie E, Krupin A, Kelley MW. 2004. Cellular growth and rearrangement during the development of the mammalian organ of Corti. *Dev Dyn* 229: 802-12

McNeill H. 2002. Planar polarity: location, location, location. *Curr Biol* 12: R449-51

Metzger RJ, Krasnow MA. 1999. Genetic control of branching morphogenesis. *Science* 284: 1635-9

Miranda KC, Khromykh T, Christy P, Le TL, Gottardi CJ, et al. 2001. A dileucine motif targets E-cadherin to the basolateral cell surface in Madin-Darby canine kidney and LLC-PK1 epithelial cells. *J Biol Chem* 276: 22565-72

Mlodzik M. 2002. Planar cell polarization: do the same mechanisms regulate Drosophila tissue polarity and vertebrate gastrulation? *Trends Genet* 18: 564-71

Murray JW, Wolkoff AW. 2003. Roles of the cytoskeleton and motor proteins in endocytic sorting. *Adv Drug Deliv Rev* 55: 1385-403

Murray RZ, Jolly LA, Wood SA. 2004. The FAM deubiquitylating enzyme localizes to multiple points of protein trafficking in epithelia, where it associates with E-cadherin and beta-catenin. *Mol Biol Cell* 15: 1591-9

Nagafuchi A, Ishihara S, Tsukita S. 1994. The roles of catenins in the cadherin-mediated cell adhesion: functional analysis of E-cadherin-alpha catenin fusion molecules. *J Cell Biol* 127: 235-45

Nardi J, Magee-Adams S. 1986. Formation of scale spacing patterns in a moth wing. *Dev Biol* 116: 278-90

Nikko E, Marini AM, Andre B. 2003. Permease recycling and ubiquitination status reveal a particular role for Bro1 in the multivesicular body pathway. *J Biol Chem* 278: 50732-43

Nilsson D. 1989. Optics and Evolution of the Compound Eye. In *Facets of Vision*, ed. Stavenga/Hardie, pp. 30-73. Berlin Heidelberg: Springer-Verlag

Noselli S, Agnes F. 1999. Roles of the JNK signaling pathway in Drosophila morphogenesis. *Curr Opin Genet Dev* 9: 466-72

Oda H, Tsukita S. 1999. Dynamic features of adherens junctions during Drosophila embryonic epithelial morphogenesis revealed by a Dalpha-catenin-GFP fusion protein. *Dev Genes Evol* 209: 218-25

Oda H, Tsukita S. 2001. Real-time imaging of cell-cell adherens junctions reveals that Drosophila mesoderm invagination begins with two phases of apical constriction of cells. *J Cell Sci* 114: 493-501

Oda H, Uemura T, Harada Y, Iwai Y, Takeichi M. 1994. A Drosophila homolog of cadherin associated with armadillo and essential for embryonic cell-cell adhesion. *Dev Biol* 165: 716-26

Palacios F, Price L, Schweitzer J, Collard JG, D'Souza-Schorey C. 2001. An essential role for ARF6-regulated membrane traffic in adherens junction turnover and epithelial cell migration. *Embo J* 20: 4973-86

Palacios F, Schweitzer JK, Boshans RL, D'Souza-Schorey C. 2002. ARF6-GTP recruits Nm23-H1 to facilitate dynamin-mediated endocytosis during adherens junctions disassembly. *Nat Cell Biol* 4: 929-36

Palacios F, Tushir JS, Fujita Y, D'Souza-Schorey C. 2005. Lysosomal targeting of E-cadherin: a unique mechanism for the down-regulation of cell-cell adhesion during epithelial to mesenchymal transitions. *Mol Cell Biol* 25: 389-402

Pan WJ, Pang SZ, Huang T, Guo HY, Wu D, Li L. 2004. Characterization of function of three domains in dishevelled-1: DEP domain is responsible for membrane translocation of dishevelled-1. *Cell Res* 14: 324-30

Paricio N, Feiguin F, Boutros M, Eaton S, Mlodzik M. 1999. The Drosophila STE20-like kinase misshapen is required downstream of the Frizzled receptor in planar polarity signaling. *Embo J* 18: 4669-78

Paterson AD, Parton RG, Ferguson C, Stow JL, Yap AS. 2003. Characterization of E-cadherin endocytosis in isolated MCF-7 and chinese hamster ovary cells: the initial fate of unbound E-cadherin. *J Biol Chem* 278: 21050-7

Pece S, Gutkind JS. 2002. E-cadherin and Hakai: signalling, remodeling or destruction? *Nat Cell Biol* 4: E72-4

Pelissier A, Chauvin JP, Lecuit T. 2003. Trafficking through Rab11 endosomes is required for cellularization during Drosophila embryogenesis. *Curr Biol* 13: 1848-57

Penton A, Wodarz A, Nusse R. 2002. A mutational analysis of dishevelled in Drosophila defines novel domains in the dishevelled protein as well as novel suppressing alleles of axin. *Genetics* 161: 747-62

Perez-Moreno M, Jamora C, Fuchs E. 2003. Sticky business: orchestrating cellular signals at adherens junctions. *Cell* 112: 535-48

Pfeffer SR. 2001. Rab GTPases: specifying and deciphering organelle identity and function. *Trends Cell Biol* 11: 487-91

Phillips HM, Murdoch JN, Chaudhry B, Copp AJ, Henderson DJ. 2005. Vangl2 acts via RhoA signaling to regulate polarized cell movements during development of the proximal outflow tract. *Circ Res* 96: 292-9

Povelones M, Howes R, Fish M, Nusse R. 2005. Genetic evidence that Drosophila frizzled controls planar cell polarity and Armadillo signaling by a common mechanism. *Genetics* 171: 1643-54

Price MH, Roberts DM, McCartney BM, Jezuit E, Peifer M. 2006. Cytoskeletal dynamics and cell signaling during planar polarity establishment in the Drosophila embryonic denticle. *J Cell Sci* 119: 403-15

Prigent M, Dubois T, Raposo G, Derrien V, Tenza D, et al. 2003. ARF6 controls post-endocytic recycling through its downstream exocyst complex effector. *J Cell Biol* 163: 1111-21

Pruyne DW, Schott DH, Bretscher A. 1998. Tropomyosin-containing actin cables direct the Myo2p-dependent polarized delivery of secretory vesicles in budding yeast. *J Cell Biol* 143: 1931-45

Rawls AS, Wolff T. 2003. Strabismus requires Flamingo and Prickle function to regulate tissue polarity in the Drosophila eye. *Development* 130: 1877-87

Riezman H, Munn A, Geli MI, Hicke L. 1996. Actin-, myosin- and ubiquitin-dependent endocytosis. *Experientia* 52: 1033-41

Riggleman B, Schedl P, Wieschaus E. 1990. Spatial expression of the Drosophila segment polarity gene armadillo is posttranscriptionally regulated by wingless. *Cell* 63: 549-60

Roberts WM, Howard J, Hudspeth AJ. 1988. Hair cells: transduction, tuning, and transmission in the inner ear. *Annu Rev Cell Biol* 4: 63-92

Robinson MS. 2004. Adaptable adaptors for coated vesicles. *Trends Cell Biol* 14: 167-74

Robinson MS, Bonifacino JS. 2001. Adaptor-related proteins. *Curr Opin Cell Biol* 13: 444-53

Rousset R, Mack JA, Wharton KA, Jr., Axelrod JD, Cadigan KM, et al. 2001. Naked cuticle targets dishevelled to antagonize Wnt signal transduction. *Genes Dev* 15: 658-71

Rulifson EJ, Wu CH, Nusse R. 2000. Pathway specificity by the bifunctional receptor frizzled is determined by affinity for wingless. *Mol Cell* 6: 117-26

Saburi S, McNeill H. 2005. Organising cells into tissues: new roles for cell adhesion molecules in planar cell polarity. *Curr Opin Cell Biol* 17: 482-8

Sahai E, Marshall CJ. 2002. ROCK and Dia have opposing effects on adherens junctions downstream of Rho. *Nat Cell Biol* 4: 408-15

Seabra MC, Coudrier E. 2004. Rab GTPases and myosin motors in organelle motility. *Traffic* 5: 393-9

Sever S. 2002. Dynamin and endocytosis. *Curr Opin Cell Biol* 14: 463-7

Shimada Y, Usui T, Yanagawa S, Takeichi M, Uemura T. 2001. Asymmetric colocalization of Flamingo, a seven-pass transmembrane cadherin, and Dishevelled in planar cell polarization. *Curr Biol* 11: 859-63

Shipitsin M, Feig LA. 2004. RalA but not RalB enhances polarized delivery of membrane proteins to the basolateral surface of epithelial cells. *Mol Cell Biol* 24: 5746-56

Simonsen A, Lippe R, Christoforidis S, Gaullier JM, Brech A, et al. 1998. EEA1 links PI(3)K function to Rab5 regulation of endosome fusion. *Nature* 394: 494-8

Sommer B, Oprins A, Rabouille C, Munro S. 2005. The exocyst component Sec5 is present on endocytic vesicles in the oocyte of Drosophila melanogaster. *J Cell Biol* 169: 953-63

Struhl G, Barbash DA, Lawrence PA. 1997. Hedgehog acts by distinct gradient and signal relay mechanisms to organise cell type and cell polarity in the Drosophila abdomen. *Development* 124: 2155-65

Strutt D. 2003. Frizzled signalling and cell polarisation in Drosophila and vertebrates. *Development* 130: 4501-13

Strutt DI. 2001. Asymmetric localization of frizzled and the establishment of cell polarity in the Drosophila wing. *Mol Cell* 7: 367-75

Strutt DI. 2002. The asymmetric subcellular localisation of components of the planar polarity pathway. *Semin Cell Dev Biol* 13: 225-31

Strutt DI, Weber U, Mlodzik M. 1997. The role of RhoA in tissue polarity and Frizzled signalling. *Nature* 387: 292-5

Strutt H, Mundy J, Hofstra K, Strutt D. 2004. Cleavage and secretion is not required for Four-jointed function in Drosophila patterning. *Development* 131: 881-90

Strutt H, Strutt D. 2002a. Nonautonomous planar polarity patterning in Drosophila: dishevelled-independent functions of frizzled. *Dev Cell* 3: 851-63

Strutt H, Strutt D. 2002b. Planar polarity: photoreceptors on a high fat diet. *Curr Biol* 12: R384-5

Strutt H, Strutt D. 2003. EGF signaling and ommatidial rotation in the Drosophila eye. *Curr Biol* 13: 1451-7

Strutt H, Strutt D. 2005. Long-range coordination of planar polarity in Drosophila. *Bioessays* 27: 1218-27

Tanaka-Matakatsu M, Uemura T, Oda H, Takeichi M, Hayashi S. 1996. Cadherin-mediated cell adhesion and cell motility in Drosophila trachea regulated by the transcription factor Escargot. *Development* 122: 3697-705

Tardieu A. 1988. Eye lens proteins and transparency: from light transmission theory to solution X-ray structural analysis. *Annu Rev Biophys Biophys Chem* 17: 47-70

Taylor J, Abramova N, Charlton J, Adler PN. 1998. Van Gogh: a new Drosophila tissue polarity gene. *Genetics* 150: 199-210

Tepass U, Gruszynski-DeFeo E, Haag TA, Omatyar L, Torok T, Hartenstein V. 1996. shotgun encodes Drosophila E-cadherin and is preferentially required during cell rearrangement in the neurectoderm and other morphogenetically active epithelia. *Genes Dev* 10: 672-85

Tepass U, Hartenstein V. 1994. The development of cellular junctions in the Drosophila embryo. *Dev Biol* 161: 563-96

Tepass U, Tanentzapf G, Ward R, Fehon R. 2001. Epithelial cell polarity and cell junctions in Drosophila. *Annu Rev Genet* 35: 747-84

TerBush DR, Maurice T, Roth D, Novick P. 1996. The Exocyst is a multiprotein complex required for exocytosis in Saccharomyces cerevisiae. *Embo J* 15: 6483-94

Tilney L, Saunders JC. 1983. Actin Filaments, stereocilia, and hair cells of the bird cochlea I. Length, number, width, and distribution of stereocilia of each hair cell are related to the position of the hair cell on the cochlea. *J. Cell Biol.*: 807-21

Tilney LG, Tilney MS, Saunders JS, DeRosier DJ. 1986. Actin filiaments, stereocilia, and hair cells of the bird cochlea III. The development and differentiation of hair cells and stereocilia. *Dev. Biol.* 116: 100-18

Tree DR, Ma D, Axelrod JD. 2002a. A three-tiered mechanism for regulation of planar cell polarity. *Semin Cell Dev Biol* 13: 217-24.

Tree DR, Shulman JM, Rousset R, Scott MP, Gubb D, Axelrod JD. 2002b. Prickle mediates feedback amplification to generate asymmetric planar cell polarity signaling. *Cell* 109: 371-81

Turner CM, Adler PN. 1998. Distinct roles for the actin and microtubule cytoskeletons in the morphogenesis of epidermal hairs during wing development in Drosophila. *Mech Dev* 70: 181-92

Uemura T, Oda H, Kraut R, Hayashi S, Kotaoka Y, Takeichi M. 1996. Zygotic Drosophila E-cadherin expression is required for processes of dynamic epithelial cell rearrangement in the Drosophila embryo. *Genes Dev* 10: 659-71

Ueno N, Greene ND. 2003. Planar cell polarity genes and neural tube closure. *Birth Defects Res C Embryo Today* 69: 318-24

Ulrich F, Concha ML, Heid PJ, Voss E, Witzel S, et al. 2003. Slb/Wnt11 controls hypoblast cell migration and morphogenesis at the onset of zebrafish gastrulation. *Development* 130: 5375-84

Ulrich F, Krieg M, Schotz EM, Link V, Castanon I, et al. 2005. Wnt11 Functions in Gastrulation by Controlling Cell Cohesion through Rab5c and E-Cadherin. *Dev Cell* 9: 555-64

Ungermann C, Langosch D. 2005. Functions of SNAREs in intracellular membrane fusion and lipid bilayer mixing. *J Cell Sci* 118: 3819-28

Usui T, Shima Y, Shimada Y, Hirano S, Burgess RW, et al. 1999. Flamingo, a seven-pass transmembrane cadherin, regulates planar cell polarity under the control of Frizzled. *Cell* 98: 585-95

van Dam EM, Stoorvogel W. 2002. Dynamin-dependent transferrin receptor recycling by endosome-derived clathrin-coated vesicles. *Mol Biol Cell* 13: 169-82

Veeman MT, Axelrod JD, Moon RT. 2003. A second canon. Functions and mechanisms of beta-catenin-independent Wnt signaling. *Dev Cell* 5: 367-77

Vinson CR, Adler PN. 1987. Directional non-cell autonomy and the transmission of polarity information by the frizzled gene of Drosophila. *Nature* 329: 549-51

Vinson CR, Conover S, Adler PN. 1989. A Drosophila tissue polarity locus encodes a protein containing seven potential transmembrane domains. *Nature* 338: 263-4

Waddington CH. 1941. The genetic control of wing development in Drosophila. *Journal of Genetics* 41: 75-139

Wang J, Mark S, Zhang X, Qian D, Yoo SJ, et al. 2005. Regulation of polarized extension and planar cell polarity in the cochlea by the vertebrate PCP pathway. *Nat Genet* 37: 980-5

Webb SD, Owen MR. 2004. Intra-membrane ligand diffusion and cell shape modulate juxtacrine patterning. *J Theor Biol* 230: 99-117

Wehrli M, Tomlinson A. 1995. Epithelial planar polarity in the developing Drosophila eye. *Development* 121: 2451-9

Wehrli M, Tomlinson A. 1998. Independent regulation of anterior/posterior and equatorial/polar polarity in the Drosophila eye; evidence for the involvement of Wnt signaling in the equatorial/polar axis. *Development* 125: 1421-32

Wheelock MJ, Johnson KR. 2003. Cadherin-mediated cellular signaling. *Curr Opin Cell Biol* 15: 509-14

Winter CG, Wang B, Ballew A, Royou A, Karess R, et al. 2001. Drosophila Rho-associated kinase (Drok) links Frizzled-mediated planar cell polarity signaling to the actin cytoskeleton. *Cell* 105: 81-91

Wolff T, Rubin GM. 1998. Strabismus, a novel gene that regulates tissue polarity and cell fate decisions in Drosophila. *Development* 125: 1149-59

Wong HC, Bourdelas A, Krauss A, Lee HJ, Shao Y, et al. 2003. Direct binding of the PDZ domain of Dishevelled to a conserved internal sequence in the C-terminal region of Frizzled. *Mol Cell* 12: 1251-60

Wong LL, Adler PN. 1993. Tissue polarity genes of Drosophila regulate the subcellular location for prehair initiation in pupal wing cells. *J Cell Biol* 123: 209-21

Wootton R. 1992. Functional morphology of insect wings. *Annu. Rev. Entomol.* 37: 113-40

Yan D, Wallingford JB, Sun TQ, Nelson AM, Sakanaka C, et al. 2001. Cell autonomous regulation of multiple Dishevelled-dependent pathways by mammalian Nkd. *Proc Natl Acad Sci U S A* 98: 3802-7

Yang CH, Axelrod JD, Simon MA. 2002. Regulation of Frizzled by fat-like cadherins during planar polarity signaling in the Drosophila compound eye. *Cell* 108: 675-88

Yap AS, Brieher WM, Gumbiner BM. 1997. Molecular and functional analysis of cadherin-based adherens junctions. *Annu Rev Cell Dev Biol* 13: 119-46

Yeaman C, Grindstaff KK, Nelson WJ. 2004. Mechanism of recruiting Sec6/8 (exocyst) complex to the apical junctional complex during polarization of epithelial cells. *J Cell Sci* 117: 559-70

Yun UJ, Kim SY, Liu J, Adler PN, Bae E, et al. 1999. The inturned protein of Drosophila melanogaster is a cytoplasmic protein located at the cell periphery in wing cells. *Dev Genet* 25: 297-305

Zajac A, Sun X, Zhang J, Guo W. 2005. Cyclical regulation of the exocyst and cell polarity determinants for polarized cell growth. *Mol Biol Cell* 16: 1500-12

Zallen J, Zallen R. 2004. Cell-pattern disordering during convergent extension in Drosophila. *Journal of Physics: Condensed Matter* 44: S5073-S80

Zerial M, McBride H. 2001. Rab proteins as membrane organizers. *Nat Rev Mol Cell Biol* 2: 107-17

Zhang XM, Ellis S, Sriratana A, Mitchell CA, Rowe T. 2004. Sec15 is an effector for the Rab11 GTPase in mammalian cells. *J Biol Chem* 279: 43027-34

Zhu S, Liu L, Korzh V, Gong Z, Low BC. 2006. RhoA acts downstream of Wnt5 and Wnt11 to regulate convergence and extension movements by involving effectors Rho Kinase and Diaphanous: Use of zebrafish as an in vivo model for GTPase signaling. *Cell Signal* 18: 359-72

Appendix I

Planar cell polarity during larval and pupal development

Appendix I A

A wing imaginal disc stained for Flamingo. Ventral and dorsal wing pouch regions are labeled on top of the image. A schematic representation of global Flamingo polarity is given. Compare with Appendix I B. Frizzled-GFP localizes in a similar fashion (Appendix I J).

Schematic representation of flamingo polarity in wing pouch

Ventral Dorsal Hinge folds

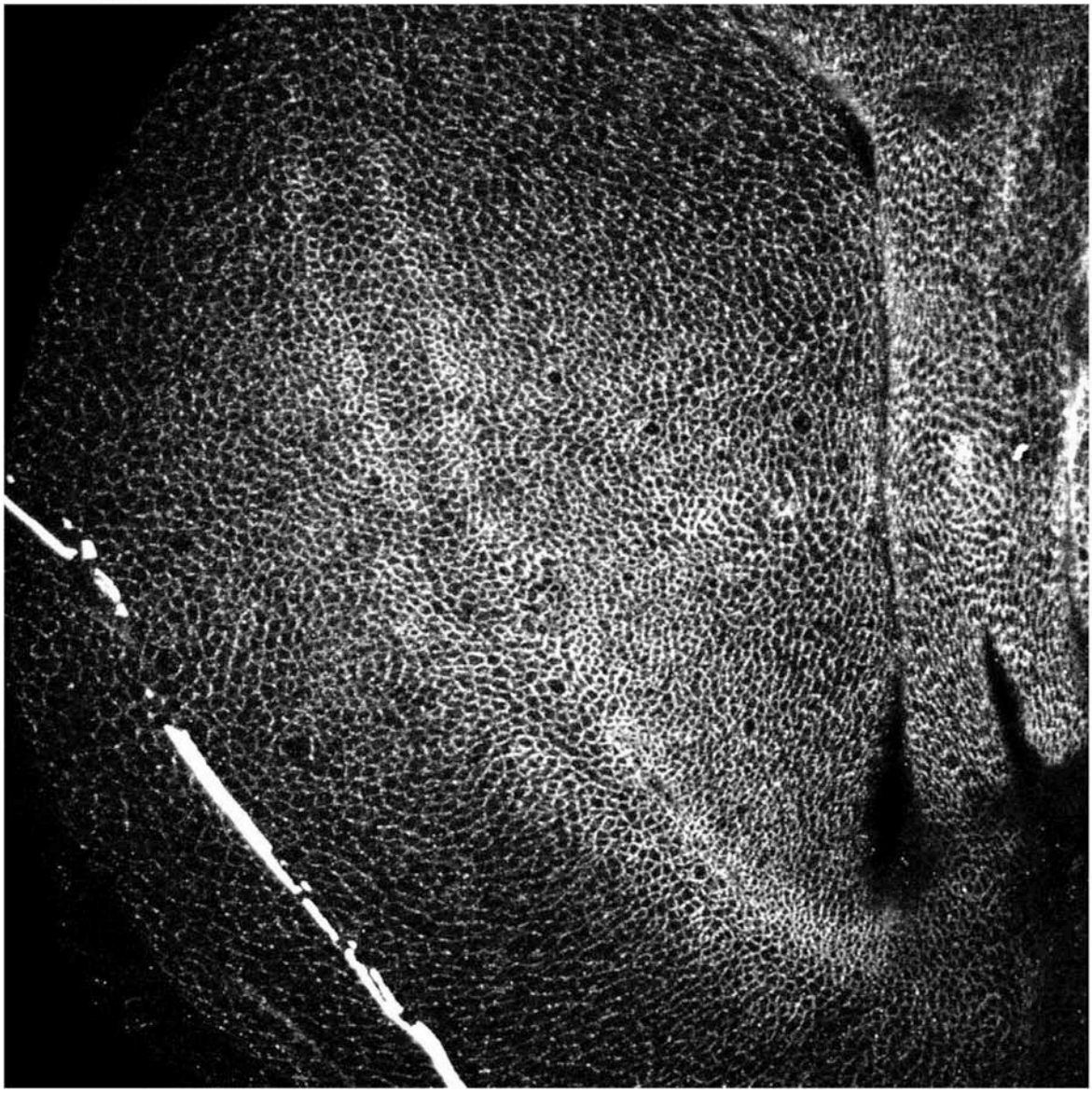

Appendix I B

The same wing imaginal disc as in Appendix I B stained for E-cadherin.

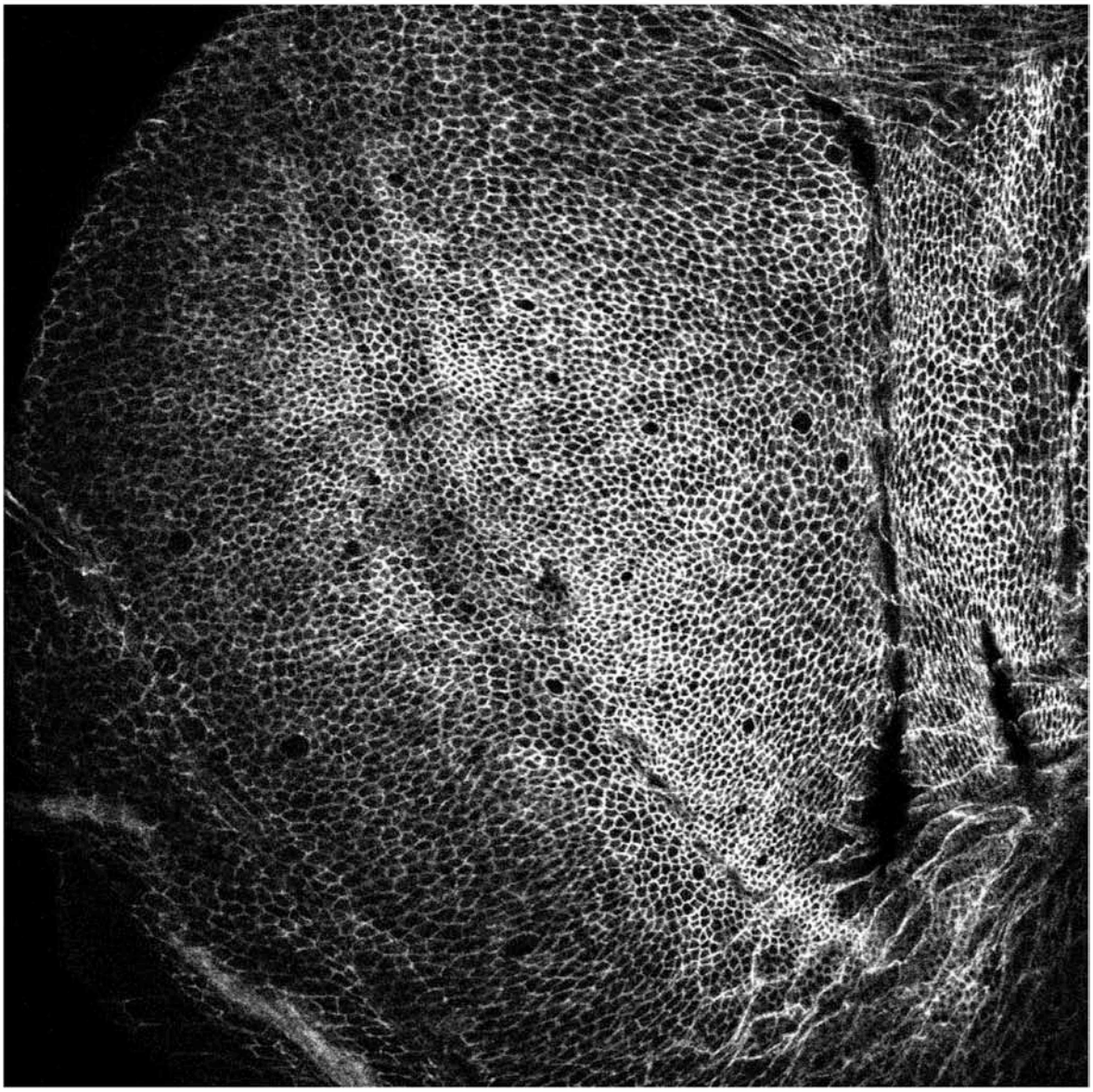

Appendix I C

A late prepupal wing (7hrs APF at 25ºC – Waddington stage PP3) stained for Flamingo. Compare with Appendix I D. A schematic representation of Flamingo polarity is given.

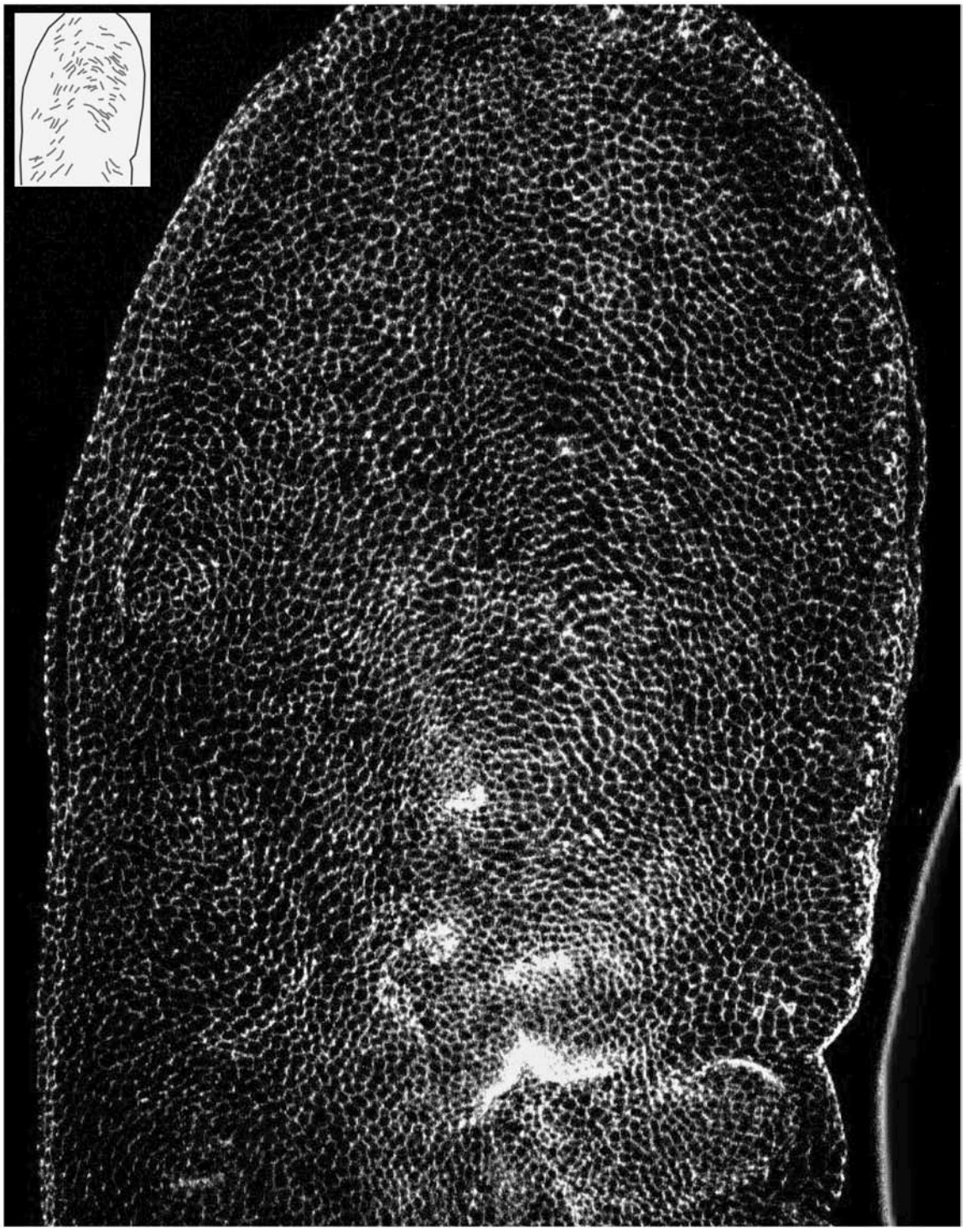

Appendix I D

The same late prepupal wing (7hrs APF at 25ºC – Waddington stage PP3) as in Appendix I C stained for E-cadherin.

Appendix I E

An early pupal wing (Waddington stage P1/P2A) stained for Flamingo. Compare with Appendix I F. Anterior/posterior and distal/proximal axis are indicated and a schematic representation of Flamingo polarity is given.

Appendix I F

The same early pupal wing (Waddington stage P1/P2A) as in Appendix I E stained for E-cadherin.

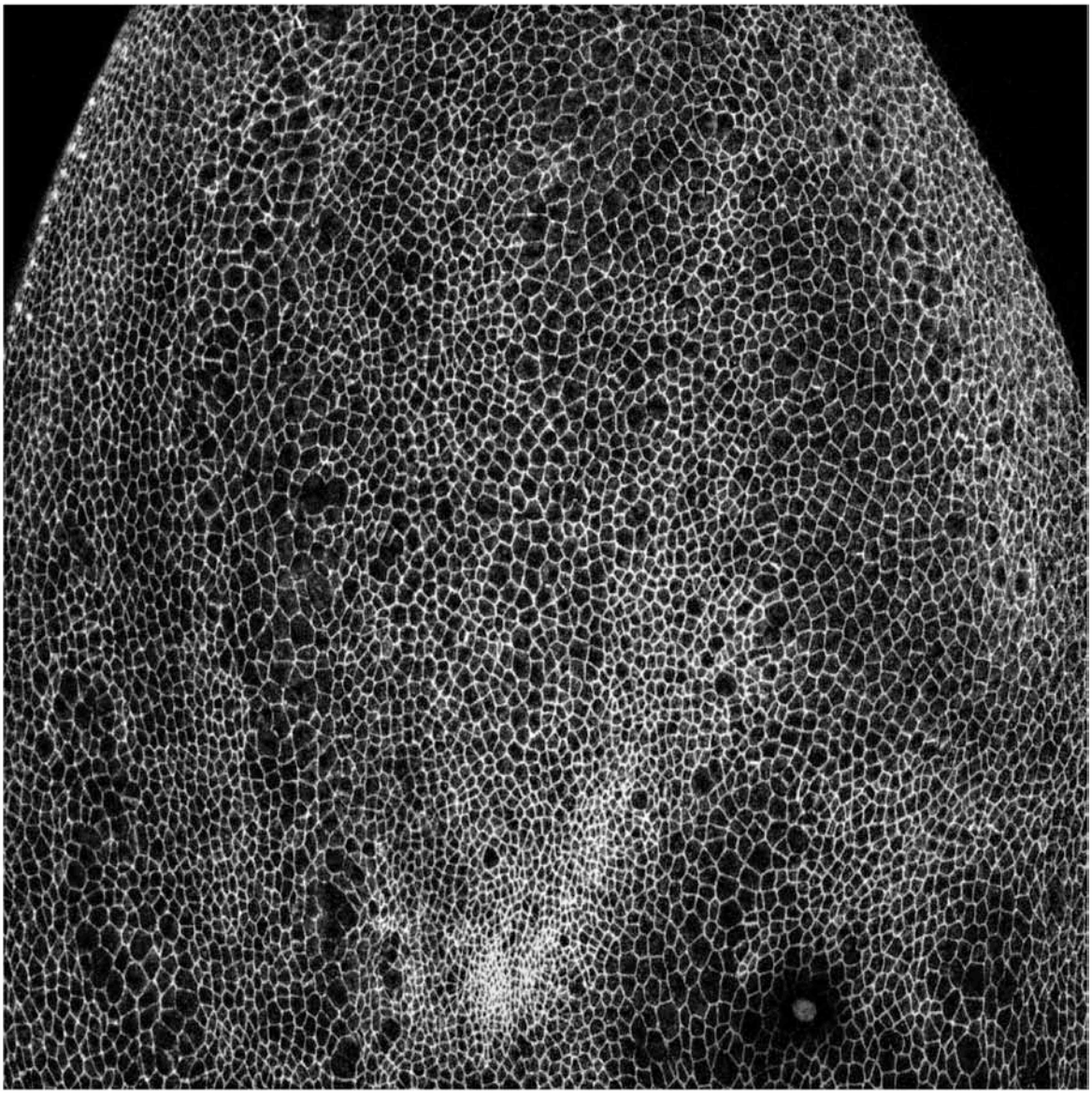

Appendix I G

An early pupal wing (Waddington stage P1/P2A) stained for Flamingo. Compare with Appendix I H. The distal/proximal axis is indicated and a schematic representation of Flamingo polarity is given.

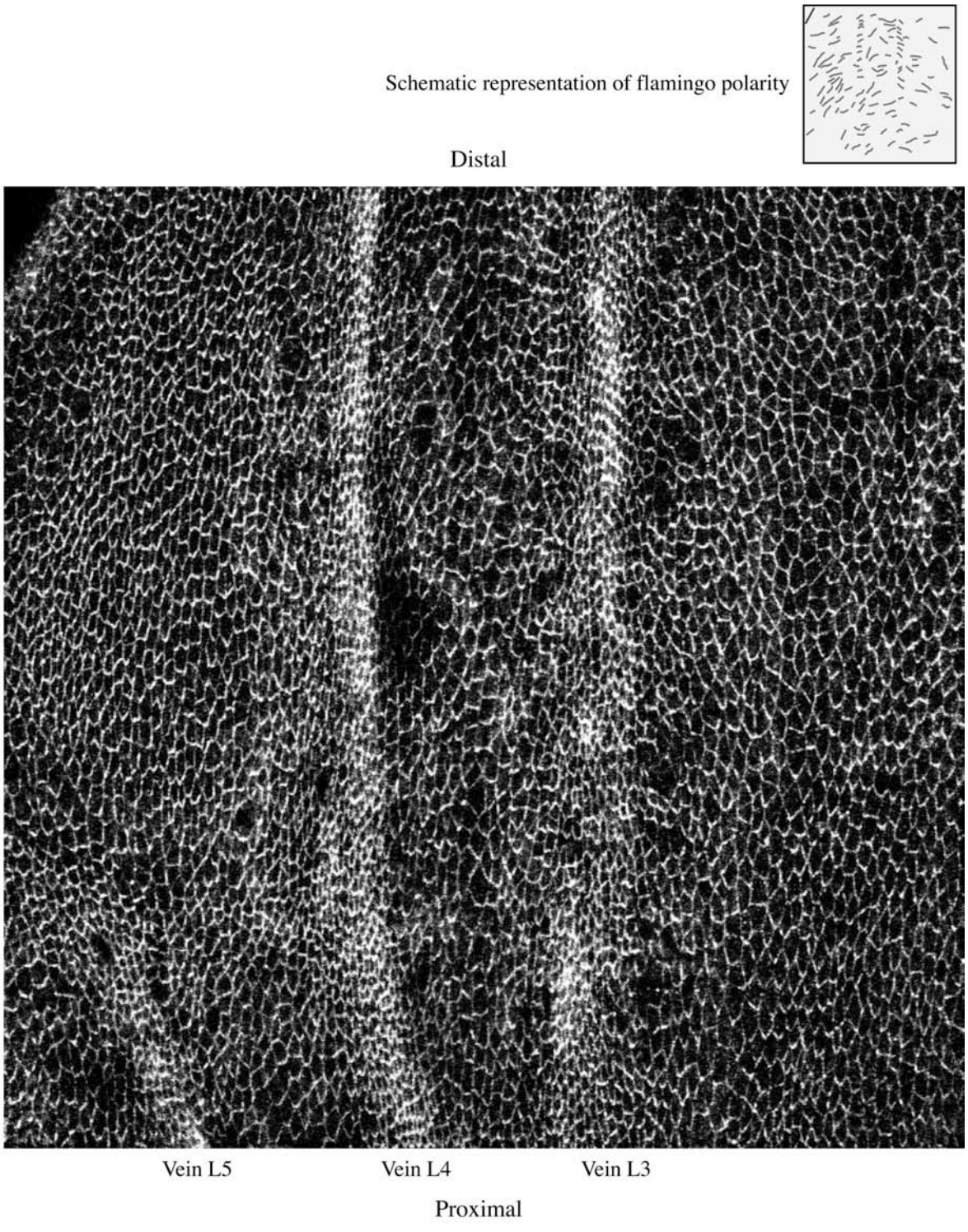

Appendix I H

The same early pupal wing (Waddington stage P1/P2A) as in Appendix I G stained for E-cadherin.

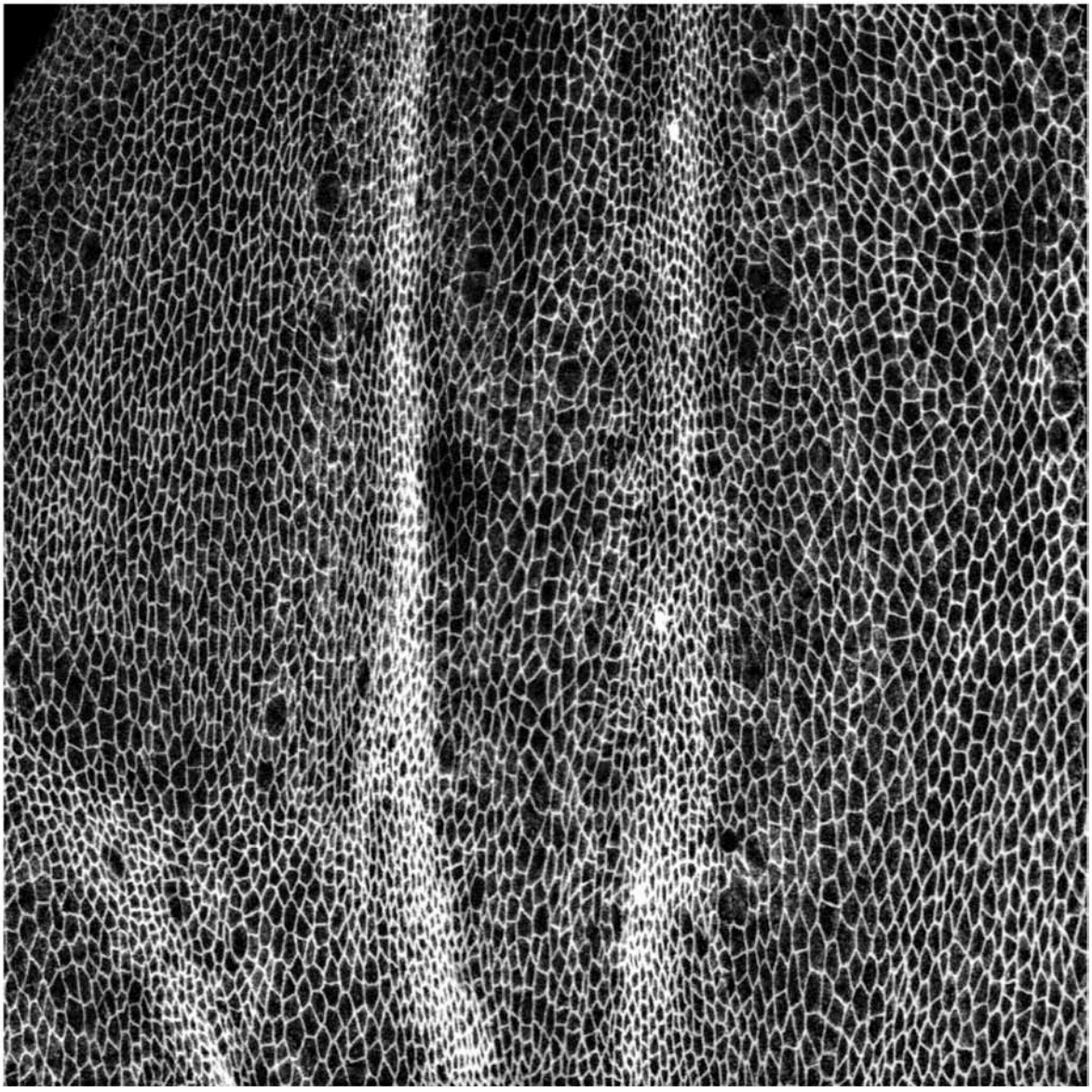

Appendix I I

A pupal wing (Waddington stage early P2C, equivalent to packing analysis time point 2) stained for Flamingo.

Appendix I J

A wing imaginal disc expressing Frizzled-GFP. Compare to Appendix I A. A schematic representation of Frizzled-polarity in the wing pouch is given.

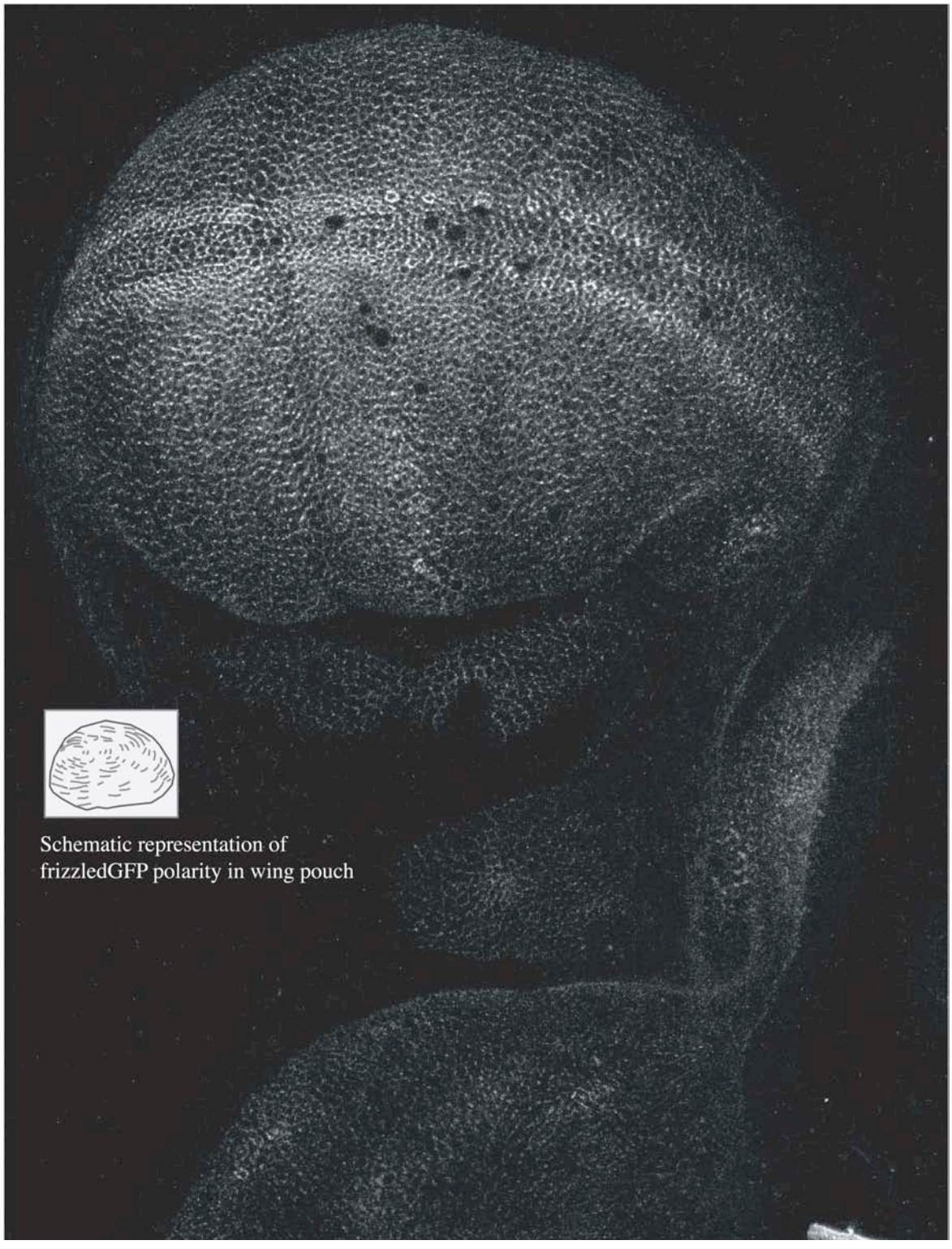

Appendix I K

An early prepupal wing expressing Frizzled-GFP.

Appendix I L

A *pk30*/*pk30* mutant wing imaginal disc stained for Flamingo. Flamingo localizes in a punctate pattern, which is not coordinated between neighboring cells. Compare to wild type in Appendix I A.

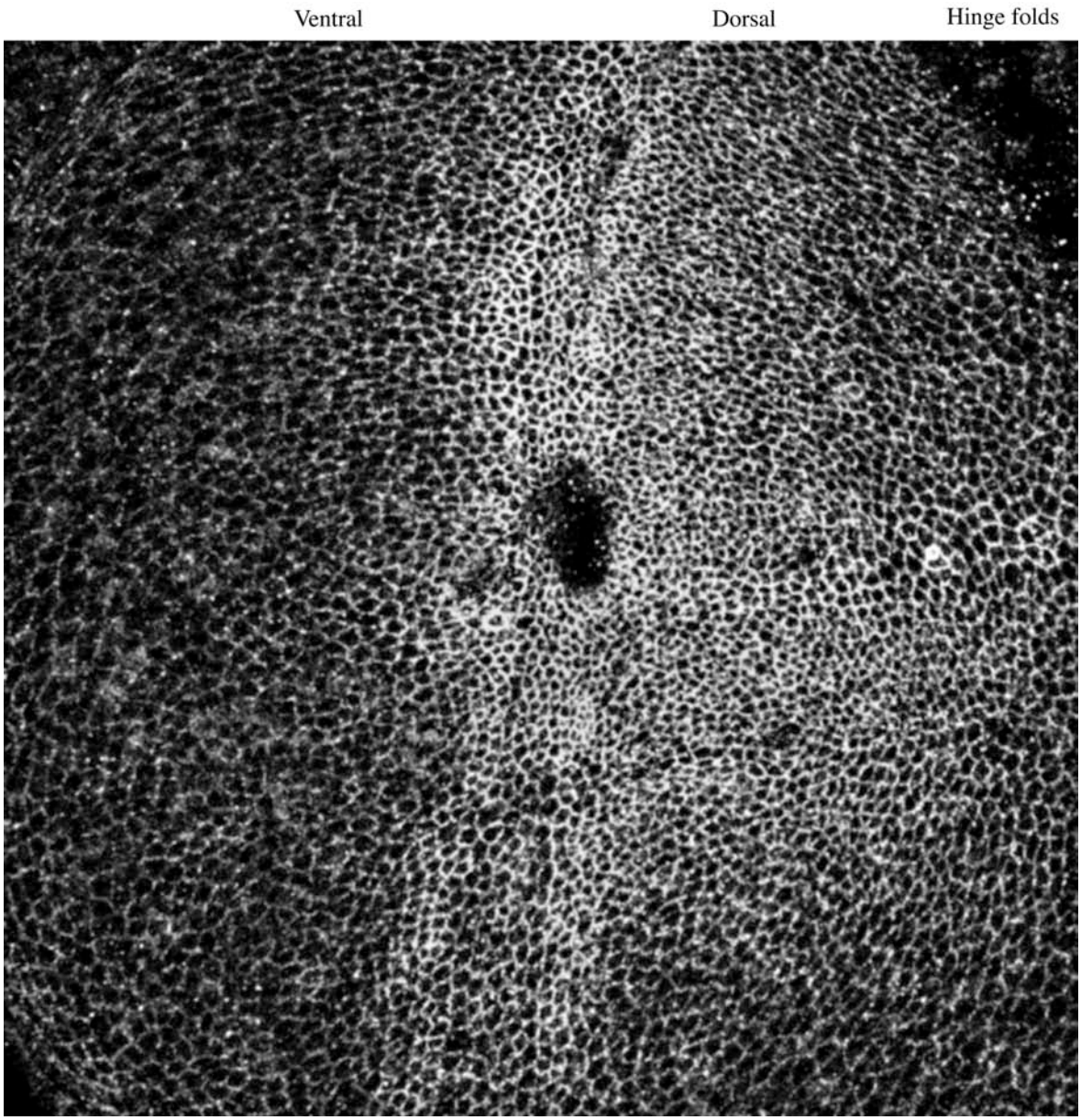

Appendix II

Cellenger Cell Packing Analysis

Data and Statistics

Area, cell-cell (border) contact and perimeter lengths are given for all cells

Perimeters are also given for individual polygon classes

Area, cell-cell (border) contact and perimeter lengths are given in pixels

Imaginal Disc	1pxl=0.05μm
Prepupal wings	1pxl=0.12μm
Pupal wings	1pxl=0.12μm

Polygon identity and counts are given in absolute numbers or percentage of total count

Vertex identity and counts are given in absolute numbers or percentage of total count

Hexagonality expresses the average number of neighbors per cell

Oregon R intervein cells between vein L2 and L4 - Summary

	cell count	hexagonality	area	SD	perimeter	SD	area min	perimeter min	area max	perimeter max
ORK disc										
W1	**628**	**5,680**	**2854**	1468	**265**	69	615	122	9857	496
W2	**930**	**5,657**	**1971**	780	**224**	45	502	112	7168	408
W3	**975**	**5,704**	**1942**	902	**219**	53	311	82	9422	470
average	844	5,670	2255		236		476	105	8816	458
ORK prepupal 12hAPF21.5C										
W1	490	**5,641**	**1653**	446	**199**	28	374	92	3053	272
W2	476	**5,609**	**1656**	569	**203**	34	177	88	3159	284
W3	409	**5,812**	**2121**	735	**223**	38	524	128	4614	338
average	458	**5,687**	1810		208		358	103	3609	298
ORK pupal TP1 29hAPF21.5C										
W1	**944**	**5,697**	**761**	328	**142**	31	79	42	3136	278
W2	**1153**	**5,710**	**645**	261	**133**	28	67	38	2670	256
W3	**1133**	**5,717**	**743**	299	**141**	29	166	58	2502	256
average	1077	5,717	716		139		104	46	2769	263
ORK pupal TP2 32.5hAPF21.5C										
W1	**1128**	**5,852**	**700**	271	**129**	25	6	12	1732	202
W2	**1202**	**5,873**	**660**	227	**123**	23	176	62	1461	184
W3	**1048**	**5,869**	**719**	268	**127**	25	165	66	1676	208
average	1126	5,869	693		126		116	47	1623	198
ORK pupal TP3 36hAPF21.5C										
W1	**1136**	**5,920**	**711**	244	**124**	23	226	68	1712	206
W2	**1390**	**5,919**	**566**	175	**111**	19	191	64	1125	170
W3	**1409**	**5,917**	**567**	185	**111**	19	203	62	1243	178
average	1312	5,919	614		115		207	65	1360	185
ORK pupal TP4 39.5hAPF21.5C										
W1	**1322**	**5,933**	**596**	176	**113**	17	204	66	1180	160
W2	**1634**	**5,950**	**484**	119	**103**	13	169	58	1002	152
average	1478	5,942	540		108		187	62	1091	156
ORK pupal TP5 43hAPF21.5C										
W1	**1026**	**5,967**	**830**	310	**137**	24	225	74	1880	208
W2	**1031**	**5,947**	**842**	261	**138**	21	244	74	1623	196
W3	**881**	**5,950**	**943**	300	**145**	23	203	74	2026	224
average	979	5,955	872		140		224	74	1843	209

Oregon R between vein L2 and L4 - Polygon counts

	cell count	count 3er	count 4er	count 5er	count 6er	count 7er	count 8er
ORK disc							
W1	628		61	210	239	106	11
W2	930	3	78	327	366	139	17
W3	975	1	74	352	350	182	16
average %	844	**0,20%**	**9,15%**	**34,57%**	**37,75%**	**16,24%**	**2,03%**
SD %		0,18%	1,47%	1,28%	1,43%	1,93%	0,58%
ORK prepupal 12hAPF21.5C							
W1	490	1	23	187	220	58	1
W2	476	3	32	180	204	55	3
W3	409		13	129	194	68	5
average %	458	**0,42%**	**4,87%**	**35,84%**	**45,06%**	**13,34%**	**0,69%**
SD %		0,30%	1,78%	3,73%	2,29%	2,85%	0,51%
ORK pupal TP1 29hAPF21.5C							
W1	944	2	55	345	375	151	15
W2	1153	3	62	389	527	156	16
W3	1133	1	58	353	553	154	14
average %	1077	**0,19%**	**5,44%**	**33,81%**	**44,75%**	**14,37%**	**1,40%**
SD %		0,00%	0,36%	2,70%	4,62%	1,41%	0,18%
ORK pupal TP2 32.5hAPF21.5C							
W1	1128	1	17	303	642	157	8
W2	1202		5	295	752	148	2
W3	1048		6	237	680	123	2
average %	1126	**0,09%**	**0,83%**	**24,67%**	**61,45%**	**12,66%**	**0,36%**
SD %		0,00%	0,59%	2,13%	4,10%	1,13%	0,31%
ORK pupal TP3 36hAPF21.5C							
W1	1136		1	208	809	117	1
W2	1390		2	225	1047	116	
W3	1409		2	272	976	159	
average %	1312		**0,1%**	**17,9%**	**71,9%**	**10,0%**	**0,0%**
SD %			0%	2%	3%	1%	0%
ORK pupal TP4 39.5hAPF21.5C							
W1	1322		2	196	1012	112	
W2	1634			235	1261	138	2
average %	1478		**0,15%**	**14,60%**	**76,86%**	**8,46%**	**0,06%**
SD %				0,31%	0,44%	0,02%	0,09%
ORK pupal TP5 43hAPF21.5C							
W1	1026		1	122	817	86	1
W2	1031			142	800	87	1
W3	881			115	696	69	1
average %	979		**0,10%**	**12,91%**	**78,74%**	**8,22%**	**0,10%**
SD %				0,95%	1,04%	0,34%	0,01%

Oregon R between vein L2 and L4 - Polygon perimeters

	cell count	perimeter 3er	perimeter 4er	perimeter 5er	perimeter 6er	perimeter 7er	perimeter 8er
ORK disc							
W1	628		219	249	271	306	288
W2	930	188	182	212	229	252	292
W3	975	248	188	203	225	248	271
average	844	**218**	**196**	**221**	**242**	**269**	**284**
SD		42	20	24	25	32	11
ORK prepupal 12hAPF21.5C							
W1	490	154	182	193	203	206	234
W2	476	157	177	197	207	220	182
W3	409		192	212	224	246	247
average	458	**155**	**183**	**201**	**211**	**224**	**221**
SD		2	8	10	11	20	34
ORK pupal TP1 29hAPF21.5C							
W1	944	221	196	146	115	172	223
W2	1153	107	105	128	135	144	187
W3	1133	96	122	133	143	159	178
average	1077	**141**	**141**	**136**	**131**	**158**	**196**
SD		69	48	9	14	14	24
ORK pupal TP2 32.5hAPF21.5C							
W1	1128	12	107	123	130	139	156
W2	1202		118	119	124	130	140
W3	1048		114	118	128	139	115
average	1126	**12**	**113**	**120**	**127**	**136**	**137**
SD			5	3	3	5	21
ORK pupal TP3 36hAPF21.5C							
W1	1136		86	116	124	137	166
W2	1390		96	105	112	121	
W3	1409		99	104	111	121	
average	1312		**94**	**108**	**115**	**126**	**166**
SD			7	7	8	9	
ORK pupal TP4 39.5hAPF21.5C							
W1	1322		100	104	114	126	
W2	1634		97	103	111	119	
average	1478		**99**	**104**	**112**	**122**	
SD			2	1	2	5	
ORK pupal TP5 43hAPF21.5C							
W1	1026		86	121	138	145	158
W2	1031			127	139	146	176
W3	881			135	146	158	172
average	979		**86**	**128**	**141**	**149**	**169**
SD				7	4	7	9

Oregon R intervein cells between vein L2 and L4 - Cell-cell contacts - Summary

	border count	border length	SD	mode	min	max
ORK pupal TP1 29hAPF21.5C						
W1	5364	21,3	11,0	13	2	66
W2	6504	19,3	10,7	19	2	69
W3	6472	20,9	11,0	16	2	76
average	**6113**	**20,5**		**16**	**2**	**70**
ORK pupal TP2 32.5hAPF21.5C						
W1	6553	18,9	8,9	17	2	55
W2	7036	18,0	7,9	15	2	52
W3	6152	18,7	8,0	18	2	53
average	**6580**	**18,5**		**17**	**2**	**53**
ORK pupal TP3 36hAPF21.5C						
W1	6690	18,4	6,8	20	2	48
W2	8169	16,0	6,2	14	2	41
W3	8277	16,1	6,1	17	2	41
average	**7712**	**16,8**		**17**	**2**	**43**
ORK pupal TP4 39.5hAPF21.5C						
W1	7791	16,4	5,5	17	2	37
W2	9630	14,6	5,1	14	2	37
average	**8711**	**15,5**		**16**	**2**	**37**
ORK pupal TP5 43hAPF21.5C						
W1	6079	19,9	7,1	22	2	42
W2	6102	20,3	7,0	19	2	48
W3	5218	21,5	7,2	22	2	47
average	**5800**	**20,6**		**21**	**2**	**46**

Oregon R intervein cells between vein L2 and L4 - Vertex counts - Summary

	vertex count	3er vertex	%	4er vertex	%
ORK pupal TP1 29hAPF21.5C					
W1	2020	1879	92,97%	141	6,98%
W2	2407	2231	92,57%	176	7,30%
W3	2345	2202	93,90%	143	6,10%
average	**2257**	**2104**	**93,15%**	**153**	**6,79%**
SD	208	195	0,68%	20	0,62%
ORK pupal TP2 32.5hAPF21.5C					
W1	2454	2358	96,09%	96	3,91%
W2	2649	2564	96,79%	85	3,21%
W3	2315	2243	96,89%	72	3,11%
average	**2473**	**2388**	**96,59%**	**84**	**3,41%**
SD	168	163	0,44%	12	0,44%
ORK pupal TP3 36hAPF21.5C					
W1	2530	2476	97,87%	54	2,13%
W2	3063	2996	97,81%	67	2,19%
W3	3108	3044	97,94%	64	2,06%
average	**2900**	**2839**	**97,87%**	**62**	**2,13%**
SD	322	315	0,06%	7	0,06%
ORK pupal TP4 39.5hAPF21.5C					
W1	2914	2858	98,08%	56	1,92%
W2	3585	3533	98,55%	52	1,45%
average	**3250**	**3196**	**98,31%**	**54**	**1,69%**
SD	474	477	0,33%	3	0,33%
ORK pupal TP5 43hAPF21.5C					
W1	2265	2238	98,81%	27	1,19%
W2	2220	2182	98,29%	38	1,71%
W3	1925	1895	98,44%	30	1,56%
average	**2137**	**2105**	**98,51%**	**32**	**1,49%**
SD	185	184	0,27%	6	0,27%

Oregon R between anterior wing margin and vein L2 - Summary

	cell count	hexagonality	area	SD	perimeter	SD	area min	perimeter min	area max	perimeter max
ORK pupal TP1 29hAPF21.5C										
W1	**151**	**5,641**	**1140**	304	**178**	26	627	160	1121	182
W2	**223**	**5,767**	**862**	264	**152**	24	300	90	1619	206
W3	**200**	**5,850**	**1013**	297	**171**	26	428	106	1964	236
average	191	5,753	1005		167		452	119	1568	208
ORK pupal TP2 32.5hAPF21.5C										
W1	**182**	**5,934**	**914**	137	**147**	12	589	116	1234	184
W2	**147**	**5,884**	**1306**	309	**181**	23	377	92	2217	236
W3	**178**	**5,848**	**1000**	198	**160**	17	468	100	1546	198
W4	**154**	**5,922**	**1227**	291	**175**	22	627	128	1948	236
average	165	5,897	1111		166		515	109	1736	214
ORK pupal TP3 36hAPF21.5C										
W1	**179**	**5,939**	**1049**	207	**154**	17	401	98	1692	208
W2	**224**	**5,911**	**883**	194	**148**	17	345	102	1762	228
average	202	5,925	966		151		373	100	1727	218
ORK pupal TP4 39.5hAPF21.5C										
W1	**176**	**5,960**	**1046**	235	**159**	19	430	98	1630	202
W2	**317**	**5,918**	**631**	177	**121**	19	201	72	1001	158
average	247	5,939	838		140		316	85	1316	180
ORK pupal TP5 43hAPF21.5C										
W1	**122**	**5,984**	**1580**	263	**189**	17	1096	156	2303	230
W2	**125**	**5,992**	**1543**	268	**187**	16	978	142	2276	224
W3	**134**	**6,000**	**1419**	194	**178**	13	1018	152	2016	216
average	127	5,992	1514		185		1031	150	2198	223

Oregon R between anterior wing margin and vein L2 - Polygon counts

	cell count	count 3er	count 4er	count 5er	count 6er	count 7er	count 8er
ORK pupal TP1 29hAPF21.5C							
W1	151		2	47	84	18	
W2	223		4	73	120	23	3
W3	200		7	52	108	30	3
average %	**191**		**2,21%**	**29,95%**	**54,48%**	**12,41%**	**1,42%**
SD %			1,14%	3,52%	1,00%	2,38%	0,11%
ORK pupal TP2 32.5hAPF21.5C							
W1	147		1	40	82	23	1
W2	178			42	121	15	
W3	154			30	106	18	
W4	182		1	26	139	16	
average %	**165**		**0,23%**	**23,43%**	**64,20%**	**11,92%**	**0,23%**
SD %			0,39%	3,87%	7,30%	3,62%	0,39%
ORK pupal TP3 36hAPF21.5C							
W1	179		1	27	133	18	
W2	224		1	46	150	26	1
average %	**202**		**0,50%**	**17,81%**	**70,63%**	**10,83%**	**0,50%**
SD %			0,08%	3,86%	5,19%	1,10%	0,08%
ORK pupal TP4 39.5hAPF21.5C							
W1	176			17	149	10	
W2	317		1	47	246	23	
average %	**247**		**0,16%**	**12,24%**	**81,13%**	**6,47%**	
SD %			0,22%	3,65%	4,99%	1,11%	
ORK pupal TP5 43hAPF21.5C							
W1	122			10	104	8	
W2	125			13	100	12	
W3	134			9	116	9	
average %				**8,44%**	**83,94%**	**7,62%**	
SD %				1,85%	3,47%	1,71%	

Oregon R between anterior wing margin and vein L2 - Polygon perimeters

	cell count	perimeter 3er	perimeter 4er	perimeter 5er	perimeter 6er	perimeter 7er	perimeter 8er
ORK pupal TP1 29hAPF21.5C							
W1	151		171	174	178	183	
W2	223		131	144	158	152	182
W3	200		155	164	173	181	201
average	**191**		**152**	**161**	**170**	**172**	**192**
SD			20	15	11	18	14
ORK pupal TP2 32.5hAPF21.5C							
W1	147		162	174	181	193	194
W2	178			155	160	173	
W3	154			173	174	184	
	182		136	145	147	148	
average	**165**		**149**	**162**	**166**	**175**	**194**
SD			18	14	15	19	
ORK pupal TP3 36hAPF21.5C							
W1	179		176	146	154	165	
W2	224		122	141	150	152	190
average	**202**		**149**	**143**	**152**	**159**	**190**
SD			38	3	3	9	
ORK pupal TP4 39.5hAPF21.5C							
W1	176			147	160	157	
W2	317		78	111	122	131	
average	**247**		**78**	**129**	**141**	**144**	
SD				25	27	19	
ORK pupal TP5 43hAPF21.5C							
W1	122			184	189	196	
W2	125			177	186	201	
W3	134			168	178	188	
average	**127**			**176**	**184**	**195**	
SD				8	5	6	

Oregon R between vein L4 and L5 - Summary

	cell count	hexagonality	area	SD	perimeter	SD	area min	perimeter min	area max	perimeter max
ORK pupal TP1 29hAPF21.5C										
W1	**1095**	**5,725**	**772**	295	**141**	27	175	70	2515	242
W2	**1113**	**5,747**	**664**	270	**131**	26	177	72	2814	258
W3	**1114**	**5,774**	**746**	319	**136**	29	13	18	2434	250
average	1107	5,749	727		136		122	53	2588	250
ORK pupal TP2 32.5hAPF21.5C										
W1	**1250**	**5,822**	**630**	206	**123**	22	10	16	1768	254
W2	**1285**	**5,847**	**592**	179	**119**	21	11	20	1363	192
W3	**1363**	**5,859**	**588**	184	**117**	20	151	62	1261	184
average	1299	5,843	603		120		57	33	1464	210
ORK pupal TP3 36hAPF21.5C										
W1	**1094**	**5,926**	**693**	169	**123**	17	164	64	1284	176
W2	**1394**	**5,909**	**574**	147	**113**	16	216	66	1522	188
W3	**1284**	**5,908**	**593**	142	**115**	15	216	66	1413	172
average	1257	5,914	620		117		199	65	1406	179
ORK pupal TP4 39.5hAPF21.5C										
W1	**1352**	**5,948**	**571**	125	**113**	14	152	56	1137	166
W2	**1564**	**5,956**	**465**	97	**100**	12	40	26	832	146
average	1458	5,952	518		107		96	41	985	156
ORK pupal TP5 43hAPF21.5C										
W1	**1071**	**5,955**	**774**	201	**133**	19	186	62	1755	216
W2	**1129**	**5,932**	**752**	186	**132**	16	221	70	1401	182
average	1100	5,943	763		132		204	66	1578	199

Oregon R between vein L4 and L5 - Polygon counts

	cell count	count 3er	count 4er	count 5er	count 6er	count 7er	count 8er
ORK pupal TP1 29hAPF21.5C							
W1	1095		45	380	521	129	20
W2	1113		47	383	505	161	17
W3	1114	1	43	368	515	169	18
average %		**0,03%**	**4,06%**	**34,05%**	**46,39%**	**13,81%**	**1,66%**
SD %		0,05%	0,19%	0,89%	1,11%	1,79%	0,15%
ORK pupal TP2 32.5hAPF21.5C							
W1	1250	1	23	363	679	178	6
W2	1285	2	24	327	752	176	4
W3	1363		14	336	844	166	3
average %		**0,08%**	**1,58%**	**26,38%**	**58,25%**	**13,37%**	**0,34%**
SD %		0,08%	0,48%	2,34%	3,81%	1,07%	0,13%
ORK pupal TP3 36hAPF21.5C							
W1	1094		1	200	772	121	
W2	1394		3	277	961	150	3
W3	1284		5	268	853	156	2
average %			**0,23%**	**19,67%**	**68,65%**	**11,32%**	**0,12%**
SD %			0,15%	1,31%	2,08%	0,73%	0,11%
ORK pupal TP4 39.5hAPF21.5C							
W1	1352		2	191	1034	125	
W2	1564		1	222	1189	149	3
average %	**1458**		**0,11%**	**14,16%**	**76,25%**	**9,39%**	**0,10%**
SD %			0,06%	0,05%	0,32%	0,20%	0,14%
ORK pupal TP5 43hAPF21.5C							
w1	1021		1	139	785	96	
W1	1071			155	810	105	1
W2	1129		1	163	877	88	
average %	**1100**		**0,04%**	**14,46%**	**76,65%**	**8,80%**	**0,05%**
SD %			0,06%	0,02%	1,45%	1,42%	0,07%

Oregon R between vein L4 and L5 - Polygon perimeters

	cell count	perimeter 3er	perimeter 4er	perimeter 5er	perimeter 6er	perimeter 7er	perimeter 8er
ORK pupal TP1 29hAPF21.5C							
W1	1095		130	133	142	159	186
W2	1113		110	125	131	147	186
W3	1114	18	120	127	137	151	179
average	**1107**	**18**	**120**	**128**	**137**	**152**	**184**
SD			10	4	6	6	4
ORK pupal TP2 32.5hAPF21.5C							
W1	1250	16	110	118	125	132	152
W2	1285	20	102	113	120	126	143
W3	1363		100	109	118	127	132
average	**1299**	**18**	**104**	**113**	**121**	**128**	**142**
SD		3	5	4	4	3	10
ORK pupal TP3 36hAPF21.5C							
W1	1094		64	116	124	134	
W2	1394		101	108	113	121	133
W3	1284		116	108	116	126	132
average	**1257**		**94**	**110**	**117**	**127**	**133**
SD			27	5	6	7	1
ORK pupal TP4 39.5hAPF21.5C							
W1	1352		82	106	113	120	
W2	1564		26	95	100	108	120
average	**1458**		**54**	**101**	**107**	**114**	**120**
SD			40	8	9	9	
ORK pupal TP5 43hAPF21.5C							
	1021		112	127	136	142	
W1	1071			123	134	137	202
W2	1129		114	126	133	134	
average	**1074**		**113**	**125**	**134**	**138**	**202**
SD				2	2	4	

pk-sple 13/26 between vein L2 and L4 - General

	cell count	hexagonality	area	SD	perimeter	SD	area min	perimeter min	area max	perimeter max
pk-sple13/26 pupal TP1 30hAPF21.5C										
W1	**1078**	**5,694**	**784**	283	**141**	26	37	26	2020	224
W2	**991**	**5,632**	**886**	324	**153**	30	194	80	3752	332
W3	**908**	**5,655**	**975**	374	**155**	30	214	66	2629	242
W4	**587**	**5,647**	**910**	339	**153**	28	245	92	5150	366
average	891	5,657	889		151		173	66	3388	291
pk-sple13/26 pupal TP2 33.5hAPF21.5C										
W1	**1267**	**5,704**	**646**	250	**131**	24	169	68	169	68
W2	**1179**	**5,755**	**721**	210	**130**	20	215	70	215	70
W3	**1160**	**5,803**	**732**	246	**130**	23	177	60	177	60
average	1202	5,754	700		130		187	66	187	66
pk-sple13/26 pupal TP3 37hAPF21.5C										
W1	**1196**	**5,844**	**720**	230	**128**	21	190	66	1819	282
W2	**1423**	**5,797**	**559**	141	**113**	15	140	68	1083	164
W3	**1321**	**5,824**	**634**	175	**119**	17	59	34	1188	166
average	1313	5,822	638		120		130	56	1363	204
pk-sple13/26 pupal TP4 40.5hAPF21.5C										
W1	**1181**	**5,854**	**731**	221	**129**	18	219	74	1648	190
W2	**1314**	**5,825**	**635**	185	**119**	17	165	58	1383	190
W3	**1211**	**5,846**	**686**	197	**126**	17	183	68	1640	196
average	1248	5,841	684		125		189	67	1557	192
pk-sple13/26 pupal TP5 44hAPF21.5C										
W1	**1055**	**5,967**	**829**	251	**138**	19	199	80	1611	198
W2	**1272**	**5,947**	**681**	240	**124**	22	170	60	1411	186
W3	**1140**	**5,950**	**763**	278	**132**	22	184	64	1726	198
average	1156	5,955	758		131		184	68	1583	194

pk-sple 13/26 between vein L2 and L4 - General

	cell count	hexagonality	area	SD	perimeter	SD	area min	perimeter min	area max	perimeter max
pk-sple13/26 pupal TP1 30hAPF21.5C										
W1	**1078**	**5,694**	**784**	283	**141**	26	37	26	2020	224
W2	**991**	**5,632**	**886**	324	**153**	30	194	80	3752	332
W3	**908**	**5,655**	**975**	374	**155**	30	214	66	2629	242
W4	**587**	**5,647**	**910**	339	**153**	28	245	92	5150	366
average	891	5,657	889		151		173	66	3388	291
pk-sple13/26 pupal TP2 33.5hAPF21.5C										
W1	**1267**	**5,704**	**646**	250	**131**	24	169	68	169	68
W2	**1179**	**5,755**	**721**	210	**130**	20	215	70	215	70
W3	**1160**	**5,803**	**732**	246	**130**	23	177	60	177	60
average	1202	5,754	700		130		187	66	187	66
pk-sple13/26 pupal TP3 37hAPF21.5C										
W1	**1196**	**5,844**	**720**	230	**128**	21	190	66	1819	282
W2	**1423**	**5,797**	**559**	141	**113**	15	140	68	1083	164
W3	**1321**	**5,824**	**634**	175	**119**	17	59	34	1188	166
average	1313	5,822	638		120		130	56	1363	204
pk-sple13/26 pupal TP4 40.5hAPF21.5C										
W1	**1181**	**5,854**	**731**	221	**129**	18	219	74	1648	190
W2	**1314**	**5,825**	**635**	185	**119**	17	165	58	1383	190
W3	**1211**	**5,846**	**686**	197	**126**	17	183	68	1640	196
average	1248	5,841	684		125		189	67	1557	192
pk-sple13/26 pupal TP5 44hAPF21.5C										
W1	**1055**	**5,967**	**829**	251	**138**	19	199	80	1611	198
W2	**1272**	**5,947**	**681**	240	**124**	22	170	60	1411	186
W3	**1140**	**5,950**	**763**	278	**132**	22	184	64	1726	198
average	1156	5,955	758		131		184	68	1583	194

pk-sple 13/26 between vein L2 and L4 - Polygon perimeters

	cell count	perimeter 3er	perimeter 4er	perimeter 5er	perimeter 6er	perimeter 7er	perimeter 8er
pk-sple13/26_TP1 30hAPF21.5C							
W1	1078	120	128	135	144	151	180
W2	991		151	151	152	164	179
W3	908		148	152	155	163	177
W4	587	109	140	145	156	168	200
average	891	**115**	**142**	**146**	**152**	**161**	**184**
SD		8	10	7	6	7	11
pk-sple13/26_TP2 33.5hAPF21.5C							
W1	1267	12	118	126	134	140	162
W2	1179		124	127	131	138	
W3	1160		116	126	130	140	177
average	1202	**12**	**119**	**126**	**131**	**139**	**169**
SD			4	1	2	1	10
pk-sple13/26_TP3 37hAPF21.5C							
W1	1196		128	123	129	136	
W2	1423		109	111	113	120	
W3	1321		103	116	120	123	104
average	1313		**113**	**117**	**121**	**126**	**104**
SD			13	6	8	9	
pk-sple13/26_TP4 40.5hAPF21.5C							
W1	1181		124	124	130	136	
W2	1314		109	113	120	126	124
W3	1211		121	122	126	134	194
average	1248		**118**	**120**	**126**	**132**	**159**
SD			8	6	5	5	49
pk-sple13/26_TP5 44hAPF21.5C							
W1	1055		118	132	139	145	
W2	1272		107	119	126	130	
W3	1140		82	124	133	141	
average	1156		**103**	**125**	**133**	**139**	
SD			19	7	7	7	

PCP mutants and Ecad:aCat fusion protein between vein L2 and L4 - Summary

	cell count	hexagonality	area	SD	perimeter	SD	area min	perimeter min	area max	perimeter max
ORK										
W1	**1026**	**5,967**	**830**	310	**137**	24	225	74	1880	208
W2	**1031**	**5,947**	**842**	261	**138**	21	244	74	1623	196
W3	**881**	**5,950**	**943**	300	**145**	23	203	74	2026	224
average	979	5,955	872		140		224	74	1843	209
pk 1										
W1	**1153**	**5,819**	**753**	201	**133**	18	255	74	1882	210
W2	**1344**	**5,825**	**629**	174	**122**	17	179	66	1142	168
W3	**1273**	**5,805**	**633**	167	**122**	16	217	74	1292	184
average	1257	5,816	672		126		217	71	1439	187
pk-sple13/26										
W1	**1055**	**5,967**	**829**	251	**138**	19	199	80	1611	198
W2	**1272**	**5,947**	**681**	240	**124**	22	170	60	1411	186
W3	**1140**	**5,950**	**763**	278	**132**	22	184	64	1726	198
average	1156	5,955	758		131		184	68	1583	194
stbm 6										
W1	**1280**	**5,912**	**658**	171	**125**	16	151	60	1125	164
W2	**1073**	**5,915**	**744**	210	**130**	18	146	60	1484	190
W3	**1224**	**5,931**	**676**	181	**124**	17	235	70	1331	178
average	1192	5,919	692		127		17	63	1313	177
dgo 380										
W1	**1112**	**5,944**	**775**	210	**133**	18	244	74	1355	174
W2	**1246**	**5,929**	**689**	191	**126**	17	191	76	1253	168
W3	**1143**	**5,927**	**761**	221	**134**	18	241	80	1368	182
average	1167	5,933	742		131		18	77	1325	175
stan 3										
W1	**1381**	**5,921**	**645**	186	**122**	16	203	74	1287	170
W2	**1234**	**5,918**	**719**	181	**130**	16	267	82	1418	184
W3	**1352**	**5,916**	**659**	169	**125**	15	175	76	1157	170
average	1322	5,919	675		126		215	77	1287	175
fz P21 with hairs										
W1	**1381**	**5,946**	**611**	177	**118**	17	213	68	1162	168
W2	**1032**	**5,950**	**809**	287	**137**	23	249	74	1847	204
W3	**1277**	**5,966**	**666**	203	**124**	18	243	80	1612	200
average	1230	5,954	695		127		235	74	1540	191
fz P21 without hairs										
W1	**1141**	**5,897**	**729**	253	**130**	23	118	58	2028	216
W2	**1093**	**5,917**	**824**	208	**137**	19	308	82	1686	202
W3	**1288**	**5,901**	**671**	227	**125**	22	207	70	1346	188
average	1174	5,905	741		131		211	70	1687	202
FRT42 fmi E59										
cl 1	**350**	**5,774**	**490**	63	**109**	9	337	84	691	134
cl 2	**30**	**5,633**	**341**	76	**95**	9	207	80	497	116
cl 3	**56**	**5,821**	**521**	74	**111**	10	351	86	727	134
cl 4	**263**	**5,802**	**421**	66	**102**	8	242	72	660	128
cl 5	**48**	**5,813**	**1424**	158	**192**	11	1084	170	1842	224
cl 6	**65**	**5,708**	**1612**	216	**201**	15	1126	168	2162	242
cl 7	**176**	**5,875**	**1171**	156	**168**	12	852	142	1722	200
average	141	5,775	854		140		600	115	1186	168
ptcGAL4/80; UAS E-cad-a-Cat										
W1	**830**	**5,912**	**987**	304	**154**	25	69	52	1819	212
W2	**1016**	**5,907**	**766**	238	**136**	21	192	66	1496	194
W3	**805**	**5,917**	**1031**	305	**159**	24	282	84	1948	218
average	884	5,912	928		150		181	67	1754	208

PCP mutants and Ecad:aCat fusion protein between vein L2 and L4 - Polygon counts

	cell count	count 3er	count 4er	count 5er	count 6er	count 7er	count 8er
ORK							
W1	1026		1	122	817	86	1
W2	1031			142	800	87	1
W3	881			115	696	69	1
average %	979		**0,10%**	**12,91%**	**78,74%**	**8,22%**	**0,10%**
SD %	85			0,95%	1,04%	0,34%	0,01%
pk 1							
W1	1153		4	299	752	98	
W2	1344		5	345	874	120	
W3	1273		3	345	822	103	
average %	1257		**0,32%**	**26,23%**	**64,94%**	**8,51%**	
SD %	97		0,07%	0,76%	0,33%	0,42%	
pk-sple13/26							
W1	1055		8	220	748	79	
W2	1272		11	292	884	85	
W3	1140		2	234	810	94	
average %	1156		**0,60%**	**21,45%**	**70,48%**	**7,47%**	
SD %	109		0,37%	1,32%	0,86%	0,78%	
stbm 6							
W1	1280			219	955	106	
W2	1073		3	191	775	102	2
W3	1224		1	192	923	107	1
average %	1192		**0,18%**	**16,87%**	**74,08%**	**8,84%**	**0,09%**
SD %	107		0,14%	1,08%	1,65%	0,62%	0,09%
dgo 380							
W1	1112			155	864	93	
W2	1246		1	198	936	111	
W3	1143		3	188	843	108	1
average %	1167		**0,11%**	**15,43%**	**75,52%**	**8,91%**	**0,03%**
SD %	70		0,13%	1,32%	2,00%	0,54%	0,05%
stan 3							
W1	1381			236	1018	127	
W2	1234		4	192	939	99	
W3	1352		3	208	1040	101	
average %	1322		**0,182%**	**16,01%**	**75,58%**	**8,23%**	**0,00%**
SD %	78		0,166%	0,94%	1,67%	0,88%	0,00%
fz P21 with hairs							
W1	1381		1	205	1043	131	1
W2	1032		2	153	773	103	1
W3	1277			161	998	118	
average %	1230		**0,09%**	**14,09%**	**76,19%**	**9,57%**	**0,06%**
SD %	179		0,10%	1,29%	1,72%	0,38%	0,05%
fz P21 without hairs							
W1	1141		9	225	782	124	1
W2	1093		3	204	767	119	
W3	1288		4	262	883	136	3
average %	1174		**0,46%**	**19,58%**	**69,09%**	**10,77%**	**0,11%**
SD %	102		0,29%	0,85%	0,94%	0,18%	0,12%
FRT42 fmi E59							
cl 1	350		3	94	232	21	
cl 2	30			11	19		
cl 3	56			14	38	4	
cl 4	263		2	60	189	12	
cl 5	48			11	35	2	
cl 6	65			22	40	3	
cl 7	176			32	134	10	
average %	141		**0,00**	**26,61**	**68,56**	**4,60**	
SD %			0,40	6,52	5,32	2,27	
ptcGAL4; UAS E-cad-a-Cat							
W1	830			156	592	81	1
W2	1016			195	720	101	
W3	805		2	159	548	96	
average %	884		**0,08%**	**19,25%**	**70,09%**	**10,54%**	**0,04%**
SD %	115		0,14%	0,48%	1,76%	1,20%	0,07%

PCP mutants and Ecad-aCat fusion protein between vein L2 and L4 - Polygon perimeters

	cell count	perimeter 3er	perimeter 4er	perimeter 5er	perimeter 6er	perimeter 7er	perimeter 8er
ORK							
W1	1026		86	121	138	145	158
W2	1031			127	139	146	176
W3	881			135	146	158	172
average	979		**86**	**128**	**141**	**149**	**169**
SD				7	4	7	9
pk 1							
W1	1153		137	129	134	140	
W2	1344		122	116	124	122	
W3	1273		103	120	123	125	
average	1257		**121**	**122**	**127**	**129**	
SD			17	7	6	10	
pk-sple13/26							
W1	1055		118	132	139	145	
W2	1272		107	119	126	130	
W3	1140		82	124	133	141	
average	1156		**103**	**125**	**133**	**139**	
SD			19	7	7	7	
stbm 6							
W1	1280			122	125	131	
W2	1073		82	123	131	140	167
W3	1224		90	120	124	132	148
average	1192		**86**	**122**	**127**	**134**	**158**
SD			6	1	4	5	13
dgo 380							
W1	1112			126	134	144	
W2	1246		116	121	126	133	
W3	1143		98	124	135	140	154
average	1167		**107**	**123**	**132**	**139**	**154**
SD			13	3	5	5	
stan 3							
W1	1381			116	123	128	
W2	1234		113	124	131	135	
W3	1352		107	120	126	133	
average	1322		**110**	**120**	**127**	**132**	
SD			4	4	4	4	
fz P21 with hairs							
W1	1381		126	110	118	127	128
W2	1032		104	125	138	151	144
W3	1277			117	124	138	
average	1230		**115**	**117**	**127**	**139**	**136**
SD			16	8	10	12	11
fz P21 without hairs							
W1	1141		101	124	130	143	160
W2	1093		131	132	136	146	
W3	1288		104	119	125	140	133
average	1174		**112**	**125**	**131**	**143**	**146**
SD			17	7	6	3	19
FRT42 fmi E59							
cl 1	350		108	109	109	113	
cl 2	30			93	96		
cl 3	56			108	112	112	
cl 4	263		103	100	103	106	
cl 5	48			190	191	203	
cl 6	65			196	204	195	
cl 7	176			165	167	179	
average	141		**106**	**137**	**140**	**151**	
SD			4	45	46	46	
ptcGAL4; UAS E-cad-a-Cat							
W1	830			150	154	160	170
W2	1016			133	136	141	
W3	805		161	152	159	166	
average	884		**161**	**145**	**150**	**156**	**170**
SD				10	12	13	

PCP mutants and Ecad:aCat fusion protein - Cell-Cell contacts - General

	border count	border length	SD	mode	min	max
ORK pupal TP5 43hAPF21.5C						
W1	6079	19,94	7,06	22	2	42
W2	6102	20,26	7,03	19	2	48
W3	5218	21,50	7,18	22	2	47
average	**5800**	**20,56**		**21**	**2**	**46**
pk 1						
W1	3578	19,66	7,75	19	2	46
W2	7749	17,76	7,33	21	2	42
W3	7316	18,06	7,49	17	2	52
average %	**6214**	**18**		**19**	**2**	**47**
pk-sple13/26						
W1	6148	20,53	7,09	20	2	47
W2	7351	18,21	6,90	18	2	43
W3	6676	19,35	7,32	19	2	45
average %	**6725**	**19**		**19**	**2**	**45**
stbm 6						
W1	7539	17,89	6,52	20	2	45
W2	6325	19,10	6,84	22	2	44
W3	7219	17,99	6,02	19	2	39
average %	**7028**	**18**		**20**	**2**	**43**
dgo 380						
W1	6576	19,35	6,55	21	2	40
W2	7358	18,13	6,20	20	2	39
W3	6739	19,38	6,72	20	2	43
average %	**6891**	**19**		**20**	**2**	**41**
stan 3						
W1	8093	17,49	6,10	18	3	39
W2	7276	18,83	6,19	19	2	43
W3	7971	17,75	5,90	18	2	39
average %	**7780**	**18**		**18**	**2**	**40**
fz P21 with hairs						
W1	8165	16,84	6,12	15	2	37
W2	6128	20,02	7,33	17	2	47
W3	7603	17,75	6,31	17	2	42
average %	**7299**	**18**		**16**	**2**	**42**
fz P21 without hairs						
W1	6709	19,00	7,58	19	2	51
W2	7554	18,07	7,48	18	3	44
W3	6423	20,41	8,04	22	3	51
average %	**6895**	**19**		**20**	**3**	**49**
FRT42 fmi E59						
cl 1	2011	31,33	11,46	28	6	110
cl 2	168	25,32	9,83		6	46
cl 3	326	31,48	11,50	28	6	64
cl 4	1502	28,35	10,92	36	4	66
cl 5	279	59,35	19,39	56	12	122
cl 6	371	64,33	22,85	68	6	138
cl 7	576	51,47	17,25		6	100
average %		*diff. scales*	*diff. scales*	*diff. scales*	*diff. scales*	*diff. scales*
ptcGAL4; UAS E-cad-a-Cat						
W1	4872	22,68	8,76	25	2	49
W2	5939	19,71	7,88	18	2	48
W3	4731	23,35	8,97	20	2	53
average %	**5181**	**22**		**21**	**2**	**50**

PCP mutants and Ecad:aCat fusion protein - Vertex counts

	vertex count	3er vertex	%	4er vertex	%
ORK pupal TP5 43hAPF21.5C					
W1	2265	2238	98,81%	27	1,19%
W2	2220	2182	98,29%	38	1,71%
W3	1925	1895	98,44%	30	1,56%
average	**2137**	**2105**	**98,51%**	**32**	**1,49%**
SD	185	184	0,27%	6	0,27%
pk 1					
W1	2438	2329	95,53%	109	4,47%
W2	2881	2745	95,28%	136	4,72%
W3	2737	2585	94,45%	152	5,55%
average %	**2685**	**2553**	**95,09%**	**132**	**4,91%**
SD	226	210	0,57%	22	0,57%
pk-sple13/26					
W1	2237	2137	95,53%	100	4,47%
W2	2651	2519	95,02%	132	4,98%
W3	2413	2329	96,52%	84	3,48%
average %	**2434**	**2328**	**95,69%**	**105**	**4,31%**
SD	208	191	0,76%	24	0,76%
stbm 6					
W1	2824	2746	97,24%	78	2,76%
W2	2354	2289	97,24%	65	2,76%
W3	2629	2584	98,29%	45	1,71%
average %	**2602**	**2540**	**97,59%**	**63**	**2,41%**
SD	236	232	0,61%	17	0,61%
dgo 380					
W1	2414	2381	98,63%	33	1,37%
W2	2727	2674	98,06%	53	1,94%
W3	2452	2398	97,80%	54	2,20%
average %	**2531**	**2484**	**98,16%**	**47**	**1,84%**
SD	171	164	0,43%	12	0,43%
stan 3					
W1	2999	2925	97,53%	74	2,47%
W2	2652	2597	97,93%	55	2,07%
W3	2928	2866	97,88%	62	2,12%
average %	**2860**	**2796**	**97,78%**	**64**	**2,22%**
SD	183	175	0,22%	10	0,22%
fz P21 with hairs					
W1	3095	3044	98,35%	51	1,65%
W2	2293	2261	98,60%	32	1,40%
W3	2856	2829	99,05%	27	0,95%
average %	**2748**	**2711**	**98,67%**	**37**	**1,33%**
SD	412	405	0,36%	13	0,36%
fz P21 without hairs					
W1	2555	2484	97,22%	71	2,78%
W2	2820	2752	97,59%	68	2,41%
W3	2333	2289	98,11%	44	1,89%
average %	**2569**	**2508**	**97,64%**	**61**	**2,36%**
SD	244	232	0,45%	15	0,45%
FRT42 fmi E59					
cl 1	2011	725	94,52%	42	5,48%
cl 2	168	72	92,31%	6	7,69%
cl 3	326	160	98,16%	3	1,84%
cl 4	1502	592	95,95%	25	4,05%
cl 5	279	136	96,45%	5	3,55%
cl 6	371	157	95,15%	8	4,85%
cl 7	576	394	97,52%	10	2,48%
average %	**748**	**319**	**1**	**14**	**4,28%**
SD	715	255	0	14	1,97%
ptcGAL4; UAS E-cad-a-Cat					
W1	1801	1750	97,17%	51	2,83%
W2	2246	2176	96,88%	70	3,12%
W3	1781	1738	97,59%	43	2,41%
average %	**1943**	**1888**	**97,21%**	**55**	**2,79%**
SD	263	249	0,35%	14	0,35%

PCP mutants and Ecad:aCat fusion protein - Cell-cell contact and perimeter variation

	ratio: SD of average cell area / average cell area	ratio: SD of average cell perimeter / average cell perimeter	ratio: SD of average junction length / average junction length	ratio: ratio junction length / ratio perimeter	junction length variation relative to ORK (normalized for perimeter variation)	SD of normalized junction length variation relative to ORK
ORK_TP5						
W1	0,374	0,178	0,354	1,990		
W2	0,310	0,155	0,347	2,242		
W3	0,318	0,162	0,334	2,063		
average	**0,334**	**0,165**	**0,345**	**2,098**	**1,000**	0,062
SD	0,035	0,012	0,010	0,130		
pk 1						
W1	0,302	0,138	0,345	2,498		
W2	0,353	0,179	0,379	2,116		
W3	0,365	0,169	0,379	2,234		
average %	**0,340**	**0,162**	**0,367**	**2,282**	**1,088**	0,086
SD	0,033	0,021	0,019	0,196		
pk-sple13/26						
W1	0,268	0,136	0,394	2,899		
W2	0,277	0,138	0,412	2,983		
W3	0,264	0,128	0,390	3,033		
average %	**0,269**	**0,134**	**0,399**	**2,972**	**1,416**	0,023
SD	0,007	0,005	0,012	0,068		
stbm 6						
W1	0,261	0,128	0,365	2,842		
W2	0,282	0,140	0,358	2,556		
W3	0,268	0,137	0,335	2,443		
average %	**0,270**	**0,135**	**0,353**	**2,614**	**1,246**	0,079
SD	0,011	0,006	0,016	0,205		
dgo 380						
W1	0,289	0,134	0,349	2,611		
W2	0,252	0,121	0,329	2,708		
W3	0,256	0,119	0,332	2,784		
average %	**0,266**	**0,125**	**0,336**	**2,701**	**1,287**	0,032
SD	0,020	0,008	0,011	0,087		
stan 3						
W1	0,272	0,133	0,338	2,541		
W2	0,277	0,133	0,342	2,568		
W3	0,290	0,135	0,347	2,575		
average %	**0,280**	**0,134**	**0,343**	**2,561**	**1,221**	0,007
SD	0,010	0,001	0,004	0,018		
fz P21 with hairs						
W1	0,290	0,143	0,363	2,549		
W2	0,355	0,164	0,366	2,228		
W3	0,305	0,146	0,356	2,442		
average %	**0,316**	**0,151**	**0,362**	**2,406**	**1,147**	0,068
SD	0,034	0,012	0,005	0,164		
fz P21 without hairs						
W1	0,347	0,178	0,399	2,236		
W2	0,252	0,141	0,414	2,943		
W3	0,338	0,173	0,394	2,274		
average %	**0,313**	**0,164**	**0,402**	**2,484**	**1,184**	0,160
SD	0,052	0,020	0,010	0,398		
FRT42 fmi E59						
cl 1		0,078	0,366	4,688		
cl 2		0,092	0,388	4,202		
cl 3		0,090	0,365	4,073		
cl 4		0,083	0,385	4,654		
cl 5		0,058	0,327	5,618		
cl 6		0,076	0,355	4,662		
cl 7		0,073	0,335	4,601		
average %		**0,079**	**0,360**	**4,643**	**2,213**	0,107
SD		0,011	0,023	0,496		
ptcGAL4; UAS E-cad-a-Cat						
W1	0,308	0,160	0,386	2,413		
W2	0,311	0,157	0,400	2,545		
W3	0,295	0,152	0,384	2,532		
average %	**0,305**	**0,156**	**0,390**	**2,497**	**1,190**	0,029
SD	0,008	0,004	0,009	0,073		

Appendix III

Cellenger Cell Packing Analysis

Image Output

Oregon R Wing Imaginal Disc and Prepupal Packing (12hrs APF at 21.5°C)

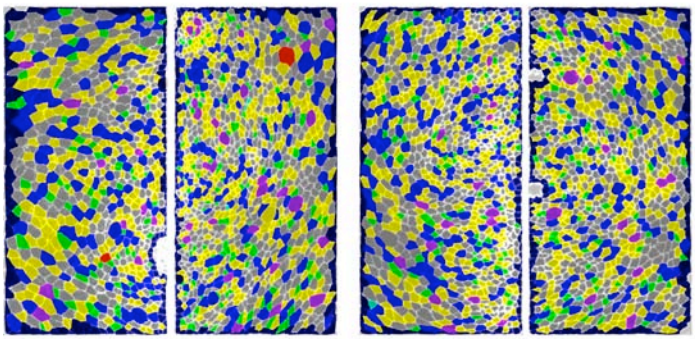

Wing Imaginal Disc 1+2 (ventral side left;dorsal side right)

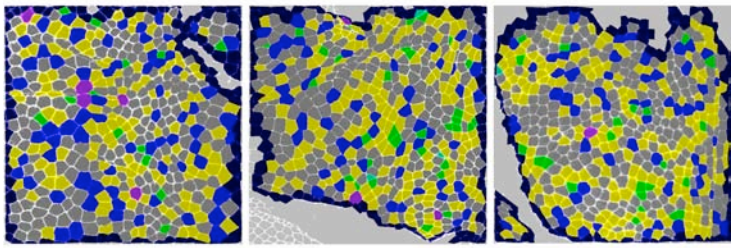

Prepupal wing (Live imaging of E-cadherin GFP at 12hrsAPF 21.5°C)

Oregon R Pupal Packing Time Point 1 (29 hrs APF at 21.5°C)

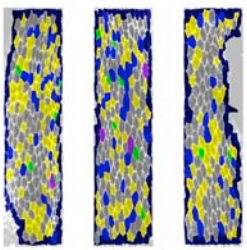

between anterior wing margin and L2

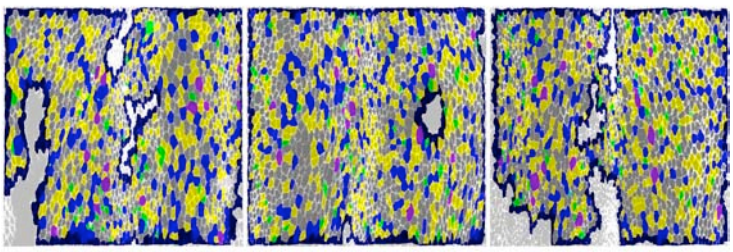

between L2 and L4 distal to anterior crossvein

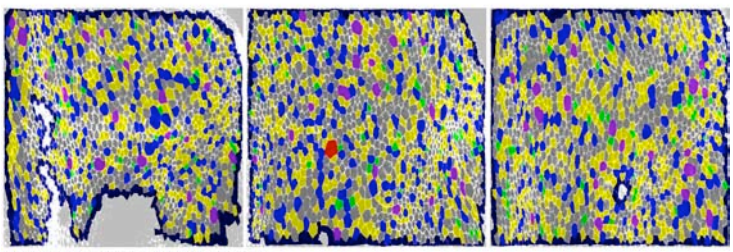

between L4 and L5 distal to posterior crossvein

Oregon R Pupal Packing Time Point 2 (32.5 hrs APF at 21.5°C)

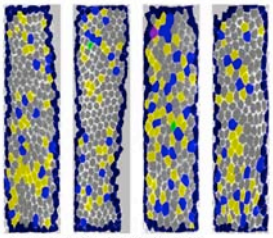

between anterior wing margin and L2

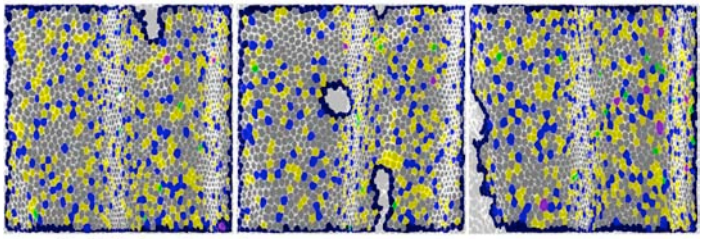

between L2 and L4 distal to anterior crossvein

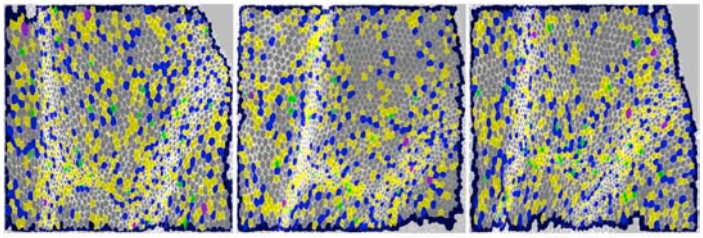

between L4 and L5 distal to posterior crossvein

Oregon R Pupal Packing Time Point 3 (36 hrs APF at 21.5°C)

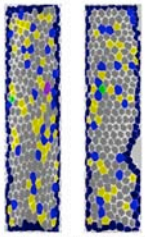

between anterior wing margin and L2

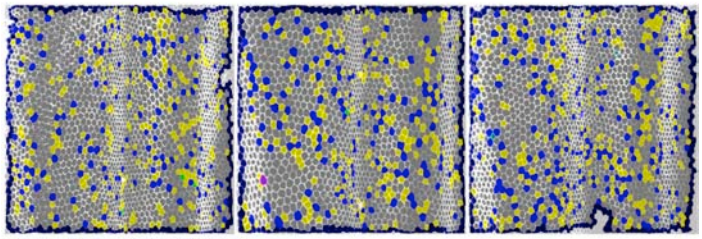

between L2 and L4 distal to anterior crossvein

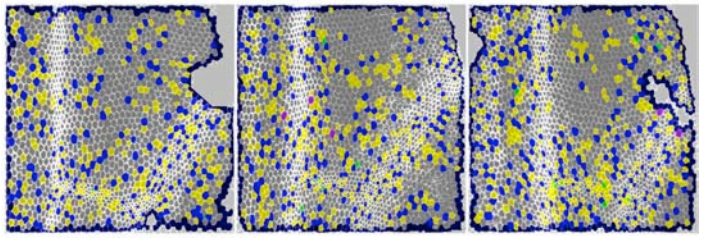

between L4 and L5 distal to posterior crossvein

Oregon R Pupal Packing Time Point 4 (39.5 hrs APF at 21.5°C)

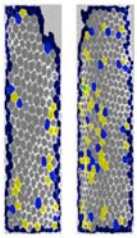

between anterior wing margin and L2

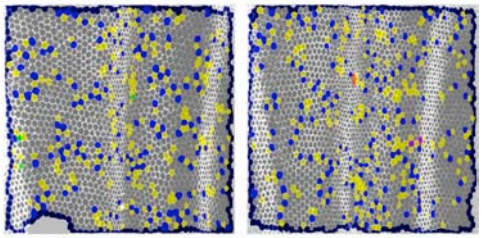

between L2 and L4 distal to anterior crossvein

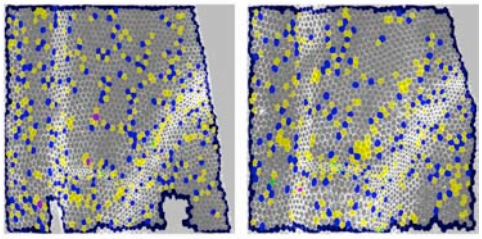

between L4 and L5 distal to posterior crossvein

Oregon R Pupal Packing Time Point 5 (43 hrs APF at 21.5°C - hair outgrowth)

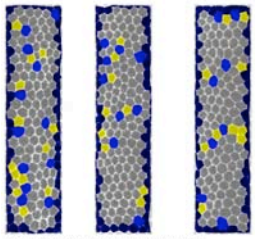

between anterior wing margin and L2

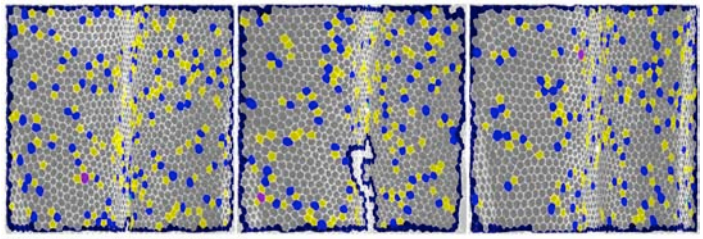

between L2 and L4 distal to anterior crossvein

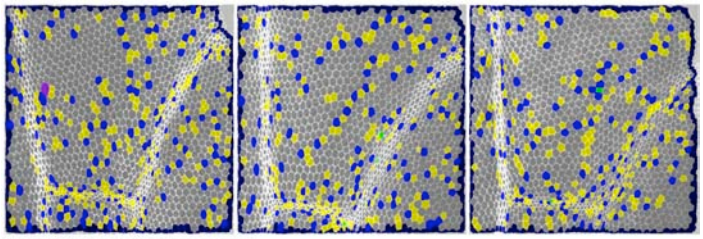

between L4 and L5 distal to posterior crossvein

Cellenger Images Oregon R and PCP mutants at hair outgrowth

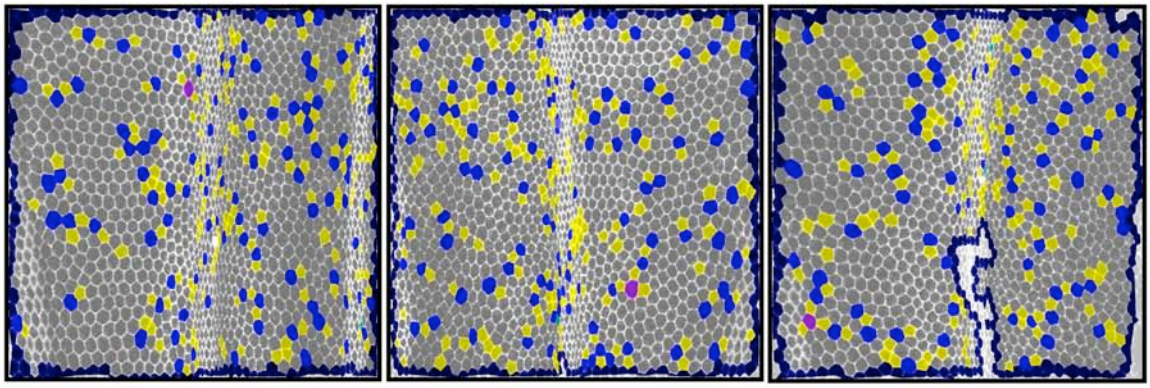

Oregon R

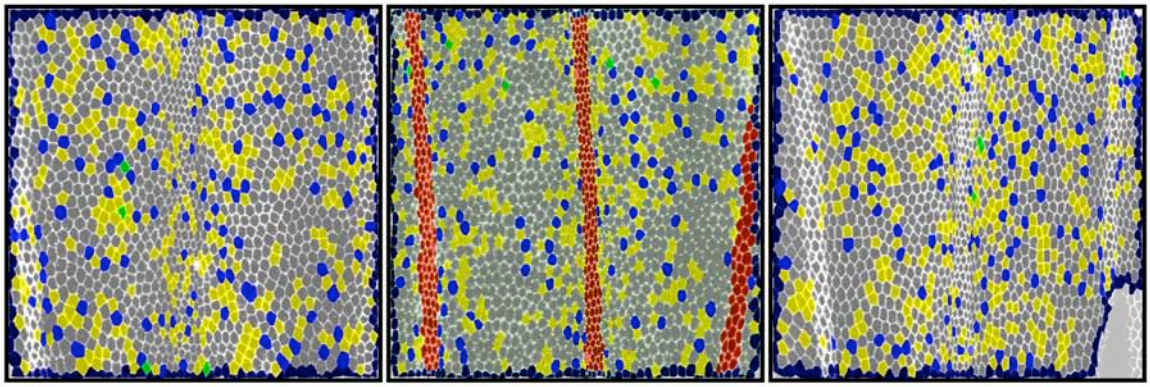

pk 1

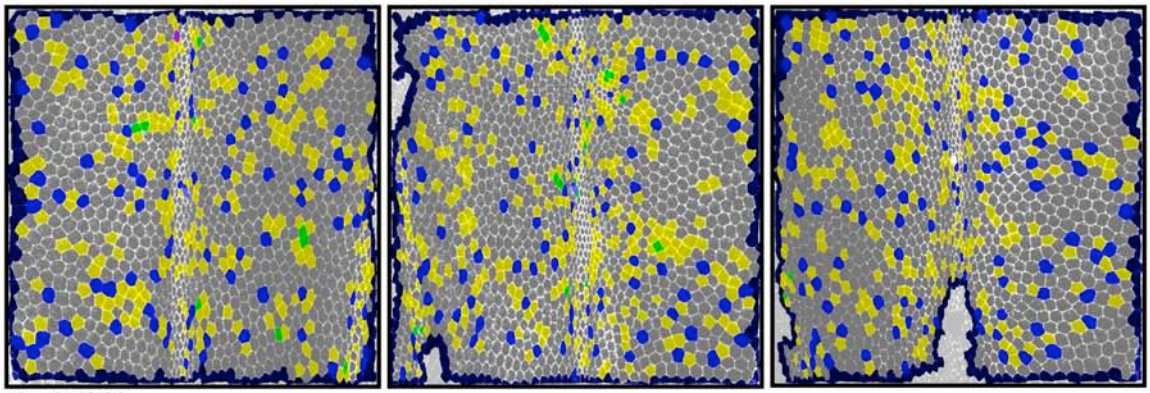

pk-sple 13/26

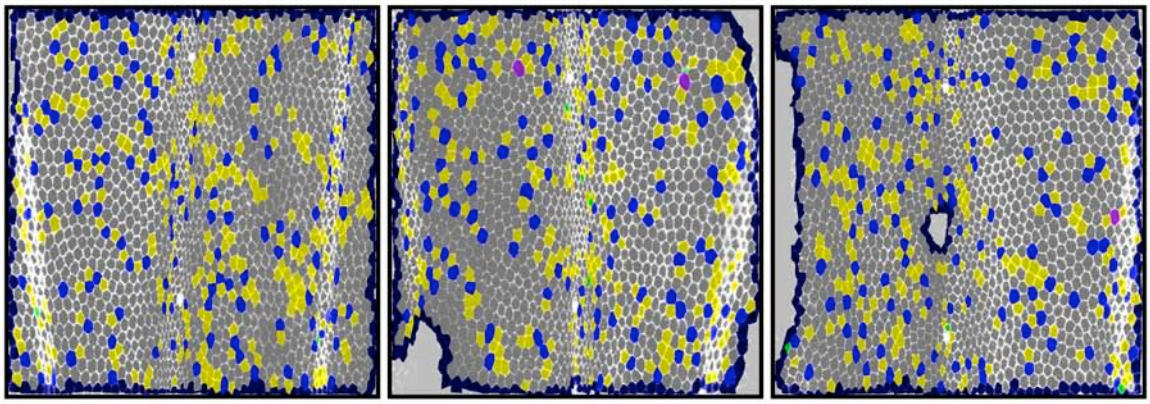

stbm 6

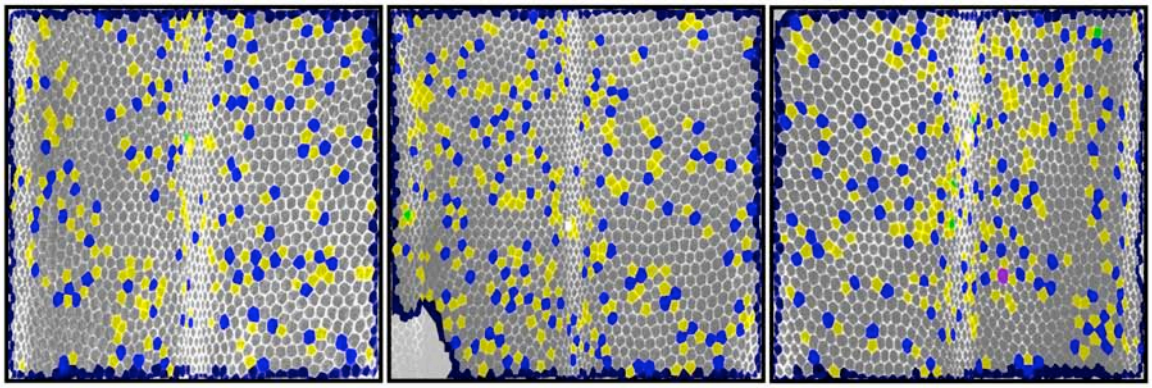

dgo 380

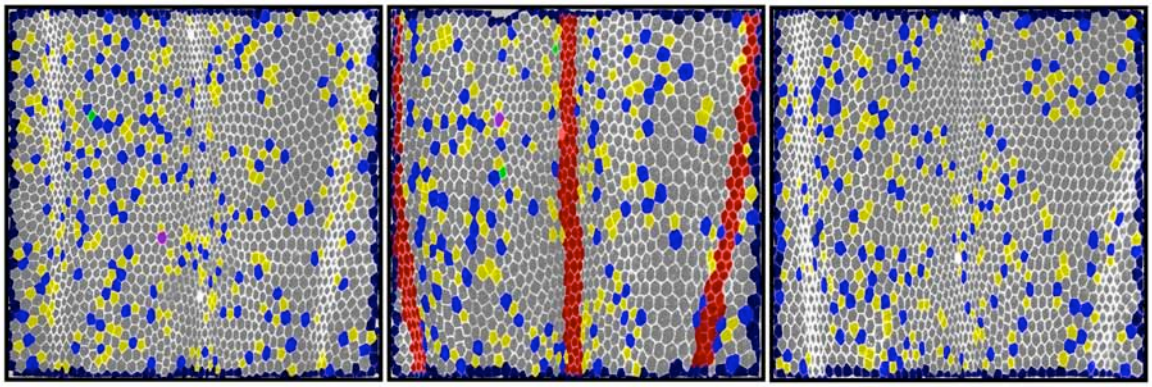

fz P21

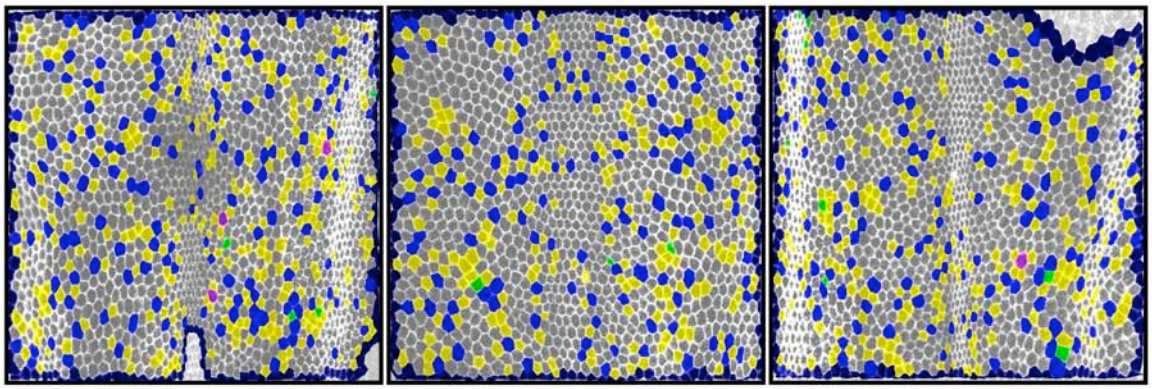

fz P21 without hair

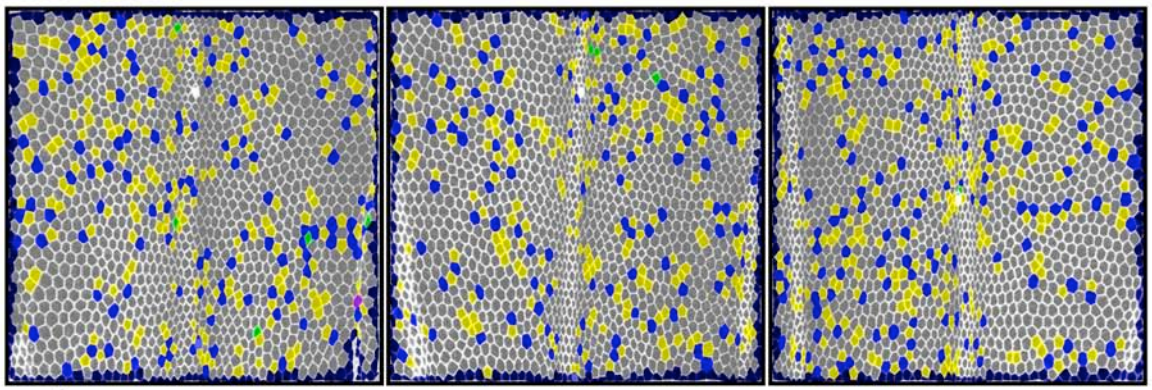

stan 3